86

ISSN 1340-3745

ICRR

ICRR-REPORT-464-2000-8

FERMILAB
OCT 16 2000
LIBRARY

INSPIRES

ICRR-Report-464-2000-8

Studies of Nuclear Components in the Energy region of 10^{15}-10^{16} eV, Electron Component in the 100GeV-10TeV, Gamma rays in the 30GeV-10TeV, Solar Neutrons and Massive Exotic Particles in the Cosmic Radiation

Fermilab Library
0 1160 0069920 1

INCA Workshop

at P. N. Lebedev Physical Institute
Moscow

Edited by T. Saito

Institute for Cosmic Ray Research

University of Tokyo

INSTITUTE FOR COSMIC RAY RESEARCH
UNIVERSITY OF TOKYO
5-1-5 Kashiwanoha, Kashiwa, Chiba 277-8582, Japan

INCA WORKSHOP (Moscow, June 7-9, 1999)

Contents

Photograph of Participants

Opening the Workshop
Academician G. T. Zatsepin.....1

I. Astrophysical goals of the INCA project

I-1. Hadron and Electron Spectra from local nearby sources
V. A. Chechin and V. A. Tsarev.....2

I-2. Negative Trend of the Cosmic Ray Flux
V. A. Chechin and V. A. Tsarev.....11

I-3. New Experiment for Strange Quark Matter Search
-How to confirm the existence of Strange Quark Matter-
T. Saito.....15

I-4. INCA Advantages for the Solar Neutrons and Gamma-Ray Observations
G. A. Bazilevskaya.....19

I-5. Massive Exotic Particles in the PCR Flux
K. A. Kotelnikov, L. M. Lyamshev, G. I. Mezon, N.G. Poluhina, N. I. Starkov, V. A. Tsarev, T. Saito and H. Sasaki.....22

II. The INCA Concept

II-1. The concept of an Ionization-Neutron Calorimeter
A. P. Chubenko.....33

II-2. Neutron Production in Nuclear and Electromagnetic cascades generated by Muons in underground experiments
O. G. Ryazafskaya.....36

II-3. Separation of Electromagnetic and Nuclear showers produced by Muons on the basis of the number of detected Neutrons
O. G. Ryazafskaya.....39

II-4. New Approach to Measurement of Energy of Primary Protons and Nuclei
R. A. Mukhamedshin.....42

II-5. New Method for Separation of Electromagnetic and Hadron Cascades in Detection of Primary Electrons and Gamma-Rays
R. A. Mukhamedshin.....46

II-6. Measurements of the neutron yield from a lead absorber for pion and proton projectiles
V. A. Ryabov.....50

II-7. Monte Carlo simulation of the efficiency of neutron detection in the INCA balloon version
N. M. Sobolevskii, A. P. Zhukov.....55

III. Realization of the INCA Project

III-1. INCA Design and Realization stages
G. I. Merzon.....59

III-2. A new Silicon detector on the basis of Matrix Bipolar structures
V. N. Murashov.....65

III-3. Scintillation and neutron detectors in the INCA
K. V. Alexandrov.....66

III-4. Detectors and Electronics of Balloon borne Strange Quark Matter Telescope
Y. Hatano, T. Yanagita.....69

III-5. Ball antenna and its application
H. Sasaki.....73

Academician
G. T. Zatsepin

Introduction words

More than 30 years ago, a problem arose: how to separate reliably a type of interaction for a muon generated a shower. Whether this interaction is electromagnetic or inelastic nuclear one. It was quite clear that this separation can be realized on the basis of studying shower composition: in the case of nuclear interaction, there would be a lot of neutrons, and we should learn to detect them. The creation of an adequate setup was performed by a group of physicists headed by O.G. Ryazhskaya. Large-scale scintillation counters based of a liquid scintillator were made. Neutrons were slowed down in the hydrogen-containing scintillator and then captured by hydrogen atoms. Delayed pulses with characteristic amplitude were recorded. Thus, features of the photo-nuclear interactions within the wide energy range were studied and the constant cross section of this interaction as demonstrated. The separation of events into two groups was the more reliable, the higher was the energy of the shower created by a muon.

Another problem now arose, which requires separating electromagnetic and nuclear-cascade showers. To do this, A.P. Chubenko has suggested using an instrument called ionization-neutron calorimeter (INCA). This calorimeter makes it possible to separate with a high reliability events generated by nuclei of primary cosmic rays and those caused by electrons. It seems to us that appearance of INCA for studying primary cosmic radiation is a rather promising step. It would be quite interesting constructing a high-volume INCA and its launching aboard a satellite for a long time to directly investigating the spectrum of primary cosmic rays in the "knee" energy region of 10^{15} - 10^{16} eV.

I would like to wish a success for our workshop.

HADRON AND ELECTRON SPECTRA FROM LOCAL NEARBY SOURCES

V. A. Chechin and V. A. Tsarev
Lebedev Physical Institute, Russian Academy of Sciences, Moscow, Russia

The INCA proposal [1] is a multipurpose project aimed at studying various aspects of cosmic ray (CR) physics and astrophysics, the studying local nearby CR sources being the most appropriate and important. In my I shall briefly remind some aspects of this problem.

1. Supernovae are the primary source of Galactic Cosmic Rays

Supernova (SN) explosions, the most energetic events observed in our Galaxy, are believed to be a primary source of high-energy CR particles up to at least 10^{14} - 10^{15} eV/n. The main arguments are well known and are based on a simple energy consideration [2]. We know that:

- CR energy density in the interstellar medium (ISM) is $w \cong$ eV/cm^3; the total power of galactic CR sources (the Galaxy- CR -luminosity)

$$L_{G,CR} \cong 10^{41} \text{ erg/s}$$

- the energy produced in a typical SN explosion (the kinetic energy of ejecta) is about

$$W_{K,SN} \cong 10^{51} \text{ erg}$$

- the rate of SN explosions in the Galaxy is estimated as

$$T^{-1} = 10^{-1} - 10^{-2} \text{ yr}^{-1}$$

- the average power produced by the Galactic SN is

$$W_{G,SN} \cong W_{K,SN} T^{-1} \cong 10^{42} \text{ erg/s}.$$

Thus, if 10% of the SN (kinetic) energy is transformed into CR energy, it can explain $L_{G,CR}$.

2. Cosmic ray spectrum

CR sources are known to concentrate in the Galactic disc. CR particles produced by different sources fill in the Galaxy, and they diffuse in random galactic magnetic fields. Due to the rigidity-dependent CR leakage from the Galaxy, the CR residence time is also rigidity-dependent

$$\tau(E) \propto E^{-\alpha}, \alpha \cong 0.75$$

with the average value $\langle\tau\rangle \cong 2 \cdot 10^7$ yr.

There appear to be three main components present in the CR spectrum, which are usually called the GCR-I, GCR-II, and EGCR components (GCR referring to "galactic CR" and EGCR to "extragalactic CR"). The spectral index of the GCR-I is about 2.75, and it is about 3.2 for GCR-II.

3. CR acceleration in supernova remnants and GCR-I

The current picture of particle acceleration in the SN remnants (SNR) was recently reviewed in [3]. From gasodynamical point of view, the expansion of the SN shell can be viewed as a motion of gas under impact of the expanding spherical, almost impenetrable shell with mass M (the mass of ejecta) and initial velocity $V_0 \cong 10^4$ km/s $\gg C_S$ (C_S is the speed of sound). Due to the ISM gas compression the shock wave (SW) appears ahead the SNR. There are essentially three distinct phases of the SNR life cycle. At the initial free expansion phase, the ejecta expands and sweeps up the IS material in front of it with velocity V_0. At this phase the shock front also moves with a constant speed $V = V_0(\gamma_a + 1)/2$, where γ_a is the adiabatic index. When (at some $t = t_0$) the mass of the swept gas becomes comparable to the mass of ejecta, the second, "adiabatic",

phase sets. At this stage the radiative losses are small compared with the total energy, i.e. the SNR energy is conserved. The onset of the third, "radiative", phase takes place when the radiative cooling timescale becomes comparable to the expansion timescale. Ultimately (after about 10^6 years), when the shell velocity decreases to 10 — 20 km/s, the SNR disappears into the ISM. The characteristic SNR size in the "active", adiabatic, phase is $R \leq R_m \cong 10$ — 100 pc.

The high-energy part of the spectrum is built up mainly at the adiabatic phase. Particle acceleration presumably occurs in the SW according to the well-known "diffusive shock acceleration" mechanism, and the CR spectrum (in the plane-wave approximation) is of power law

$$J(E) = dN/dE \propto (1/p_{inj})\,(p/p_{inj})^{-\gamma(SN)} \propto E^{-\gamma(SN)},\ \gamma(SN) = q - 2,\ q = q(t) = 3\sigma/(\sigma - 1),$$

where σ is the gas compression ratio on the shock front and p_{inj} is the injection momentum. For strong shock $\sigma = 4$, and we have the power law CR spectrum from SNR on the shock front

$$J_{SN} \propto E^{-2.0}$$

The CR flux observed at the Earth (which is supposedly close to the average Galactic one) is determined by the energy spectrum of particles accelerated in a "typical" SNR, by the average intensity of the SNR sources dI/dv dt, and the energy-dependent residence-time of CR particles in the Galaxy $\tau(E)$

$$J_{SN,\,obs.} \propto (1/p_{inj})\,(p/p_{inj})^{-\gamma(SN)-\alpha} \propto E^{-\gamma(SN)-\alpha} \cong E^{-2.75}$$

This is just what is experimentally observed.

However, the acceleration by SN shocks can produce CR only with energies up to about 10^{15} eV/n. It is difficult to reach higher energies, because when the gyroradius of the accelerated particles becomes on the order of the shock size, the shock-acceleration mechanism cannot function, as the particles escape. The gyroradius is given by

$$R = p/(e\,Z\,B) \cong (10\ \text{pc})\,(E/10^{15}\ \text{eV})\,[Z\,B(\mu G)]^{-1},$$

where the typical value of B is a few μG. Thus, this scheme can explain the total CR spectrum up to the knee region.

4. GCR-II component

An appealing way to achieve the CR spectrum continuity at the knee is to allow all particles of the first component the possibility of reacceleration up to higher energies by some other mechanism. One of the most popular scheme is acceleration by an ensemble of shocks [4]. To reach energies beyond 10^{15} eV, larger shocks are required, and those can be obtained in going to older SNR. Older SNR have weaker shocks, which produce a steeper power law. With galactic magnetic fields of about 3μG, shocks of 100 pc size could produce the observed CR spectrum (GCR-2 component) up to 3 10^{16} eV for protons and up to 10^{18} eV for iron [4]. In such a mechanism, the nonuniform distribution of SN's in the disk is taken into consideration, as well as correlation of the times of their explosions. In fact, it is known that the SN explosions have a tendency to take place mainly in associations, so they are correlated in space and time. The frequency of SN bursts in typical associations is estimated as 10^{-5} — 10^{-6} per year. Lifetime of the associations is on the order of 10^7 years, and the number of associations in the Galaxy is several thousands. A theory of CR acceleration and transport in such systems was developed by Bykov and Toptygin and some other workers (see [4] for references). In this approach the knee is caused by the change of the acceleration mechanism and turning to the acceleration by large-scale motions in a larger region. Within the uncertainties of the values of parameters of ISM, SW, and SN ensemble it is quite possible to have the increase of the spectral index $\Delta\gamma \cong 0.3$ — 0.5 and the knee at

about the experimental energy. Also the enrichment of the spectrum by heavy nuclei with E above the knee is predicted: $N(Z_2)/N(Z_1) \propto (Z_2/Z_1)^{\Delta\gamma}$.

Thus we can conclude that the observed CR spectrum is a superposition of the contributions from all sources. This fact creates the main difficulty in the astrophysical study of CR: during their confinement time CR are mixed in the IS magnetic fields, so that information about specific local sources is completely lost.

5. Local nearby sources

There are, however, some exceptions when one could derive direct information about a few nearby local sources from CR observations. These observations are:

(a) the spectrum of CR electrons at energies in the TeV-region, and

(b) the spectrum and composition of CR in the energy interval 1 — 10 PeV, the knee region.

Let us recall the arguments.

(a) Electrons.

For electrons the argumentation is especially transparent and have been originally presented as early as 1970 by Shen [5]. The essential point is that high energy electrons lose their energy mainly by synchrotron radiation and inverse Compton scattering, the energy loss being

$$dE/dt = - bE^2,\ b = 8 \cdot 10^{-17} (w_{ph} + 6 \cdot 10^{11} H^2/8\pi)\ (\text{GeV sec})^{-1}$$

Here w_{ph} is the photon energy density (expressed in eV/cm^3); H is the magnetic field (Oe); E, m, e are the electron energy (GeV), mass and charge respectively. Thus, the electron energy decreases with time as

$$E(t) = E_0/(1 + bE_0t),$$

and the electron age τ and energy E are related by the equation

$$\tau \cong 1/bE.$$

It means that from the total spectrum of electrons emitted by a source only those with energies

$$E \leq E_{max} = 1/b\tau$$

can survive diffusion over a period of time τ. In the course of this diffusion , an electron propagates to the distance $r \cong 2(D\tau)^{1/2}$. For the Galaxy with $D(E = 1\ \text{TeV}) = 10^{29}$ cm^2/s, $w_{ph} = 1$ eV/cm^3, $H = 4 \cdot 10^{-6}$ Oe, we have $b \cong (3 \cdot 10^5\ \text{yr TeV})^{-1}$, and the age of the TeV-electrons cannot significantly exceed 10^5 years. Recent experimental observation [6] of such electrons implies the existence of nearby local sources at a distance $R < 2\ (D\tau)^{1/2} \cong$ 300 — 500 pc. For 1-TeV-electrons, within their propagation domain of about 300 pc from the solar system, the expected number of SN occurrences is only 2 — 5 during the past 3 10^5 years. Only these few sources could contribute efficiently to the electron flux beyond 1 TeV.

(b) Hadrons

The situation for hadrons is not so clear and unambiguous as for electrons. Nevertheless, on the basis of some simple reasoning, one can indicate the most appropriate place to look for the local nearby source contributions [7]. The crucial point here is that due to the closeness of the nearby source, the average CR residence time in the Galaxy $\tau(E)$ is not relevant for its contribution near the Earth. Thus, its spectrum at the observation point is essentially close to that on the source, i.e., has the spectral index 2 (but not 2.75 as for the average contribution from all distant sources). With such harder spectrum, the nearby source contribution could be detectable against the average background, and the best place to look for it is at $E \cong E_{max}$, i.e., near the knee. Another specific prediction is a "fine structure" of the spectrum at $E \cong E_{max}$, produced by different groups of the CR nuclei, because of the Z-dependence of $E_{max}(Z)$. Such a

structure indeed has been seemingly found in a recent analysis of the EAS data in the knee region [7].

6. Contributions from the most important local nearby sources

An extended quantitative discussion of the electron and hadron spectra from local nearby sources has been given recently in our papers [8]. Let me first make two remarks. (a) If we want to evaluate consistently the nearby source contributions, we must calculate the absolute value of the spectrum, produced by a source whose age τ and distance from the Earth r are comparable to the characteristic values t_0 and $R(t_0)$ for typical SNR. In such a case, besides the absolute normalization of the flux, it is necessary to take into account that particles accelerated at different stages of a SNR evolution will bring different contributions to the CR spectrum observed at the Earth. Kinetic model [3] gives the most consistent treatment of the space-time CR distribution. However, combined solution of both kinetic and gasodynamic equations is a very cumbersome problem. It makes difficult to do simple estimates of spectra of the acceverated particles at arbitrary times and distances, as well as to take into account propagation effects in the IS gas. In the "onion shell model" (OSM) [9], some simplifications are used. The gas motion is described by a simple "similarity solution" typical for "strong shocks". The size of the SNR R(t) is assumed to be large, so the SW can be treated as "flat". However, OSM disregards particle diffusion from acceleration region into outer space and feed-back of the accelerated CR on SW; thus it is not completely adequate for the "running-away" high-energy particles which are important for $t > t_0$. For evaluating the high-energy spectrum from local nearby sources, we have developed a "hybrid" approach [8]. It is based on the OSM which is further constrained by some requirements following from the KM.

(b) Notice that, in principal, for young nearby source, we can encounter two rather different situations. In one (the most common) case the shock front from the SN has not reach the solar system yet, and we can observe only diffusion particles; a detectable contribution from local source can be expected at most near the knee region. In the other case, the shock front at present have already passed by the Earth, so we are now residing inside a "bubble" produced by the source. Then, we can observe particles "frozen" into the IS gas inside the bubble, the CR flux being mainly determined by convection; for the extreme conditions, almost all GCR-1 component could be caused by this local source [10]. (Such a case will be discussed in Dr. V. Chechin's talk at this workshop).

From more than the 15 known at present candidates which are within the distance 1 kpc from the solar system [11], we shall choose the following four most close and young ones: Monogem (1.1; 300), Loop 1 (2; 170), Geminga (3.4; 300), Vela [a(0.1; 500), b (0.3; 200)]. The numbers in brackets are the age (in 10^5 years) and the distance from the Earth (in pc) which are taken from [11]; for Vela we shall also consider the set (b) of parameters from [12]. The t-dependence of the distance of the Earth to the closest part of the SW from these SNR's is shown in Fig 1. We see that for the chosen set of parameters t and r for all considered sources, SW's did not reach the Earth, so we deal with the first case. Four groups of nuclei are taken into account: H(1; 1), He(2; 0.1), "light nuclei (7; 10^{-3}), and "heavy nuclei" " (28; $4 \cdot 10^{-5}$). The numbers in brackets are the charge Z and the average (standard) abundance relative hydrogen.

The calculated spectra of hadrons for the injection rate of $5 \cdot 10^{-5}$ and $2 \cdot 10^{-4}$ are shown in Figs. 2 and 3 for sets (a) and (b) respectively. The background contribution from all distant sources is approximated with two power-law functions smoothed over the energy interval 1 — 10 PeV (dotted line); the contributions from four local sources

(summed up over all groups of nuclei) are shown by dashed lines; the solid line is the sum of all four local sources plus the background; crosses and asterisks designate experimental points. Different peaks on the curves correspond to the contributions from different nuclei, since E_m is expected to be proportional to the atomic number Z. It is seen that for both sets (a) and (b), better agreement with data can be reached if the proton and helium contributions are suppressed relative heavier nuclei. The dashed-dotted line corresponds to the proton and helium contributions reduced ten times and light and heavy nuclei increased 3 times in respect to the standard values.

The slope of the spectrum S = d(logJ)/d(logE) is shown in Figs. 4 and 5. Again, the dashed-dotted line corresponds to 1/10 of the p and He abundance's, while dotted line shows the experimental values averaged according to [7].

Similar calculations have been carried out also for electron spectra. We have assumed electrons to be injected into acceleration similarly to protons with the same kinetic energy (i.e., $p_{inj} = (2mE_{inj})^{1/2}$), where m is the mass of proton or electron), and accelerated in SW at least up to energies $E \leq 10$ TeV. (The important difference of electrons is that the effective energy losses occur in the course of both acceleration and propagation).

The results of the calculations of electron spectra from the same sources are shown in Figs. 6 and 7 for (a) and (b) sets of parameter, respectively (solid line), along with experimental data and the average background due to distant sources (dotted line).

Conclusions

From inspection of the results of our calculations we can reach the following conclusions:

- With a standard set of parameters for ISM, a chosen set of the SNRs, and assuming equal injection energies for e and p, the calculated spectra both for hadrons in the knee-region and for electrons at TeV-energies are in a reasonable overall agrrement with observable data; the correct value of the e/p-flux-ratio results mainly from the mass ratio M_e/M_p and difference in energy losses. For both electrons and hadrons the contributions of the nearby sources are visible on the average background in the considered energy regions;
- For both hadrons (at E = 1 — 10 PeV) and electrons (at $E \geq 0.5$ TeV), the most important contribution comes from the youngest SNR (Monogem for the set (a) and Vela for the set (b)). For electrons it is an obvious consequence of the age-dependent energy cut-off. For hadrons it results from the diffusion factor $t^{-3/2} \exp(-r^2/4Dt)$. For all considered sources exponent is close to unity, and r-dependence vanishes: thus the relative contributions from different sources are determined only by their ages, the youngest source being the most important;
- In accord with [7], the fine structure of the knee is due to the contributions from different groups of nuclei (although, in reality, it can be smoothed);
- For better agreement with data, the lower abundance of H and He is preferable with respect to the standard one.

The general conclusion from the above discussion is rather obvious:

- Studying the primary hadron spectrum and composition in the knee region and new measurements of high-energy electron spectrum with a better accuracy and at higher energies, which can be done with INCA detector, will bring a new important insight in the astrophysics of local nearby sources.

References

1. K. V. Alexandrov et al., The INCA project, Lebedev Physical Institute preprint no. 47, Moscow, 1998
2. V. S. Beresinskii et al., Astrophysics of Cosmic Rays (North-Holland, Amsterdam, 1990)
3. E. G. Berezhko et al., JETP, 82, 1, 1996
4. A. M. Bukov and I. N. Toptygin, Proc. 25 ICRC (Durban), OG, p. 365, 1997; G. P. Zank and W. I. Axford, ibid. p. 473, A. Wandel, ibid., 413.
5. C. S. Shen, Astrophys. J. 162, L 181, 1970
6. T. Taira et al., Proc. 23 ICRC (Calgary), 1993, v. 2, p. 128
7. A. D. Erlykin and A. Wolfendale, 1997, J. Phys. G: Part. Phys., 23, 1.
8. V. A. Chechin et al., Proc. 1997 COSMION Conference, Moscow; Doklady RAN, 1999 , to be published; Kratkie Soobsheniya po Fizike, to be published.
9. T. J. Bogdan and H. J. Volk, A&A, 122, 22, 1983
10. P. A. Johnson and J. P. Dawson, Proc. 25 ICRC (Durban), 1997, OG, p. 376
11. J. Nishimura et al., Proc. 24th ICRC, Rome, 3, 29, 1996;
12. B. Aschenbach et al., Nature, v. 373, p. 587, 1995

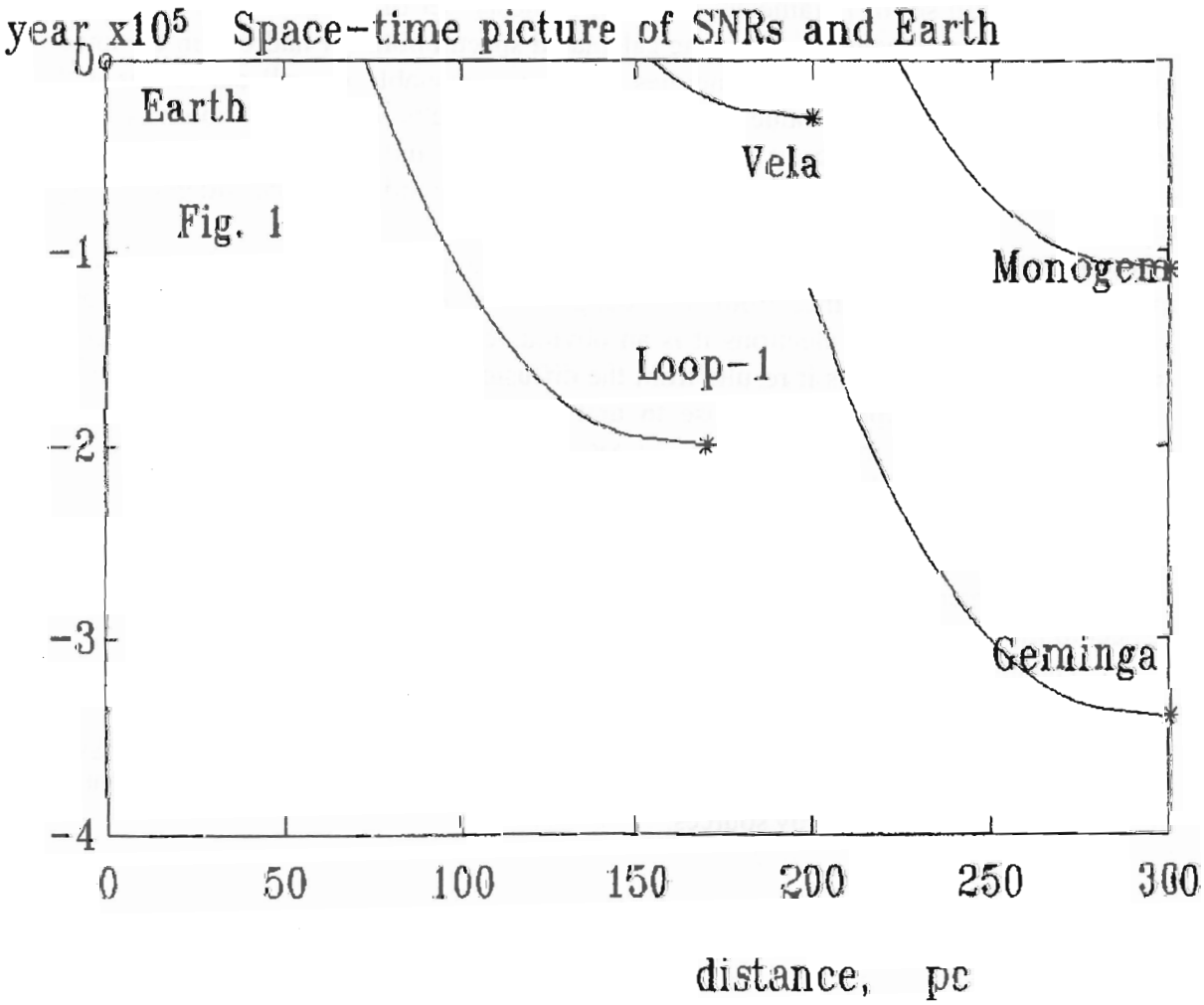

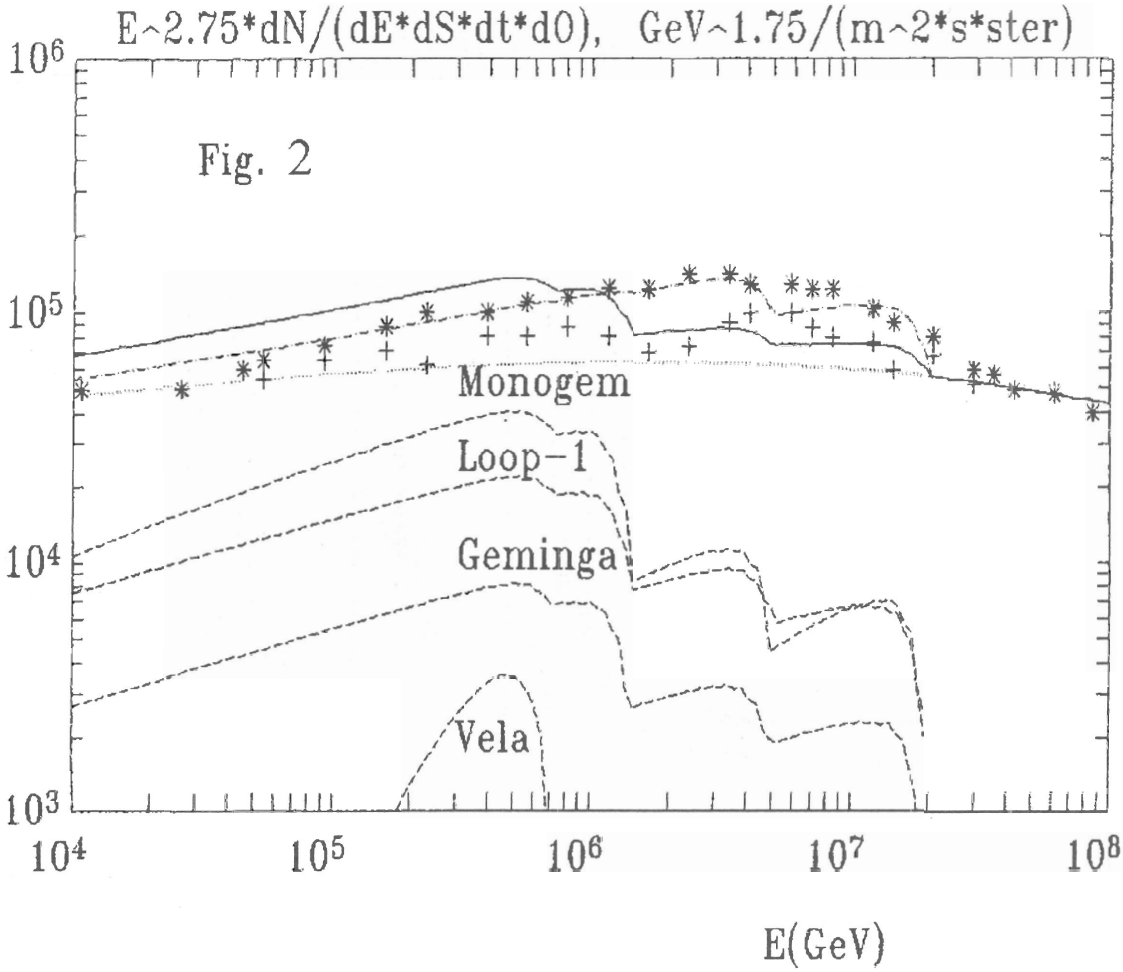
E~2.75*dN/(dE*dS*dt*d0), GeV~1.75/(m~2*s*ster)
Fig. 2
Monogem
Loop-1
Geminga
Vela
E(GeV)

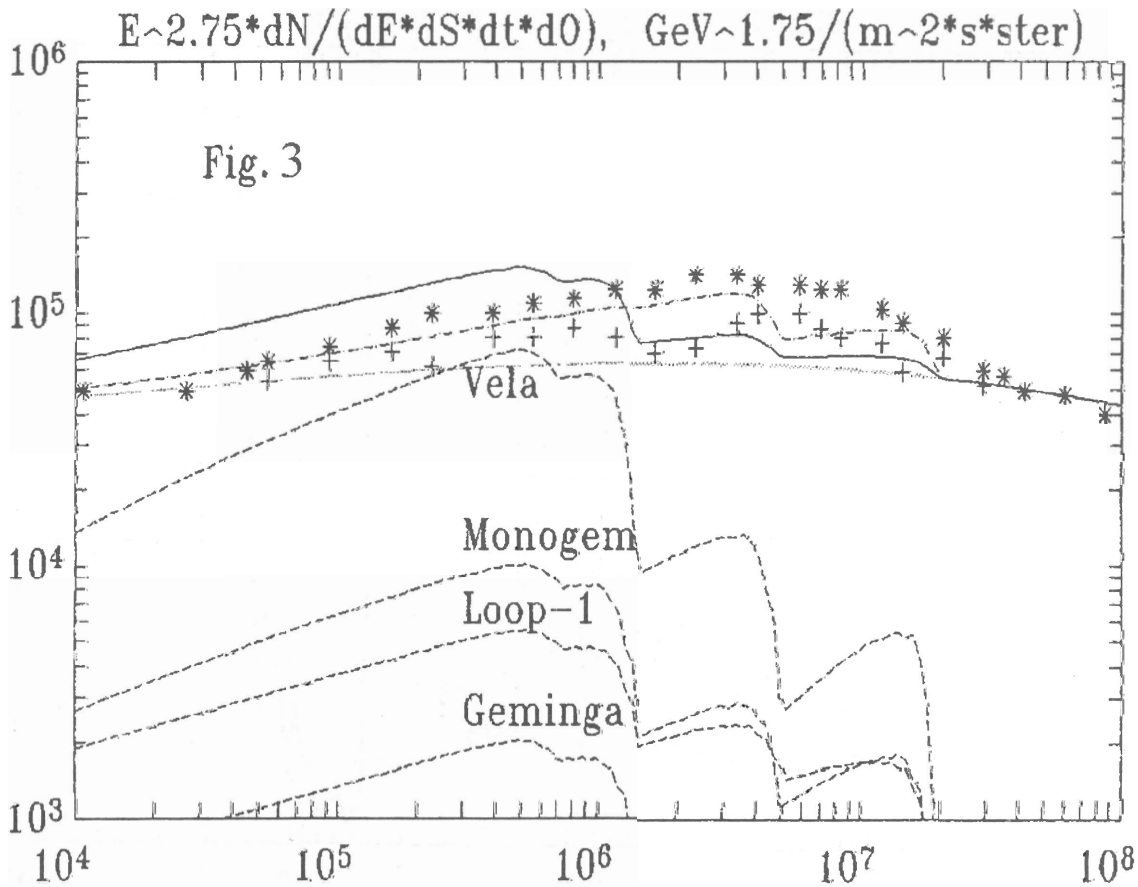
E~2.75*dN/(dE*dS*dt*d0), GeV~1.75/(m~2*s*ster)
Fig. 3
Vela
Monogem
Loop-1
Geminga
E(GeV)

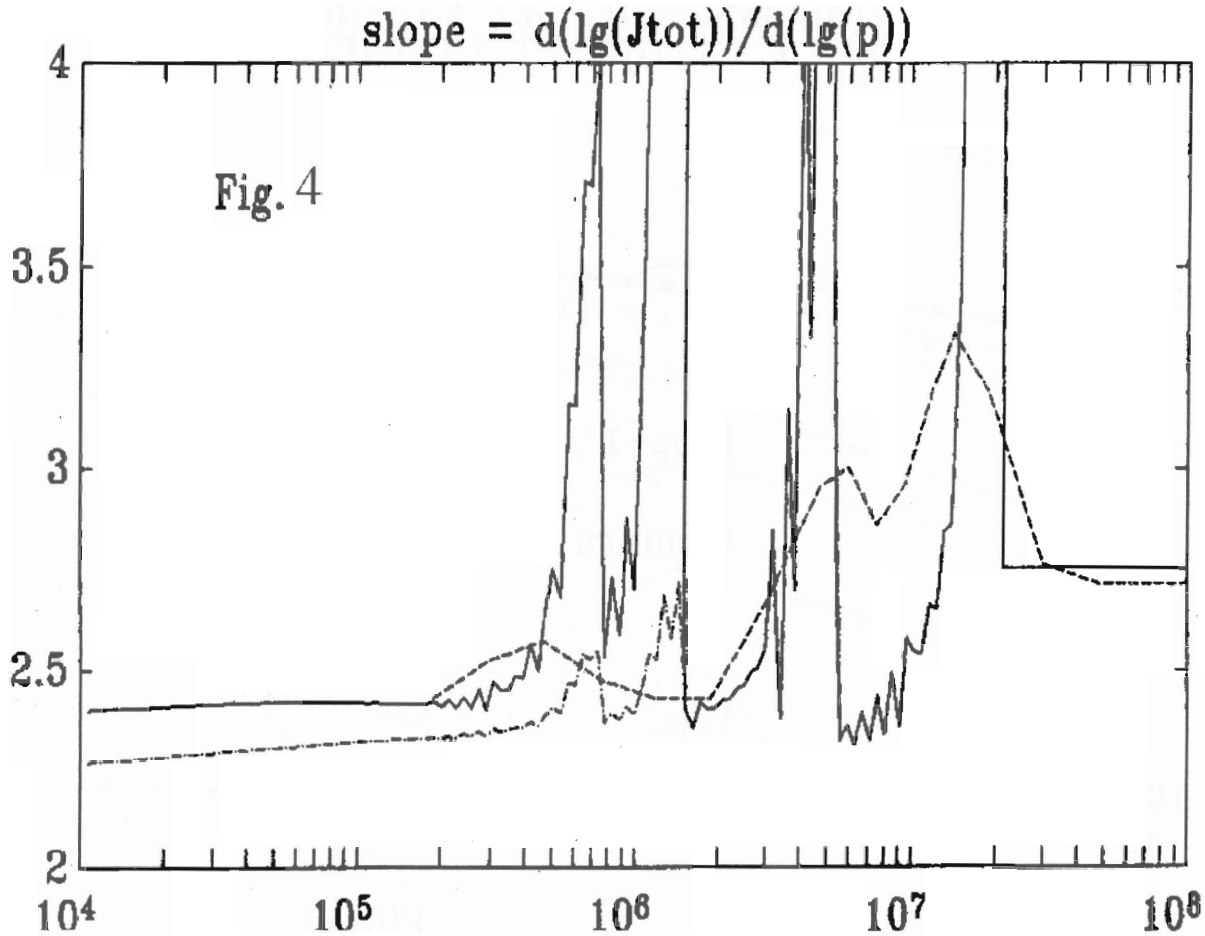
slope = d(lg(Jtot))/d(lg(p))
Fig. 4
4
3.5
3
2.5
2
10^4
10^5
10^6
10^7
10^8

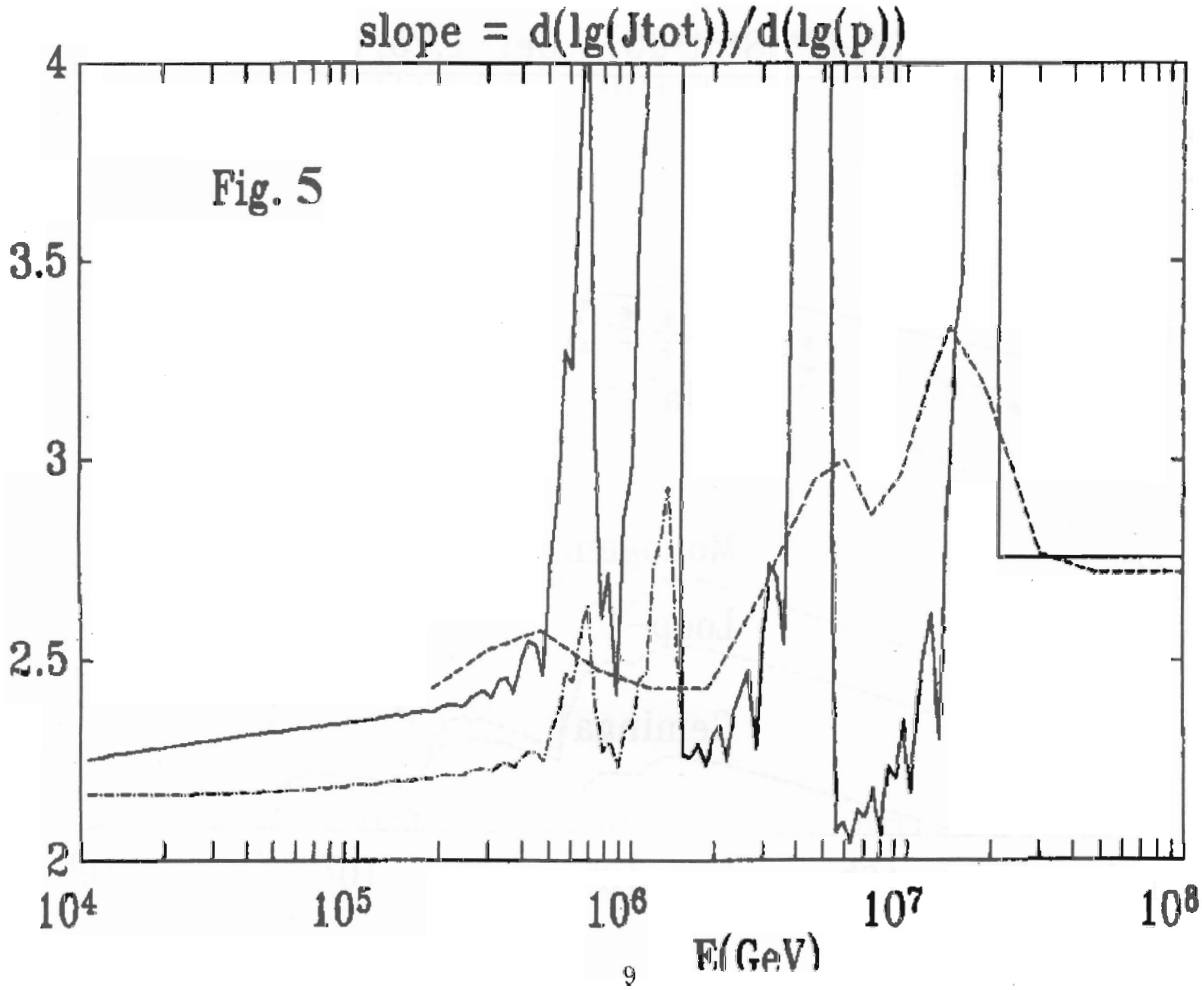
slope = d(lg(Jtot))/d(lg(p))
Fig. 5
4
3.5
3
2.5
2
10^4
10^5
10^6
10^7
10^8
E(GeV)

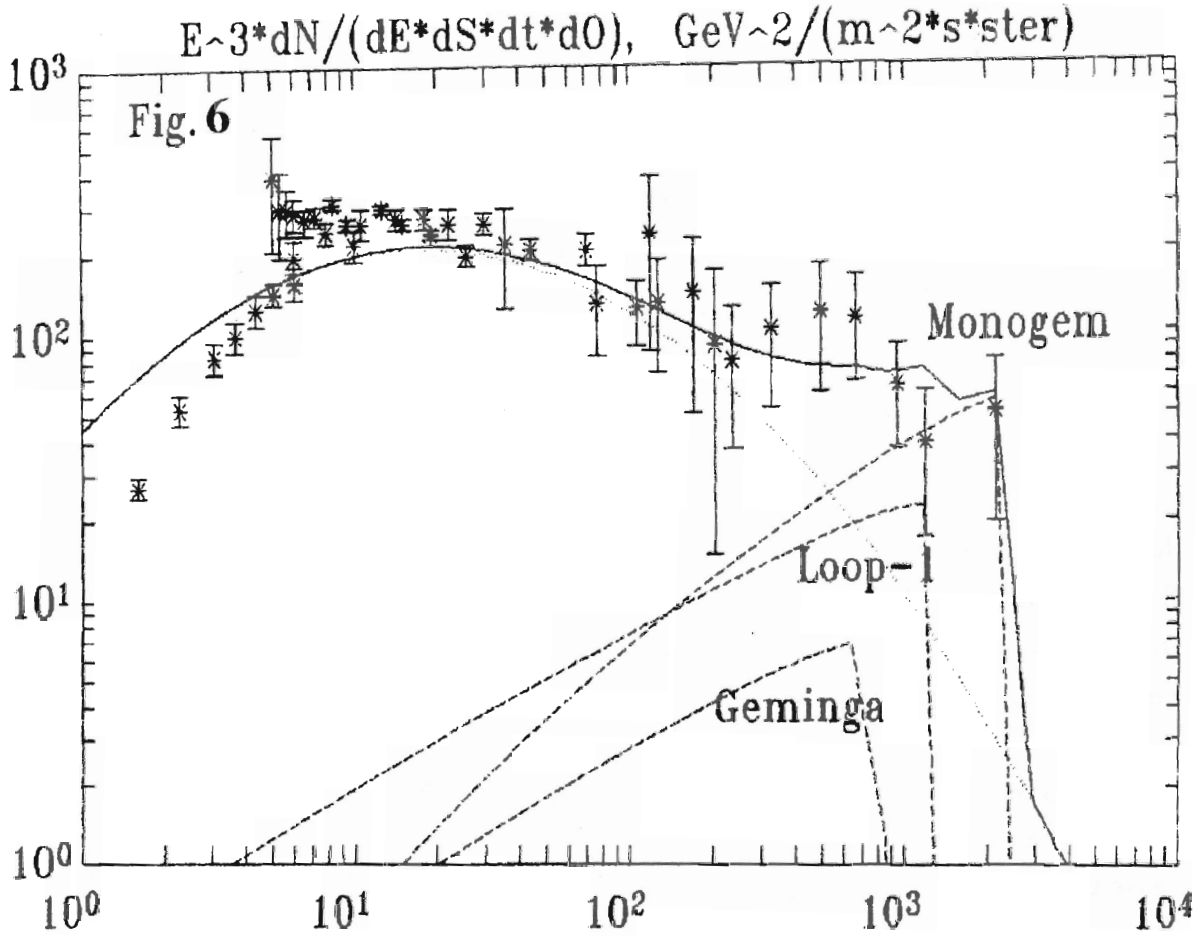
E~3*dN/(dE*dS*dt*dO), GeV~2/(m~2*s*ster)
Fig. 6
Monogem
Loop-1
Geminga
10^0
10^1
10^2
10^3
10^4

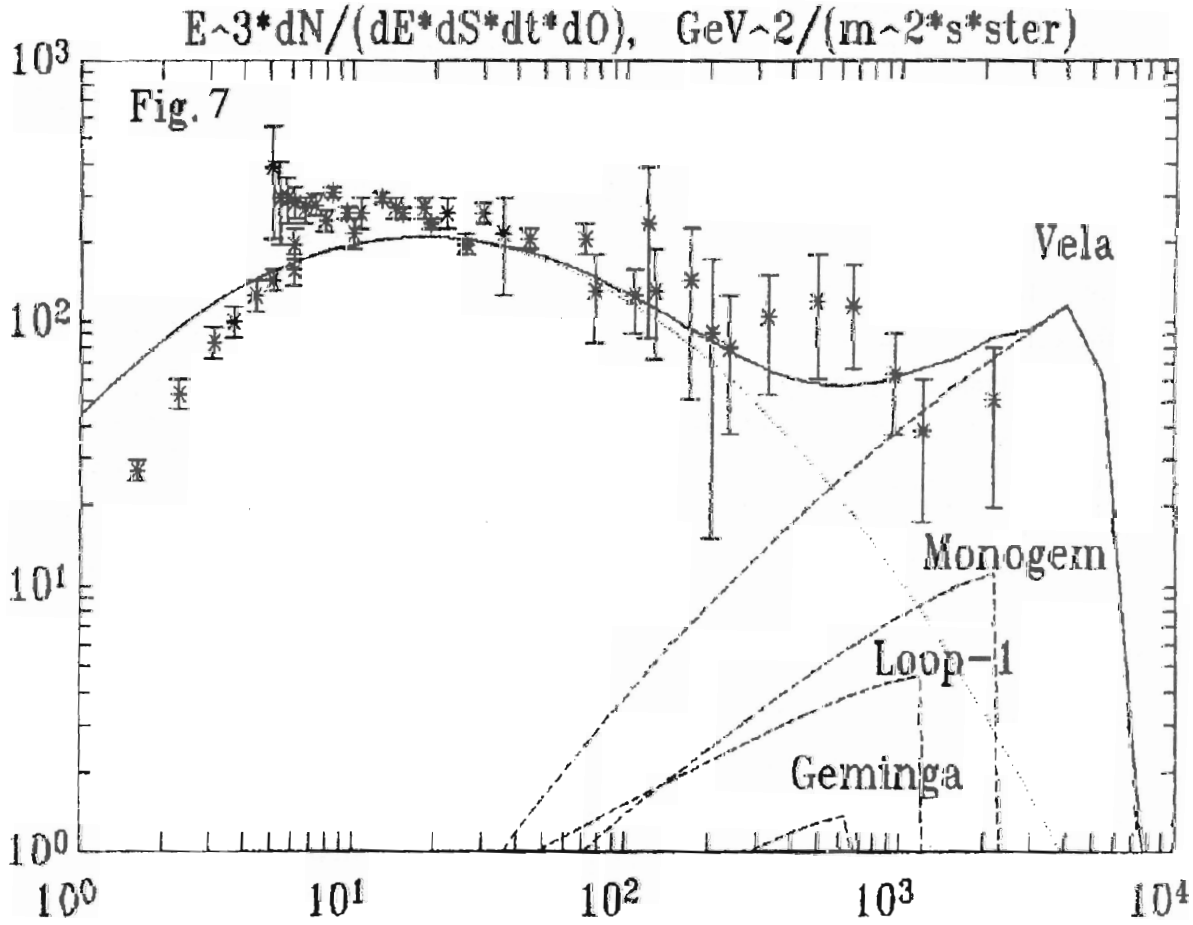
E~3*dN/(dE*dS*dt*dO), GeV~2/(m~2*s*ster)
Fig. 7
Vela
Monogem
Loop-1
Geminga
10^0
10^1
10^2
10^3
10^4
E(GeV)

Negative Trend of the Cosmic Ray Flux

V. A. Chechin and V. A. Tsarev

P.N. Lebedev Physical Institute, Moscow, Russia

The existing experimental data on cosmic rays (CR) suggest that the total CR flux in the solar system varies in time [1]. From the direct measurements carried out during the past forty years, it follows that the logarithmic time derivative T of the flux (CR "trend") is on the order of $10^{-4}\div10^{-5}$ 1/year. Hence, the age of some possible sources contributing significantly to this flux has to be about of $10^{4}\div10^{5}$ year. Furthermore, indirect evidences of the time variability of the CR flux exist. Namely, deep sea cores, polar ice , and tree samples show the presence of "bumps" in spallogenic isotopes (^{10}Be, ^{14}C, and others) [2, 3]. The most prominent "bump" (3÷7 times the average level) took place 35÷40 kiloyears ago. These "bumps" may be caused by an increase in the production of the isotopes which is associated with a corresponding increase in the CR flux in the past.

The strong shock waves produced by Supernova remnant (SNR) explosions are thought to be responsible for energetic CR particles in the Galaxy. Here, we show that the observed CR trend, the spectral index in the GeV-energy range, and the time dependence of the CR flux in the past can be qualitatively described by employing a simple approximation for the space-time distribution of the particles accelerated in such a shock wave [4], with the SNR parameters being conventional.

The time dependence of the CR flux and its energy spectrum at a given distance (relative to the SNR center) follow from the space-time distribution $f(t,r,p)$ of the accelerated particles. To calculate this function, the complicated set of kinetic and hydrodynamic equations has to be solved [4]. Physically, the distribution is a result of a "competition" between diffusion and convection processes which is governed by the relation between the diffusion coefficient $k(p)\cong10^{29}\,\mathbf{p}^{(0.3\text{-}0.6)}$ (TeV/c) cm^2/s for the accelerated particles and the value $\mathbf{R_0V_0}\cong10^{29}$ cm^2/s for a standard shock wave ($R_0\cong30$ pc and $V_0\cong10^4$ km/s are the radius and velocity of the shock at the beginning of the adiabatic stage of the SNR expansion, respectively).

For high-energy particles with $p>$TeV/c and $k(p)>R_0V_0$, the distribution is mainly determined by the diffusion from the shock front. For $t\gg r^2/4k(p)$, the flux $J(t,r,p>\text{TeV/c})=J_>$ decreases with increasing time; the corresponding "diffuse" trend is $dJ_>/J_>dt\cong3/2t$. Because the CR flux sharply diminishes with increasing energy, the observation of the "diffuse" trend is a very difficult problem.

The greater part of low-energy particles with $p<$TeV/c and $k(p)<\mathbf{R_0V_0}$ is

trapped by the interstellar matter behind the shock front (while a small part $<10^{-3}$ of such particles forms a narrow "prefront"), and their space-time distribution is determined by the motion (convection) of the matter. Low-energy particles (protons) with $p \cong$ GeV/c seem to be responsible for the CR trend under consideration. Therefore, if a significant negative CR trend actually exists the solar system should be inside a developing SNR shock wave.

According to the approximation the flux $J(t,r,p \cong (1 \div 10^3)\ \mathrm{GeV/c}) = J(t,r)$ is unambiguously determined by the distribution on the shock front $f_R(t,p)$ [4]:

$$J(t,r) \cong p^2\, f_R\{t_R(t,r),\, p\, r/R(t_R)\}. \qquad (1)$$

Here, $R(t)=R_0(t/t_0)^{2/5}$ is the shock wave radius, $t_0=R_0/V_0$, the function $t_R(t,r)$ is the time in the past when a given volume element (t,r) crossed the shock front. Approximately,

$t_R(t,r) \cong t_0(t_0/t)^3(r/R_0)^{10}$, when $t_R>t_0$, $t>t_0$,

$t_R(t,r) \cong t_0(t_0/t)^{6/5}(r/R_0)^4$, when $t_R<t_0$, $t>t_0$. (2)

The conventional form of $f_R(t,p \cong (1 \pm 10^3)\mathrm{GeV/c})$ is

$$f_R\{t,p\} \cong \mathrm{Norm}(t)/p^{q(t)}, \qquad (3)$$

where $q(t) \cong 4M^2(t)/\{M^2(t)-1\} \geq 4$, and $M(t)$ is the Mach number of the shock with the velocity V: $M(t)=V(t)/C_{sound}$.

The normalization factor Norm(t) cannot be found from the initial equations and has to be specified by physical reasons. There are two possible regimes of acceleration. In a linear regime, the accelerated particles do not influence on the shock development. In this case, $\mathrm{Norm}(t) \cong \eta\, N_p\, q(t) p_0^{q(t)-3}/4\pi$. Here, $N_p \cong \rho/m_p \cong 0.003$ cm^{-3} is the proton density in the interstellar matter, $p_0 \cong (1 \pm 10)$ MeV/c and $\eta \cong (10^{-2} \pm 10^{-5}$ are poorly defined parameters of injection. When the injection rate $\eta \geq 10^{-3}$, the backreaction of the accelerated particles changes significantly the shock structure, and the factor Norm stops increasing with η.

In the saturated regime, Norm is to be estimated from a normalization condition. Namely, the total kinetic energy and the pressure of all the accelerated particles must not exceed the kinetic energy E_{tot} of SNR and the total internal pressure $\rho V^2(t)$, respectively, and could amount to noticeable parts of them. The saturated regime is believed to be, as a rule, realized in nature. In what follows we assume the total pressure of accelerated particles to be of $0.25\,\rho V^2(t)$. In the GeV-energy range, it follows from this that

$$\mathrm{Norm}(t) \cong 0.003\ \{\rho V^2(t)/E_1\}\ p_1^{q(t)-3}, \qquad (4)$$

where $p_1 \cong 1$ GeV/c, $E_1=E(p_1)$ is the kinetic energy.

Equations (1)-(4) allow us to calculate the flux J(t,r) as a function of time provided the SNR parameters R_0, t_0 and the distance r are given.

We prefer to find the appropriate SNR parameters with using the available

experimental data.. We require the following conditions to be satisfied:
(a) the trend dJ/Jdt and (b) the value of the CR flux J at the time t_{obs} and the distance r (relative to the SNR center) should be equal to the observed ones;
(c) the maximum flux in the past should be less than $N \cong (2 \pm 7)$ times the currently observed flux at t_{obs}.

From these conditions, with V_0 given, the values of t_{obs}, t_0, and r (then, R_0 and E_{tot}) can be found. The calculation results for J(t,r) and the spectral index $\alpha(t)=q(t)-2$ are shown in Figs. 1 and 2 for $T=10^{-5}$, $J_{obs}(t_{obs}, p \cong GeV/c) \cong 0.1$, $(cm^2.s.ster.GeV)^{-1}$, $V_0 \cong 8000$ km/s. The solid and dashed curves correspond to two possible variants with N=3: $r(pc) \cong 73$ and 39; $t_{obs}(10^3\ yr) \cong 480$ and 120; $R_0(pc) \cong 14$ and 8.5; $t_0(10^3\ yr) \cong 1.8$ and 1; and $E_{tot}(10^{51} erg) \cong 0.3$ and 0.06, respectively. In these two cases, $\alpha(t_{obs})$ is close to 2 which differs from the observed values of 2.75. The experimental points are taken from [3] where only CR "archeological' data have been.

Instead of condition (c), the requirement $\alpha(t_{obs})=2.75$ can be used. This case is shown by chain-dotted curves; the corresponding SNR parameters are close to those prescribed for Geminga from recent observations [5]: $r(pc) \cong 102$; $t_{obs}(10^3 yr) \cong 210$; $R_0(pc) \cong 20$; $t_0(10^3 yr) \cong 2.4$; and $E_{tot}(10^{51} erg) \cong 0.74$.

Thus, all the physical conditions under consideration in the Gev-energy range, namely, negative CR trend ($\cong 10^{-5}$ 1/year), flux ($\cong 0.1/(cm^2.s.ster.GeV)$), and spectral index ($\cong 2.75$), can be satisfied under the assumption that a typical SNR exploded $2*10^5$ years ago at the distance 100 pc, while the particles are accelerated in the saturated regime.

REFERENCES

1. Yu. I. Stozhkov, P. E. Pokrevsky, and V. P. Okhlopkov, 1999, (submitted to Journal of the Geophysical Research)

2. C. P. Sonett, L. McIlargue, and P. E. Damon, 1997, Proc. of the 25th ICRC, Durban.

3. A. E. Ammosov, E. G. Berezhko, A. N. Konstantinov et al., 1991, Izvestiya AN USSR, v. 55, p. 2037.

4. E. G. Berezhko, V. K. Elshin, and L. T. Ksenofontov, 1996, JETP, v. 109, p.3.
G. F. Bignami, P. A. Caraveo, and S. Mereghetti, 1993, Nature, v. 361, p.704.

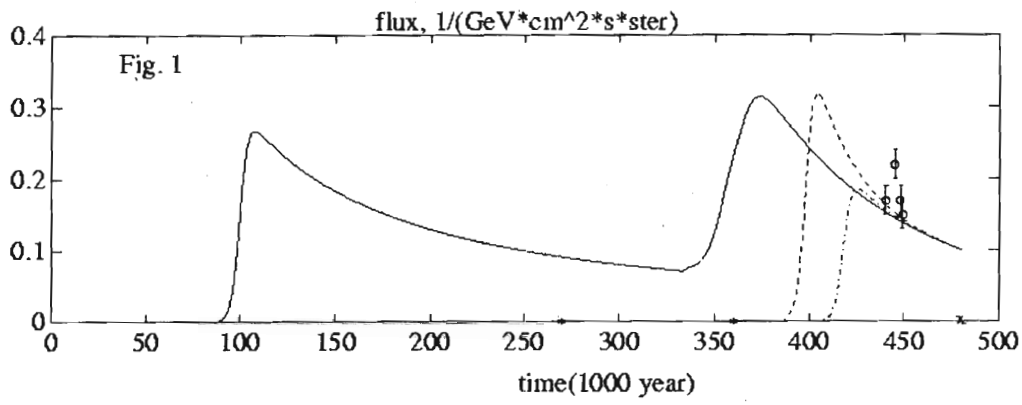

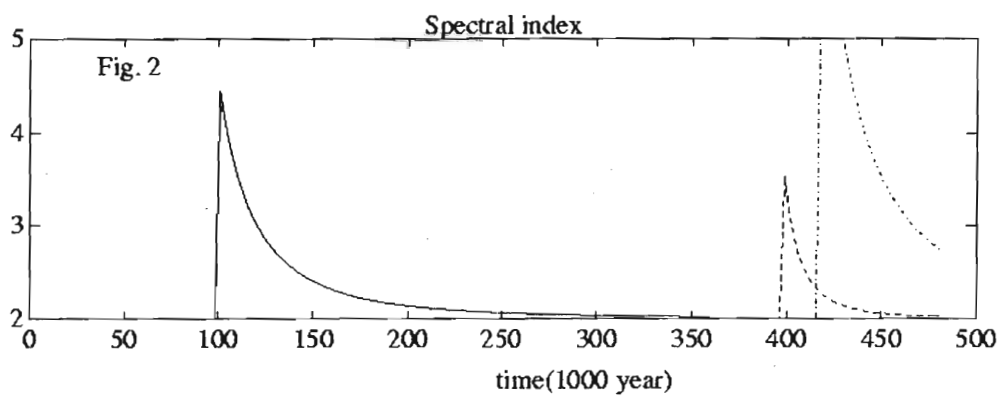

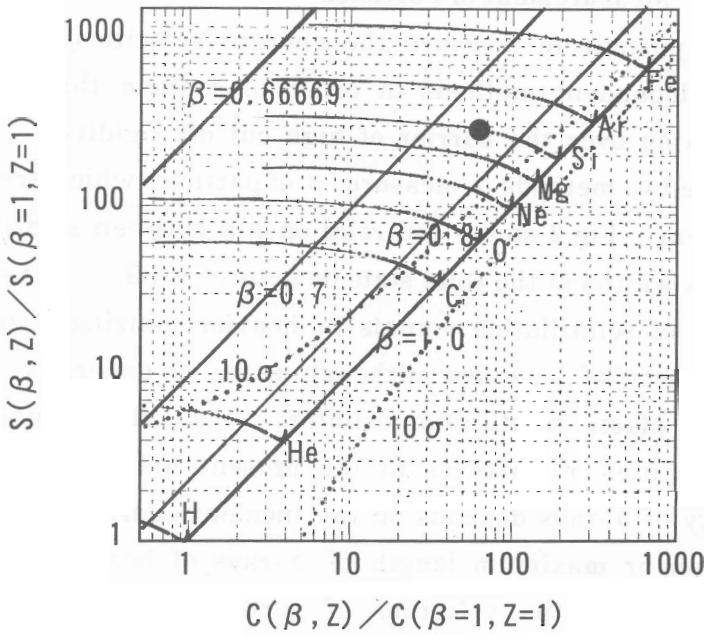

Fig.1 Relationship of Scintilation and Cherenkov Signals.
(Selection of massive candidates from normal cosmic ray particles)

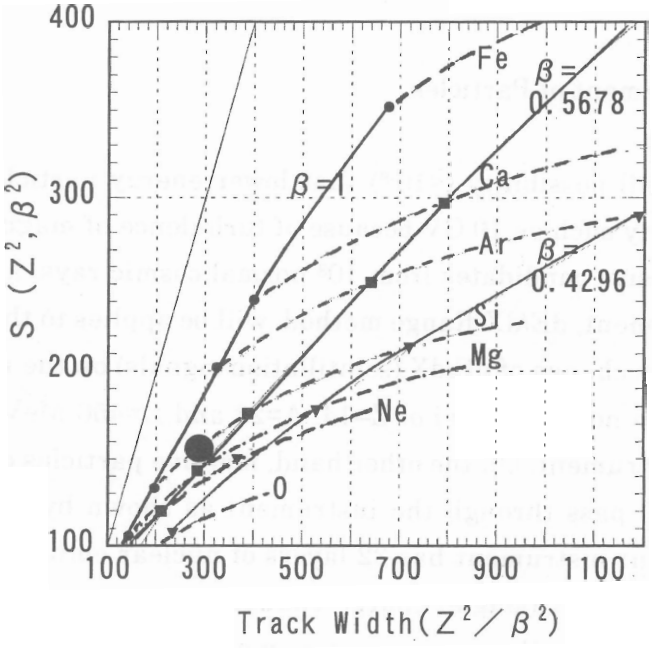

Fig.2 Saturation of Scintilation Signal
(β measuremnts of Particles.
●shows the 90's events of A/Z=370/14)

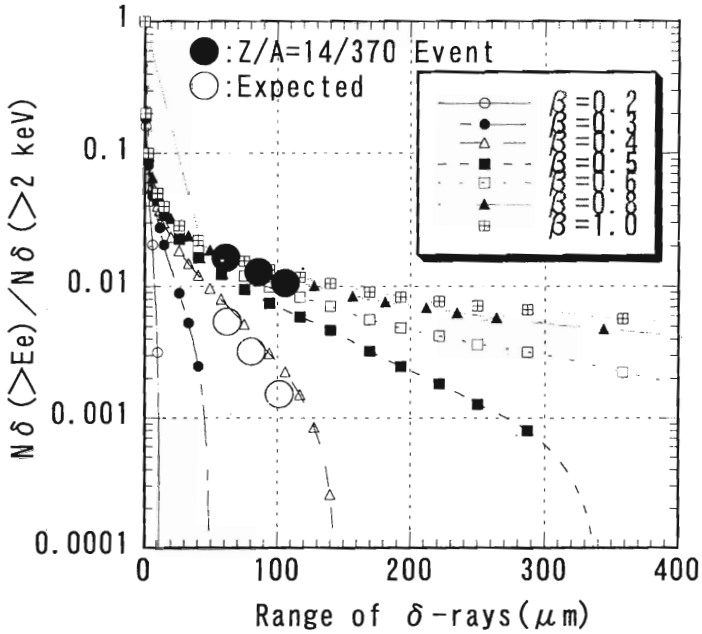

Fig.3 Distribution of δ-ray Range
(β measurement of Particles)

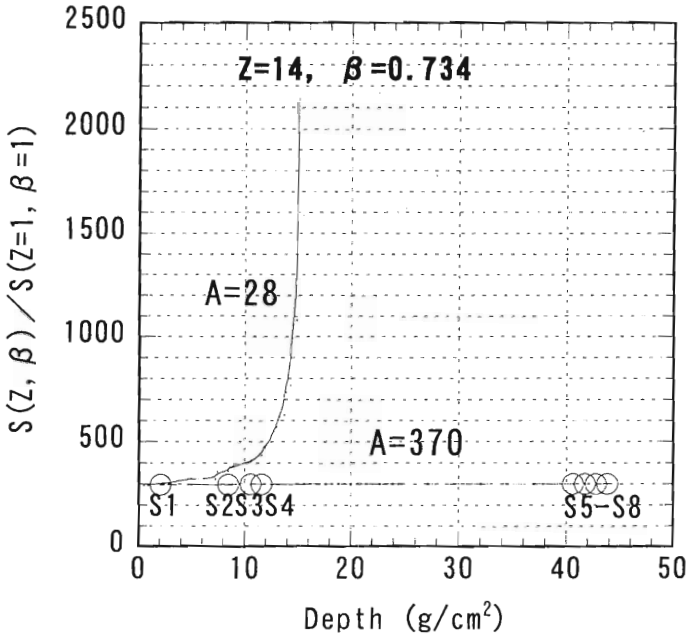

Fig.4 Mass Measurment with
dE/dX-Range Method

INCA ADVANTAGES FOR THE SOLAR NEUTRONS AND GAMMA-RAY OBSERVATIONS

G.A.Bazilevskaya
Lebedev Physical Institute, Russian Academy of Sciences

Abstract
The observational data on neutrons and gamma-rays with energies above hundreds MeV originated on the Sun are of great importance for resolving a problem of particle acceleration at astrophysical objects. At present such data are scarce. A potential of INCA for detection of energetic solar neutrons and gamma-rays is briefly discussed.

Physical problems related to solar neutrons and gamma-rays

Acceleration of charged particles in the solar flares is a manifestation of a common feature of plasma throughout a Universe and therefore is of fundamental importance. A diversity of mechanisms involved makes it extremely difficult to reconstruct a sequence of processes leading to observation nearby the Earth after powerful solar flares of charged and neutral radiation with energy up to several GeV. A significance of neutral radiation is due to the fact that contrary to charged particles it is not sensitive to the coronal and interplanetary magnetic fields and is released from the site of generation right away. That is why the observed parameters of neutral radiation serve as diagnostics of interactions between solar energetic particles and ambient solar plasma. The following information may be extracted from observations [Ramaty et al., 1988]:

time-scales of particle acceleration;
solar particle (mostly proton) energy spectrum;
number and energy content of accelerated protons;
relation of trapping and escape of the accelerated particles;
location of the interaction region;
anisotropies in electron and proton angular distribution;
abundances in solar atmosphere;
abundances in solar energetic particles.

Solar gamma-rays are generated (1) in collisions between protons with E~10-50 MeV and ambient ions (deexcitation gamma lines mainly in the range ~1 - 10 MeV); as (2) bremsstrahlung of high-energy electrons; as (3) bremsstrahlung of solar protons at E>20 MeV since at lower E contribution of electrons is much more; as (4) progenies of pions produced by solar energetic ions with E >400 MeV/n. Three latter sources would contribute to INCA observations.

Neutrons are produced in interactions with solar plasma of energetic ions with energy above ~20 MeV/n. They may escape into the interplanetary space, or may be captured on the Sun to yield 2.223 MeV gamma-ray emission. The solar neutron flux at Earth is extended in time because of velocity dispersion and is attenuated owing to neutron decay. Only ~8% of 20 MeV generated neutrons reach the Earth's orbit (and 75% for 1000 MeV neutrons). It takes 41 min for the 20 MeV neutron to travel from the Sun to the Earth, the 1000 MeV neutron will arrive in 9.523 min. The gamma-quanta will propagate with the light velocity, and arrive in 8.333 min. However, in case of time-extended emission there will be overlapping of gamma and neutron events, therefore, the selection criteria developed for separating electrons from protons in INCA will be useful here.

Current observational status

Majority of solar gamma-ray observations relates to the energy range below 100-200 MeV (spectrometers onboard spacecraft OSO7, PROGNOZ, SMM, HINOTORY, HEAO-3, YOHKOH, CGRO, GRANAT (PHEBUS), MIR (NEGA), CORONAS-I (SONG) etc.). First solar gamma-ray measurements in the range up to 2 GeV were performed by GAMMA-1 in 1990-1991 [Leikov et al., 1993; Djantemirov et al., 1995]. Only 3 events were recorded with the characteristics being different from one occasion to another. Therefore a statistics is far from enough.

Solar neutrons in the energy interval 50-100 MeV have been observed since 1980 onboard spacecraft SMM, CGRO [Chupp et al., 1982; Chupp, 1988; Debrunner et al., 1993; Ryan et al., 1993]. About 10 events with diversity of features were observed. The recording of neutrons in each event lasts from several minutes to several hours, an injection may be multiple or δ-like. The total number of the emitted neutrons with E>50 MeV ranges from $\sim 10^{28}$ to 10^{30}, the energy spectrum in the power-law form has an index from 2.4 to 3.2. The onboard neutron detectors have effective areas for neutron detection not more than 60 cm^2.

Solar neutrons with energy above 200 MeV have been observed by the ground-based instruments: standard neutron monitors [Debrunner and Lockwood, 1999], special neutron telescope network [Muraki et al., 1997] and even by the Extensive Ear Shower AKENO installation [Chiba et al., 1992], where after the flare of 4 June 1991 solar neutrons with E>10 GeV were found. The effective area of the ground-based instruments can be made large enough, however at present there is no common agreement about response function of neutron monitors for solar neutrons [Smart, 1995].

Summary of observations suggests that generation of relativistic solar particles leading to the high-energy gamma-ray and neutron production occurs only several times during an 11-year solar cycle. The need in additional observations is increased by a great diversity between individual flares. There are variety of observed time-histories but common is the occurrence of multiple episodes of gamma-ray emission (interpreted as episodes of particle acceleration). The gamma-ray observations indicate that electrons are accelerated to MeV energies in << 1 s (0.01 s is a typical value) and ions can be accelerated to GeV energy range in the order of 1 second. Theory has no difficulty with the concept of rapid particle acceleration, but there is no generally accepted dominant mechanism. More experimental data are needed to clarify the problem. One of the parameters related is an angular distribution of accelerated particles that can de investigated by study of the parent flare characteristic dependence on their distance to the center of the Sun, so called center-to-limb brightening [Vestrand, 1988]. The long-lasting gamma-ray and neutron emission may be a consequence both of long acceleration and interaction of trapped particles on the Sun. It is not known if protons and electrons are accelerated simultaneously, what is an upper energy limit for acceleration. Another question concerns a relationship between flare particles observed in the interplanetary space and those responsible for the gamma-ray and neutron emission. There are evidences that for many events they represent distinct populations of energetic particles. Only combined measurements of solar neutrons, gamma-rays and charged particles can provide an unambiguous information on complicated processes during and after the powerful solar flares. However, there are not enough well-documented solar events where gamma-ray emission and neutrons were analyzed together.

INCA advantages

Since INCA is basically a neutron monitor, it naturally provides excellent possibilities for observing solar neutrons. In addition, INCA is sensitive to gamma-radiation, which is also extremely important for high energy solar physics. INCA has a number of characteristics which make it valuable for solar observations.

- Very large effective area. For such events as 15 June 1991 thousands of neutrons would be recorded with INCA effective area at least hundred time more than that of COMPTEL

[Debrunner et al., 1993]. In the 26 March 1991 gamma-ray event a fluence of >1000 MeV gamma-emission for 10 s was 3.6 E^{-3} cm^{-2} [Rank et al., 1997]. This would result in 14 gamma-quanta recorded by INCA.

- High time resolution. It is necessary because of time-scales of processes involved.
- Possibility to estimate neutron energy spectrum via analysis of neutron penetration depth and via multiplicity analysis. This is especially important to derive absolute fluxes of the high-energy neutrons bearing in mind a controversy in response functions for neutron monitors [Smart, 1995, Debrunner and Lockwood, 1999].
- Possibility to estimate an upper energy limit. The observed flux of >10 GeV solar neutrons [Chiba et al., 1992] in event of 4 June 1991 suggests that INCA would record 2-4 n/s that makes for 20 min around 500 neutrons at E>10 GeV (with account of 20% efficiency). Therefore, more energetic neutrons, if any, would be found.
- Possibility to determine an incoming particle direction. A special mode of information acquisition may be required for solar events. A period of solar observation could be initiated by detecting of additional flux of gamma-rays incoming from the Sun's direction.
- Simultaneous observations of gamma-rays and neutrons with 100% discrimination between them. The importance of this opportunity is clear from the previous part of the paper.

First order estimation suggests that a background will be low due to the high energy threshold (only particles with E> 10^9ev will be recorded). However, a problem of a background needs a special consideration including both calculations and INCA exposition to the low-energy neutron beam.

Thus, the parameters that INCA will provide in the solar mode of observation concern (1) the real absolute flux values of neutrons with E>200 MeV and gamma-rays with E up to several GeV, (2) timing of neutron and gamma-emission, (3) energy spectra and upper energy limit of neutral radiation, (4)center-to-limb brightening.

Acknowledgement

This work was partly supported by the Russian Foundation for Basic Research, grants No. 98-02-16420 and 99-02-18222.

References

Chiba N. et al., *Astropaticle Physics*, v. 1(1), p. 27, 1992.
Chupp E.L., *Solar Physics*, v. 118(1/2), p. 137, 1988.
Chupp E.L.et al.., *Ap. J. Lett*, v. 263, p. L95, 1982.
Debrunner H. et al., *Proc. 23rd ICRC, Calgary*, v. 3, p. 115, 1993
Debrunner H. and Lockwood J.A., *Proc ISSI Workshop Cosmic Rays and Earth*, to be published in *Space Sci. Rev.*, 1999.
Djantemirov H.M. et al., *Proc. 24th ICRC, Rome*, v. 4, p. 94, 1995.
Leikov N.G., et al., *Astron. Astrophys. Suppl.* v. 97, p. 345, 1993.
Muraki Y., et al. *Proc. 25 ICRC, Durban*, v.1, p.53, 1997.
Ramaty R., Dennis B.R., and Emslie A.G., *Solar Physics*, v. 118(1/2), p. 17, 1988.
Rank G. et al. *Proc. 25 ICRC, Durban*, v.1, p.1, 1997.
Ryan J., et al. *Proc. 23rd ICRC, Calgary*, v. 3, p. 103, 1993.
Smart D.F., *Proc 24th ICRC, Invited, Rapporteurs & Highlight Papers*, p. 765, 1995
Vestrand W.T., *Solar Physics*, v.118(1/2), p. 95, 1988.

MASSIVE EXOTIC PARTICLES IN THE PCR FLUX

K.A. Kotelnikov[1], L.M.Lyamshev[2], G.I Merzon[1], N.G. Poluhina[1], N.I.Starkov[1], V.A.Tsarev[1], Saito[3], H.Sasaki[4]

1. INTRODUCTION

Existing observation data testify that 75% to 99% of the mass of the Universe is invisible. It is hidden in some non luminous objects of unknown type and until now is detectable only through its gravitational influence on luminous matter (see [1,2] for recent reviews). The problem of the "Dark matter" is one of the central problems of the modern particle physics and astrophysics. One possible explanation relates DM to various astronomical objects like brown dwarfs, cosmic strings, etc. However, in this case it is hard to reconcile the expected value of matter density with popular inflationary scenario. The other hypotheses assume DM consisting of some new particles from reach variety predicted by modern particle physics. Most of the recent efforts have been so far concentrated on the search for neutral DM candidates like neutralinos, acsions, massive neutrinos, WIMPs, etc., because it is generally believed that DM particles must interact with ordinary matter only weakly. However, another wide class of candidates which includes various kinds of massive particles interacting also electromagnetically (in some models even strongly), have been shown to be compatible with DM, if their number density is low (i.e. their masses are large)[3-11]. The expected properties of these particles, which we will denote by the common symbol X, are discussed in the next section. It is believed that the overwhelming majority of X in the Universe are very slow, but some small part might be accelerated up to high energies. Recently an evidence for such particles have been reported from an experiment with high energy cosmic rays [5]. In this proposal we will concentrate on the most abundant very slow X, and propose an acoustic method for their registration in the satellite experiment.

We would like to stress that the discovery of the stable massive charged particles, besides the great fundamental importance, would be very valuable due to possible applications to the energy production [5] (in a way, similar to the muon catalysed fusion).

2. PROPERTIES OF X-PARTICLES

For our further discussion of the X-particle detection we need to specify some properties of these particles. Here we summarise the relevant features of the X expected in the current theoretical models [3-11]. In different versions of these models X could be either new elementary particles, or lumps of quarks (known or new).

(a) *"Strangelets"* [6] are lumps of strange quark matter (SQM), which consists of approximately equal number of u, d, and s - quarks. Initially SQM has been introduced for explanation of DM. Later arguments have been presented that only very heavy lumps of SQM with masses $M > 10^{46}\ GeV/c^2$, produced in the early Universe, could survive up to the present time. The lighter lumps might evaporate due to the weak forces. But on the

[1] Lebedev Physical Institute, Russian Academy of Sciences, Moscow, Russia
[2] Acoustic Institute, Russian Academy of Sciences, Moscow, Russia
[3] Institute for Cosmic Ray Research, University of Tokyo Tanashi, Tokyo, 188 Japan
[4] Kochi University, Kochi, Japan.

other hand, some objects in the Universe could exist, where strange quark matter could be preserved up to now, or be produced in the modern epoch [6]. It is possible that this matter is permanently produced in neutron or quark stars. Collision of such objects could produce small strangelets with M about $10^3 - 10^6\ GeV/c^2$, which can reach Earth.

(b) As an extension of the SQM model to the technicolor theory, a model of technibaryon matter (TBM) was proposed in [9]. The technicolor theory in turn has been introduced in order to ensure the mechanism of spontaneous violation of the electroweak symmetry, and it is very close to the QCD, but with about three orders of magnitude larger energy scale. "Technibaryons" predicted by this theory have mass scale of the order of 1 TeV. In analogy with lumps of SQM, the stranqelets, we will call the lumps of TBM "*teChnets*". It is important to stress the difference between SQM and TBM in respect to Dark Matter. In contrast to the strangelets (with $M < 10^{46}\ GeV/c^2$), which are expected to evaporate from the early Universe, technets must survive up to the present epoch, becouse their binding energy is much higher, than the critical temperature of transition from quark-gluon plasma phase to the hadron phase.

(c) Charged massive (elementary) particles (*Champs*) were suggested as Dark Matter candidates in [11], and a special case of champs with unit positive or negative charge was analysed in details. Champs with charge number Z = +1 might exist in a form of superheavy hydrogen, while their antiparticles with Z = -1 could be bound with protons and nuclei in the form of superheavy neutrons ("neutrochamps") or superheavy isotopes.

In all these models X-particles possess some common features.

2.1. **Masses**. The mass M of the X is much larger than masses of the heaviest nuclei

$$M = A\,m \gg M_{nucl}.$$

Here A is the mass number of X and m is the proton mass.

2.2. **Charge to mass ratio**. The ratio of the charge number Z of the X-particles to its mass number A is anomalously low in comparison with the ordinary nuclei

$$Z/A \ll 1.$$

In accordance with quark bag calculations [8] it is usually assumed that Z is related to A as

$$Z = b\,(M/m_0)^{1/3}.$$

Here b is close to 1, and m_0 is the characteristic mass scale, which is different in different specific models of X-particles. For example, for strangelets $m_0 = m = 1$ GeV, while for technets [9] $m_0 = 1$ TeV.

2.3. **Energy**. It is expected that the overwhelming majority of the X are nonrelativistic, and have low, "galactic" velocity v (rotational velocity at the Earth galactic radius)

$$v/c = 10^{-3},$$

so their energy is

$$E = Mv^2/2 = A\varepsilon_0,$$

where c is the speed of light, and $\varepsilon_0 = mv^2/2 \approx 500\,eV$. (It is also possible that some of the X could be accelerated up to much larger velocities in pulsars or by shock waves from supernovas and are remained in the Galaxy during about 10^7 years similarly to the moderately relativistic cosmic ray particles. It is expected [3] that in this case they could attain the velocity up to c/3 for $M = 10^3$ GeV. However, here we will discuss only the most abundant slow X with $v/c = 10^{-3}$, which constitute the main part of DM).

2.4. **Flux**. If one assumes that the X of a given type and mass m are responsible for all Galactic Dark Matter, then their number density n depends on the mass value as n =ρ(DM)/M (wherеρ(DM) = $0.3\ GeV/cm^3$ is the energy density of the Galactic halo), and the upper limit for their flux is

$$F_m = \rho(halo)v/M2\pi ster \approx 10^4\ (TeV/M)(cm^2\ s\ 2\pi ster)^{-1}$$

The strongest experimental constraints on masses of charged DM particles resulted from experiments with gamma-detectors and cosmic ray detectors[3]. From these experiments it follows that if X are responsible for all Galactic Dark Matter, their masses must be larger than about $10^9\ GeV/c^2$. However if X constitute only a part of the total Dark Matter mass, then these limits for F and M must be correspondingly changed. In general, if X are produced in various collision and spoliation processes, we would expect some sort of mass distribution for X of the form M^{-k} [10], so in our further discussion of experimental technique we will be interesting in the ability to detect X in a wide mass range with as small A_{min} (the low limit of the mass number) as it is possible.

In our estimate of the expected flux of X we must also take into account that they can be swept out from the solar system by magnetic field of the solar wind [3]. The hyromagnetic radius of particle is

$$r_g = 2\times10^{-3}\ \beta\,(M/10\ TeV)(B/G)^{-1}\ A.U.$$

Magnetic field B in the vicinity of Earth is about $5\times10^{-5}\ G$. For $\beta = 10^{-3}$ we have

$$r_g = 0.04\ (M/10\ TeV)\ A.U.$$

while the condition of penetration into the solar system is r > 1 A.U. Thus for non accelerated and non neutralised X (i.e. not dressed by electrons or nuclei, which can neutralise their charges) with mass M < 250 TeV the solar wind will prevent them from reaching Earth. On the other hand accelerated X could easily avoid this constraints [3].

The Earth's magnetosphere could also influence the X detection depending on their rigidity R = (particle momentum)/Ze = Mv/Ze. Forβ = 10^{-3} and Z = 1 R = 10^{-3} (M/GeV)GV. Thus for M >$10^3\ GeV/c^2$ the characteristic rigidity of the singly charged X is R > 1 GV, and it is of the proper order of magnitude for penetrating the Earth's magnetosphere. For Z > 1 the constraints become stronger. But if Z = $a\ (M/GeV)^{1/3}$ with a = 1, then

$$R = Mv\ (M/GeV)^{-1/3}\ 0.1\,(M/TeV)^{2/3}$$

and the Earth's magnetic field does not prevent X with M > 30 TeV from reaching Earth.

Negatively charged X are expected to be electrically neutralised due to recombination with protons and nuclei during Big Bang, so they are not suffering from solar wind.

Interaction with ordinary matter. For our discussion of the registration of very slow X we can confine ourselves, taking into account only the most important electromagnetic interaction of the X with ordinary matter, and will neglect possible strong interactions. (We will also assume the most plausible case of positively charged X [8]). Then phenomenology of the X is determined by their electric charge Ze, mass M, and size [8]

$R = a(M/m_0)^{1/3}$;

where $a = (m_0/m)R_n$, and $R_n \approx 1$ fm

X with R < R_b ("small"), and with R > R_b ("large") interact with matter in different way (here $R_b = (me\,\alpha)^{-1} \approx 5\times10^{10}\ cm$ is the Bohr radius). Charge of the large X is

neutralised by electrons, which are inside of the X, and the interaction cross section is close to the geometric one

$$\sigma_{eff} = \pi R^2$$

Such X moving in the medium with velocity v, push out atoms by elastic and quasielastic collisions, and depositing their energy according to [11]

$$dE / dx = -\sigma \rho v^2, \qquad (1)$$

where ρ is the matter density. In this case the range L is $M/(\sigma_{eff}\ \rho)$.

Small X are surrounded by electron cloud similarly to ordinary atoms. In this case the interaction cross section is determined by the size of the electron cloud (approximately of the Bohr radius), and is much larger than the geometric cross section of the bare X. X-particles with Z of about 100 resemble the superheavy isotopes of known nuclei. For charge Z > 137 e^+e^- pairs are produced, which screen the Coulomb field of X-particle. In this case the effective charge of the X is of the order of Z_{eff} = 137, the radius of the innermost electron shell

$$r_0 = (me\, Z_{eff}\ \alpha)^{-1} = 1/me \approx 4 \times 10^{-13}\ cm,$$

and the radius of the outermost orbit is of the order of the Bohr radius. For such X the energy loss due to the Coulomb scattering on the atomic electrons and nuclei is [12]

$$\frac{1}{\rho}\frac{dE}{dx} = \frac{1}{N m m_e}\left(\frac{\pi^2}{e}\frac{z Z_{eff}}{(z^{2/3}+Z_{eff}^2)^{1/2}} + \frac{8\pi\beta}{\alpha}\frac{z Z_{eff}}{(z^{2/3}+Z_{eff}^{2/3})^{3/2}}\right) \qquad (2)$$

where N and z are the mass and charge numbers of the medium respectively. Thus for "intermediate" X with Z > 137 and R < R_b their cross section is expected to be independent of A, while for lower and higher A it is an increasing function of A (assuming the same velocity v).

3.ENERGY DEPOSITION AND BACKGROUND REJECTION

The most important problems of the X detection are the registration of their signal, and rejection of the background produced by cosmic ray nuclei.

Let us consider some element of the detector which can serve as a radiator where a particle deposits an amount of energy E_d. For further discussion it is convenient to start with a typical case of plate of scintillator, say polystyrene of thickness h=1cm. Using Equations 1 and 2 we can calculate the energy E_d deposited by the slow X in this plate. Fig.1 shows the calculated values of E_d as a function of A, assuming v/c = 10^{-3} *and* $m_0 c^2 = 1GeV$. (The results can be easily rescaled for other values of v and m_0).

It is seen that the energy released by the X with A > 10^4 *is* E_d> 5 MeV, so the signal from such X can be detected in principle rather easily using the usual nuclear-physical technique. However, there is a problem with separation of this signal from that produced by the cosmic ray nuclei, especially the heaviest one, uranium-238. The energy released by this nucleus in the same plate is shown in Fig.2 as a function of the nucleus energy E^U. These values have been obtained by numerical calculations, using interpolation of the tables for protons, and the algorithm of calculation for nuclei from [13]. One can see that there is some limiting energy $E_{d,max}$= 40 GeV, which can be deposited by uranium nucleus in such a plate. It means, that using 1 cm plate of polystyrene as a radiator, we can distinguish the signals from X and nuclei for $A > A_{min} = 15\times10^8$, or $E > E_{d,max}$,

which correspond to 1 cm range of the X in polystyrene.

Note, that the decreasing of A_{min} can be reached by the rough estimation of the particle speed because that is different for TM-particles ($\beta \approx 10^{-3}$) and relativistic nuclei of cosmic ray ($\beta \approx 1$). For example the the placing of second plate on a distanse about 1 m from first one and a measurement of a particle time of flight between them can help to distinguish these two type of particles.

In fact, there is a certain limiting on value A_{min} that is determined on the basis of other requirements. These are: (a) the energy threshold of detection Eth, which is a characteristic of the method used; (b) background conditions that also depend on the detection method; and (c) certain technological limitations.

Scintillation and semiconductor detectors, that are traditional and widely used in experimental nuclear physics, have a low Eth and are, at first sight, the most adequate for solving the problem under consideration. Indeed, thin scintillating or semiconductor layers can be obtained without any technological difficulties, and methods of data acquisition and processing for these detectors are also well developed. However, both the methods have a serious disadvantage preventing identification of particles with a high energy release. The fact is that scintillation and semiconductor detectors exhibit the nonlinear response associated, in the first turn, with quenching scintillations in a scintillator or recombinating charge carriers in a semiconductor in the case of a high energy release. For example, the saturation of the output signal in organic scintillators occurs at a specific ionization energy loss on the order of 10 GeV/cm [14].

Thus, all heavily ionizing particles, independently of their nature, produce equal saturation signals that makes identification impossible. A similar situation takes place also for semiconductor detectors [15]. Thus, both scintillation and semiconductor detectors turn out to be unsuitable for separation of dark-matter particles against the background of cosmic-ray nuclei.

Track detectors based on condensed materials such as nuclear photoemulsions and film detectors (e.g., CR-39) should also be rejected due to inconveniences associated with necessity of their dismounting in space, transportation to the Earth, and long-time analysis off line.

Among gas detectors suitable for measurement of high ionization densities produced by DM particles, the most adequate is a pulse ionization chamber that has the linear response for the energy release up to about 10^{12} eV due to absence of space-charge effects inherent in proportional and other gas-discharge etectors. However, to overcome difficulties associated with development of such ionization chambers (a problem of a thin input window, a necessity to support stable gas pressure and composition for compensation of diffusion through the walls, etc.), special investigations are required. A part of these difficulties could be avoided by using arrays of thin-wall cylindrical ionization chambers instead of plane ones. To solve this problem, additional studying the long-term stability of pulse ionization chambers of various types is required in conditions approaching the space ones.

Thus, scintillation, semiconductor, and gas-discharge detectors can be used for detection of DM particles, whereas only pulse gas ionization chambers (under condition of their long-time operation stability) are suitable for identification of DM particles by the energy release in gas.

An important problem that defines efficiency of a chosen experimental method is the detector area. For investigating the low-intensity flux of DM massive particles, a method should be preferred that allows detectors of a high area to be produced and exploited. As is seen, in the case of satellite experiments, the methods indicated above become rather cumbersome and expensive.

As we show in the next section, methods of the radiation acoustics can be succesfully used for detecting DM massive charged particles. (This idea is similar to the proposal [6] to record seismic signals generated by nucleorites in the Earth's core). We may hope that the use of the modern technology of production of acoustical tranducers can make it possible to construct a light and inexpensive large-area detector of DM particles for space experiments.

4. EVALUATION OF THE ACOUSTIC SIGNAL

Let us now discuss the acoustic detection of X.From Fig.1 one can see that the energy loss DE of X for large mass becomes macroscopic, and it could produce sizeable acoustic signal. For rough estimate of this signal we can assume that the loss of the energy is distributed uniformly along the particle's track, and it has Gaussian distribution in the plane normal to the track $\propto \exp(-r^2/a^2)$, where a is the size of the region of the effective energy release. The energy released by particles in the radiator is transformed into heat, kinetic energy of the products, and acoustic waves. For the beginning we can assume that the particles incident normally to the radiator plane, and the acoustic signal propagates in the semi-infinite space without attenuation. Then we have the following equation for the pulse amplitude (the acoustic pressure) at the distance R from the track [16]

$$P = \frac{b\,\Delta E(erg)}{R(cm)\,a^2(cm)}\,Pa,$$

where b=8×10^{-4} for 1 cm plate of the polystyrene.

The possibility of reliable registration of the acoustic signal from the beam of high energy charged particles has been demonstrated in many experiments (see, for example, [16,17]), but the acoustic registration of single particles (which is close to our case of interest) was studied much less [16]. The characteristic frequency of the acoustic pulse ν_{max} is related to the size of the region of the energy release as

$$\nu_{max} = c_0/2a,$$

where c_0 is the speed of sound. For particle beams the value of a is equal to the beam transverse dimension and is typically a = 0.1 - 1 cm. For separate particle the value of a is related to the average range of delta-electrons a = 10^{-6} cm. Thus ν_{max} is about 10^5-10^6 Hz for beams, and is about 10^{11} Hz for separate particles. This 5-6 orders of magnitude difference (besides the lower value of the signal) makes the registration of the acoustic signal from single particles more complicated due to the sound absorption and need in more complex apparatus for detection in the higher frequency region.

In order to evaluate the possibility of reliable registration of the acoustic signal from DM particles we must compare this signal with the noise level, and take into account the attenuation of the signal due to its propagation. The width of the signal is of the order of magnitude

$$\Delta\nu = c_0/a \approx 10^{11}\ s^{-1},$$

and we can assume for simplicity its uniform distribution

$$dE/d\nu \approx \Delta E/\nu_{max} \approx const$$

This simplification results in some underestimate of the signal, because real amplitude of the signal is weakly increasing function of the signal frequency.

The lower boundary of the useful frequency band can be chosen rather arbitrary at the level of about $\nu_{min} \approx 10^4\ Hz$. (For installation on the ISSA one needs to take care

also of vibration noise due to the station functioning. This technical problem could be solved using specially isolation, and we will not discuss this problem here).

The upper boundary for the sensor sensitivity region can be chosen from the reasonable value of the signal to background level. The main source of the high frequency background in the experiments on satellites or on the orbital station is expected from the thermal noise of the apparatus. For longitudinal waves its value can be estimated from equation [13]

$$P_n = (< p^2 >)^{1/2} = \sqrt{\frac{4\pi kT}{3c_0}\rho(v_{max}^3 - v_{min}^3)}$$

For our estimate of the dumping we use the value 2 dB/cm for 4 MHz for polystyrene [18]. The values of the dumping coefficient for other frequencies can be estimated assuming its v^2 dependence.

Fig. 3 shows the results of our calculations of the acoustic pressure as a function of the upper limit v_{max} of the sensor's sensitivity region. Curve 1 shows the signal in the polystyrene at 20 cm distance from track of X (energy deposited by X is 100 GeV and its mass M = 5×10^8 GeV). Curve 3 corresponds to thermal noise level. This results have been calculated assuming propagation of the signal in the semi-infinite medium. In a real experiment the signal will be generated and will propagate in the plate of the radiator of thickness h which in general case is much less than the distance R from the track to the sensor . We can calculate the signal for this "wave guide" case, using results of Ref.[16]. In this case the frequency band is determined by the plate thickness h, but not the value of a:

$$\Delta v = c_o / h \approx 10^6 - 10^7 \ Hz$$

The results of the calculation for the plates of 1 cm thickness are shown in Fig.3 by solid curves. It is seen that these results are close to that for the semi-infinite case. In both cases the signal from the X exceeds the expected level of the thermal noise.

The values of the acoustic signal for this case exceed 50 and 100 Pa for v_{max} 10^6 *and* 10^7 *Hz* correspondingly. This value of the acoustic signal can be easily detected by modern acoustic sensors. In particular, the signal can be detected by means of piezo-receiver with the active elements made of piezopolymeric films on the base of polyvyniledenftoride [19].

Polymeric films based on polyvinylidene ftoride have piezoelectric properties and are widely used for development of piezoelectric detectors and dynamical-deformation tranducers [19]. The sensitive element of such a tranducer contains a folded piezoelectric film with the even number of layers. The area of each layer is (5÷10) mm x (5÷10) mm and the total thickness of the element is several tens of microns depending on the numbers of the layers. Output electric signals are taken by a coaxial cable with its screen connected to the electrode at the outer surface of the sensitive element, whereas the central wire is in contact with the internal electrode. The film layers are glued with each other by an adhesive based on epoxy resin of the cold hardening. The tranducer sensitive element is covered by a non-metallized polymeric foil for hermetization. The hermetized tranducer with the cable is glued to the surface of the plate whose dynamical deformations must be measured. The sensitivity of the piezoelectric detector can attain 10 μV/Pa depending on its design and a type of the polymeric film. It is worth mentioning that the detector sensitivity decreases in the high-frequency region (for frequences exceeding 10^5--10^6 Hz). However, in principle, a detector design is feasible for which the frequency upper boundary can be increased by the order of magnitude.

Estimates show that the detectors with an area of 1 cm x 1 cm and the thickness of 10 μm are able to record a signal induced by a DM particle of the mass within the range A

$> 3.10^7$ under consideration. These detectors could be installed on solar batteries of satellites or on the outer walls of a space station (e.g., the ALPHA International Space Station) providing the required large effective detection area.

Dealing with the acoustical method of detecting X particles, we must bear in mind one more source of background events associated with impacts of space dust particles incident onto the detector.

The dust or meteorite substance produced mainly by comets forms a dust shell around the Earth, which consists of particles with masses of 10^{17} -- 10^{-3} g. The velocities of such particles with respect to the Earth do not exceed 70 km/s, and their flux density at distances of 200--1000 km to the Earth surface (as an example, for $m < 10$g) obeys the power law [21]:

$$N\,[m^{-2}\,s^{-1}\,(2\pi\ sr)^{-1}] = 10^{12}(m/1\ g)E^{0.8}.$$

Generation of acoustical pulses by impacts of meteorites occurs through not the thermoacoustical mechanism (as is the case for X particles and atomic nuclei) but rather through dynamical mechanism. The dissimilarity in acoustical pulses corresponding to these mechanisms could be used for rejection of the space dust background. Another feasible method for such a rejection consists of detecting signals produced as a result of electromagnetic interactions of X particles (e.g., scintillations in a scintillating radiator), which are absent in the case of neutral dust particles.

However, the simplest method to suppress the acoustical background caused by dust particles would consist of using a screen or a shell capable of damping these particles. For example, in the case of the aluminum shell with a thickness of δ μm, the number of shell damages per unit area per second for a detector remoted by 200--500 km from the Earth's surface would be equal to [21]

$$N[m^{-2}s^{-1}(2\pi\ sr)^{-1}] = 3.6\cdot 10^{-8}\,\delta^{-0.94} \text{ for } 250 > \delta > 10\,\mu m$$
$$= 1.8\cdot 10^{-11}\,\delta^{-3} \text{ for } \delta > 250\,\mu m.$$

This implies that, for example, in the aluminum shell 1 mm thick, no more than one damage could arise per 3 m^2 of the shell area during the annual irradiation. This value is substantially lower than the expected number of detected X particles that is assumed in our proposal.

For detection of X particles, it is reasonable to use several layers of acoustical radiators because, in contrast to the space dust, DM particles of a large mass can easily penetrate through considerable depths of matter. For example, X particles with the mass number $A > 10^9$ are capable of penetrating four polystyrene plates each 1 cm thick. This fact can be used for detecting signals generated in several plates by these particles to obtain their additional unique signature.

In both cases, we should, of course, bare in mind that the energy loss accompanying the penetration of a particle through the additional layers of matter (a shell or several radiator plates) will lead to a certain increase in Amin. For example, the use of an aluminum shell 1 mm thick will result in the constraint $A_{min} \geq 0.5\,10^7$.

REFERENCES

1. V. Trimble, "Dark matter in the Universe: where, what and why?", Contemp. Phys. 1988, v. 29, p. 373-392.

2. V. Trimble, in "Dark Matter", 1995, eds. S.S. Holt, C.L. Bennett, New York: AIP, p. 57.
3. . S. Dimopoulos et al., "Getting a charge out dark matter", Phys. Rev. 1990, v. D41, p. 2388-2397.
4. B.L. Joffe, L.B. Okun, M.A. Shifman, M.B. Voloshin, "The heavy stable particles and could catalysis of nuclear synthesis", Acta Phys. Polonica 1981, v. B12, p. 229-235.
5. T. Saito et al., "Is there Strange-Quark matter in Galactic Cosmic Rays?", Phys. Rev. Lett. 1990, v. 65, p. 2094-2097.
6. E. Witten, "Cosmic separation of phases", Phys. Rev. 1984, v. D30, p. 272-285; A. de Rujula, S.L. Glashow, "Nuclearites - a novel form of cosmic radiation", Nature 1984, v. 312, p. 734-737.
7. C. Alkock, E. Farhi, "Evaporation of strange matter in the Universe", Phys. Rev. 1985, v. D32, p. 1273-1279; J. Madson et al., "Does strange matter evaporate in the early Universe?", Phys. Rev. 1986, v. D34, p. 2947-2955.
8. E. Farhi, R.L. Jaffe, "Strange matter", Phys. Rev. 1984, v. D30, p. 2379-2390.
9. J.A. Frieman, G.F. Giudice, "Cosmic technicolor nuggets", Nucl. Phys. 1991, v. B355, p. 162-191.
10. T. Saito, "Abundance and sources of strange quark matter", ICRR-Report-265-92-3, Preprint of Institute for Cosmic ray research of University of Tokyo, 1992, p. 1-9.
11. A. de Rujula, S.L. Glashow, Uri Sarid, "Charged dark matter", CERN-TH-5490/89, Preprint CERN, 1989, 1-24.
12. J. Lindhard, M. Scharf, "Energy dissipation by ions in the kev region", Phys. Rev. 1961, v. 124, p. 128-130.
13. Atomic Data and Nuclear Data Tables 1982, v. 27, □ 2/3.
14. J.B. Birks, "The Theory and Practice of Scintillation County", Oxford, Pergamon, 1964.
15. G. Dearnaley, D.C. Northrop, "Semiconductor Counters for Nuclear Radiation", London, E.&F.N. Spon Ltd, 1964.
16. Radiatsionnaya akustika (Radiation Acoustics), L.M. Lyamshev Ed., Moscow: Nauka, 1987; L.M. Lyamshev, Radiatsionnaya akustika (Radiation Acoustics), Moscow: Fizmatlit-Nauka, 1996.
17. Tsarev V.A. and Chechin V.A., Dal'nie neitrino. Fizicheskie osnovy i geofizicheskie primeneniya (Long-Baseline Neutrinos. Physical Principles and Geophysical Application), Fiz. Atom Yadra i Elem. Chast., 1986, vol. 17, p. 389.
18. Mason W, Piezoelectric Crystals and Their Application to Ultrasonics, New York, 1950.
19. Belova M.V., Gollmina I.P., and Pastorguev D.L., Piezoelectric Polimeric Strain Detectors, Prib. Tekh. Eksp., 1988, no. 6, pp. 160--163.
20. Ovchinnikov O.B., Pashin A.E., Puchenkov O.V., and Rastorguev D.L., On the Problem of Recording of Space-and-Time Characteristics of Short Acoustical Pulses Excited by the Optical Radiation of the Visible Spectral Range, Akust. Zhurn., 1987, vol. 33, no. 2, p. 312.
21. Veshchestvo meteornoe (Meteorite Substance), GOST 25645.128-85.

FIGURE CAPTIONS

Fig. 1. Energy loss E of DM particles in 1-cm polystyrene plate as a function of the mass number A. Curves correspond to (I) stopping DM particles and to regions of (II) small, (III) intermediate, and (IV) large DM-particle masses.

Fig. 2. Energy loss ΔE^U of a U^{238} nucleus in a polystyrene plate 1 cm of thickness as a function of the uranium nucleus energy E^U and the plate thickness h.

Fig. 3. Acoustical pressure P induced by DM particles when passing through a polysterene plate 1 cm thick at a distance of 20 cm to the point of incidence vs. the upper boundary ν_{max} of the acoustical detector sensitivity. Curves 1, 2, and 3 correspond to semiinfinite space, thin plate, and thermal-noise level, respectively.

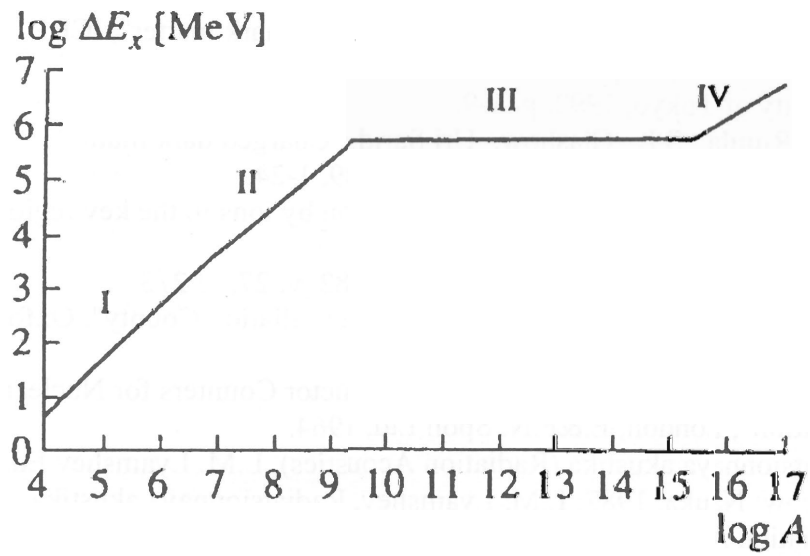

Fig. 1. (a) Dependence of energy losses ΔE of DM particles in a 1-cm thick polystyrene plate on the mass number A. (I) The area of capture of DM particles. (II) The range of small masses of DM particles. (III) the range of medium masses. (IV) The range of large masses of DM particles.

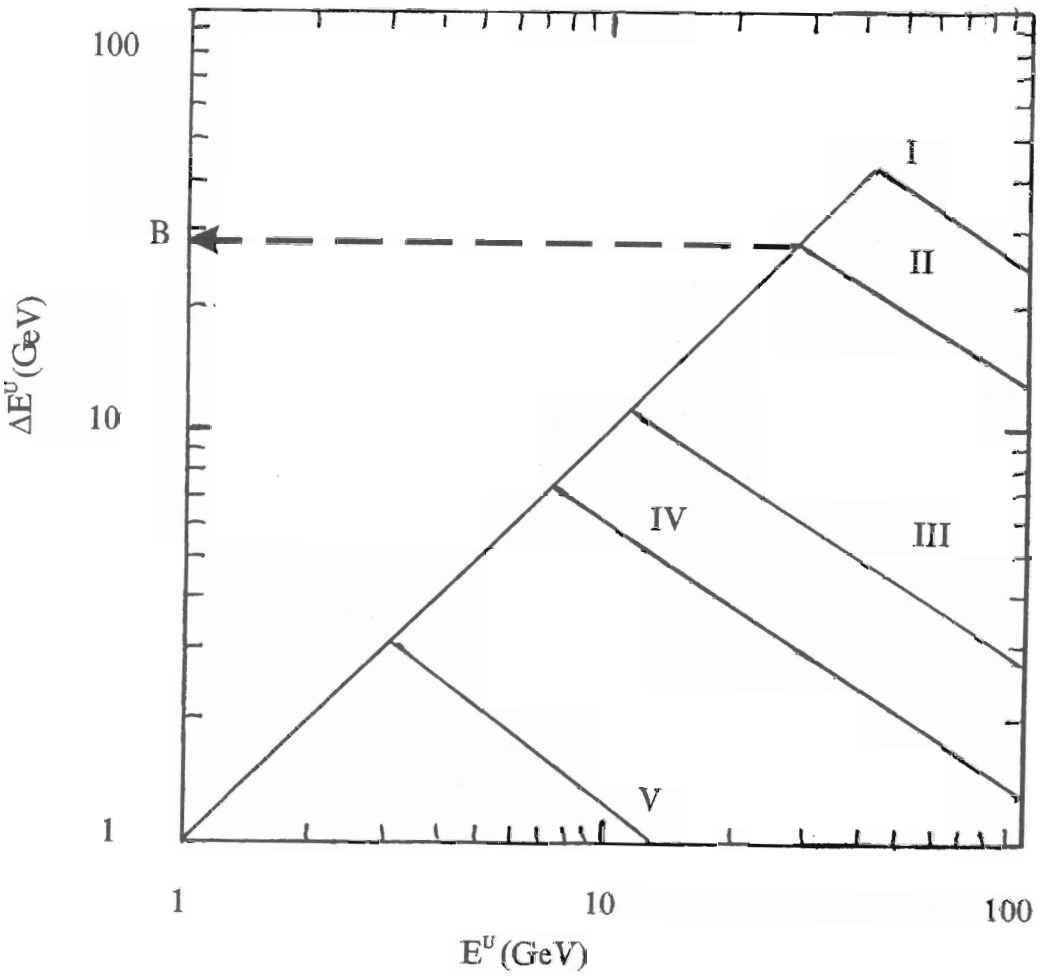

Figure 2.

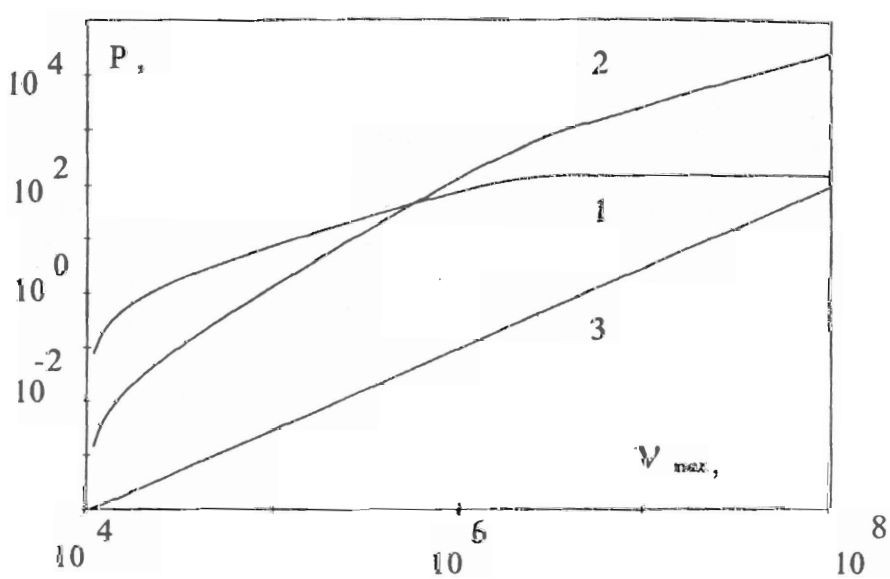

Figure 3.

The concept of an Ionization - Neutron Calorimeter

Chubenko A.P.

P.N.Lebedev Physical Institute, Russia Academy of Sciences, Moscow

Preceding experiments aimed at solving the most urgent problems in cosmic ray physics have revealed a necessity of high-aperture space instruments, capable of obtaining unambiguous information by direct methods. All these problems could be solved on the basis of the proposed INCA experiment exploiting several novel experimental ideas:

(I) A concept of an ionization-neutron calorimeter [1] for measuring particle energies, mass numbers, and separating PCR electrons and protons;

(II) A silicon detector on the basis of matrix bipolar structures [2]. for measuring primary-particle charges, spatial coordinates, energy released in cascade showers, and particle's time of flight;

(III) An acoustical detector (as a possible option) for detection of massive exotic particles [3].

Fig. 1 presents of energy spectra of various primary cosmic-ray componenets.

To perform a program of direct PCR studies, we need an experimental setup possessing the following properties:

– Geometry close to 4π;
– Geometry factor of 10–30 m^2 ster;
– Mass of not larger than 10–12 t;
– Coordinate measurement accuracy on the order of 1 mm;
– Energy measurement accuracy of about 20%;
– Particle charge measurement accuracy of about 20%;
– A negligible reverse-current effect;
– Hadron/electron rejection factor not less than 10^{-5};

To satisfy these requirements and provide an acceptable measurement accuracy for particle energy, charge and nature, we suggested recently to use a experimental setup of a new type called an ionization neutron calorimeter (INCA).

As is well known, the concept of an ionization calorimeter (ICA), proposed more than forty years ago [4] for measuring energies of cosmic-ray particles, is also used presently in accelerator experiments [5,6]. The principles of ICA are based on measuring total ionization produced as a result of cascade multiplication of secondary charged particles generated by a high- energy projectile in its interactions with matter.

Another method of particle energy determination, which is based on detection of evaporated neutrons produced in nuclear disintegrations under the action of cascade particles was also proposed more than thirty years ago [7]. This method is now used, e.g., for analyzing data obtained in the world net of neutron monitors [8]. However, total-absorption neutron calorimeters (NCA), in spite of their suggested application [9], are almost not in use up to now.

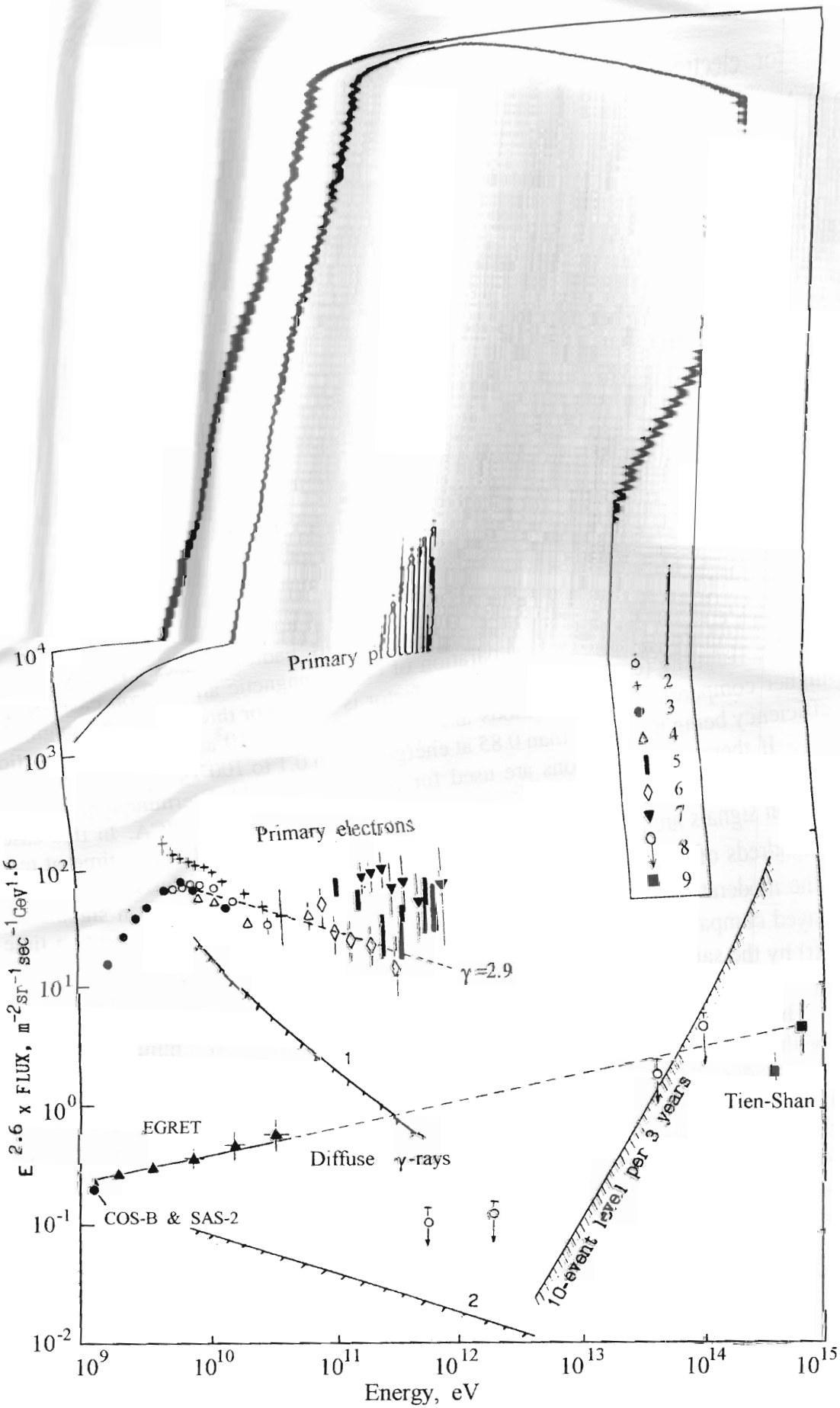

Fig. 1. Energy spectrum of primary protons, electrons, and diffuse γ-rays in the upper

electromagnetic cascades compared to hadronic ones. This yields an additional rejection factor for separation of electromagnetic and hadron cascades, so that the resulting (e, gamma)/p rejection factor is by two or three orders of magnitude higher compared to other methods and can attain 10^6 to 10^7, the electron detection efficiency being not lower than 0.85 at energies from 0.1 to 100 TeV.

If thermalized neutrons are used for the neutron yield determination, then the INCA design almost does not differ from that of a conventional ICA. In this case, neutron signals are delayed with respect to the ionization signal, because time of tens or hundreds of microseconds is required for thermalization and diffusion of neutrons in the moderating substance before they are detected. Therefore, neutron signals are delayed compared to ionization one and can be recorded (with a corresponding time shift) by the same detectors, e.g., gas proportional neutron counters filled with ^3He or BF_3.

It is important that the INCA's absorber is mainly a light substance (e.g., polyethylene) interlayered by thin plates of a heavy absorber. At a minimum weight, this provides the maximum geometry factor, the maximum absorber thickness in terms of nuclear-interaction lengths, and a reduced (according to the transition effect) effective radiation length for the development of electromagnetic cascades. Its principles were recently tested while exposing to high-energy hadron and electron beams at accelerators of the Institute for High-Energy Physics and Lebedev Physical Institute [11, 12].

Thus, INCA combines a high capability of identifying particles of electromagnetic and hadronic nature, a reliable separating of groups of nuclei, a good accuracy of energy measurements, and a relatively modest weight. INCA of the mass of 4 to 12 t installed on board of a dedicated satellite or an international space station is able to solve the "knee" problem during the 3-year orbiting. However, the problem of electron spectrum at high energies could be solved by an INCA with a mass of 0.5 to 1 t during a short 10 -day flight of a high-altitude balloon.

Thus, we show that an INCA supplemented with a charge detector and

NEUTRON PRODUCTION IN NUCLEAR AND ELECTROMAGNETIC CASCADES GENERATED BY MUONS IN UNDERGROUND EXPERIMENTS

Ryazhskaya O.G.
Institute for Nuclear Research, Russian Academy of Sciences, Moscow

In this report, we consider basic process leading to generation of neutrons in showers caused by cosmic- ray particles of super-high energies.

Nuclear-active particles are produced in nuclear showers as a result of ion-nucleus and nucleon-nucleus interactions and in electromagnetic showers due to photonuclear reactions.

In the inelastic interaction of a muon, in the case of a high energy transferred, the multiple production of hadrons $\pi^{\pm}$, π°, $K^{\pm}$, K°, n, and p, and development of a nuclear shower occur. In nuclear showers, hadrons, depending on their energy, can be arbitrarily separated into three groups: shower hadrons ($\beta > 0.7$), cascade hadrons ($\beta = 0.2 - 0.7$), and evaporation nucleons ($\beta < 0.2$). Shower $\pi^{\pm}$ mesons produce new generations of particles until particles with $\beta > 0.7$ are no longer produced. Cascade hadrons in collision with nuclei produce -cascade particles of lower energies and evaporation nucleons. The average multiplicity of cascade and evaporation particles per collision is practically constant for incident-particle energies $E \geq 20$ GeV. The shower particles move mainly in the direction of primary hadrons. Cascade nucleons and pions have a rather broad angular distribution, but still are sensitive to the direction of a primary particle. Evaporation nucleons are emitted isotropically.

Cascade neutrons are capable of further multiplication in nuclear reactions, while cascade protons rapidly lose their energy for ionization. An additional mechanism of neutron production is the capture of a slow π^{-} mesons by a nuclei. Slow π^{+} mesons produce in their decay slow muons, which in turn decay into positrons. The number of slow $\pi^{\pm}$ mesons among cascade particles depends on the number of interactions of shower particles with nuclei.

The basic process in which neutrons and pions are generated in electromagnetic showers is photoproduction on nuclei of the medium. Preferentially, evaporative and cascade particles are produced in photonuclear reactions. The main contribution to the cross section for γ-ray interaction of with production of neutrons is from the (γ,n) reaction, which has a giant resonance. In addition, it is necessary to take into account multiple photoproduction reactions (γ,in). As a result of the fact that the energy spectrum of shower photons falls off as $dE_{\gamma}/E_{\gamma}^{2}$, neutrons in electromagnetic showers are generated primarily by low-energy photons.

However, there are channels of neutron photo-production by γ rays of higher energies, primarily as a result of inelastic charge-exchange reactions

$$\gamma + p \rightarrow n + \pi^{+}, \qquad (1)$$

$$\gamma + A \rightarrow (A-1) + n + \pi^{+} \qquad (2)$$

and secondarily, as a result of two-step reactions such as

$$\gamma + A \rightarrow A + \pi^{+} \pi^{-}$$

$$\pi^{-} + A \rightarrow (A-1) + n. \qquad (3)$$

Pions are produced in photoproduction reactions $(\gamma, i\pi^{+}\pi^{-})$ and also in charge-

exchange reactions $\gamma+p\rightarrow n+\pi^{+}$, $\gamma+n\rightarrow p+\pi^{-}$.

Neutrons are also produced in capture of a slow π^{-} meson by a nucleus of matter. This effect leads to an increase of the multiplicity of neutrons.

The dependence of the average multiplicity of neutrons and π mesons in electromagnetic showers on the shower energy E_s, is satisfactorily approximated by a linear function $\overline{N}^{e.m}_{n,\pi} = A\cdot E_s^{1.0}$. If we take into account, that in the interaction of a high-energy shower photon high-energy π mesons can be produced which are less capable of producing nuclear cascades, then the dependence $\overline{N}^{e.m}_{n,\pi} = f(E_s)$ changes to $\overline{N}^{e.m}_{n,\pi} = A\cdot E_s^{1.05}$.

The underground study of hadrons was carried out in the 100-metric-ton scintillation detector at the Artemovsk Scientific Station of the Nuclear Research Institute and in the LVD detector. As a result of the low natural radioactivity of the environment and of the construction materials, for detection of neutrons it turned out to be possible to use the reaction of neutron capture in hydrogen

$$n+p \rightarrow d+\gamma \qquad (4)$$

A neutron produced in the scintillator is decelerated colliding with carbon and hydrogen nuclei to thermal energies, diffuses, and is captured by a hydrogen nucleus, forming an excited deuterium nucleus. The excitation is removed by γ ray radiation with the energy of 2.23 MeV. The average time of neutron capture in the scintillator of the C_nH_{2n+2} type is about 170 μsec. The detection of single neutrons with a high efficiency is possible as a result of the low counting rate of background pulses. The neutron-detection efficiency averaged over the entire detector is (84 ± 3) %, and the efficiency averaged over the inner volume of the detector, at a distance about of 57 cm away from the walls, is (92 ± 3)%.

The spectra of detected neutrons are presented in Fig. 1 and 2.

The high efficiency of the neutron detection and the calorimetric nature of our detector provides the possibility of studying not only the dependence of the average number of neutrons in a shower on the energy, but also the distribution of the showers in the number of neutrons. However, for this purpose, it is necessary to have good separation of electromagnetic and nuclear showers generated by muons. Although the average numbers of neutrons for electromagnetic and nuclear cascades of the same energy differ significantly, as a result of fluctuations of the number of neutrons in the showers of the two types an answer to the question of the true dependence of the average number of neutrons on the energy and also the question of the distribution of showers in the number of neutrons can only be given by experiment.

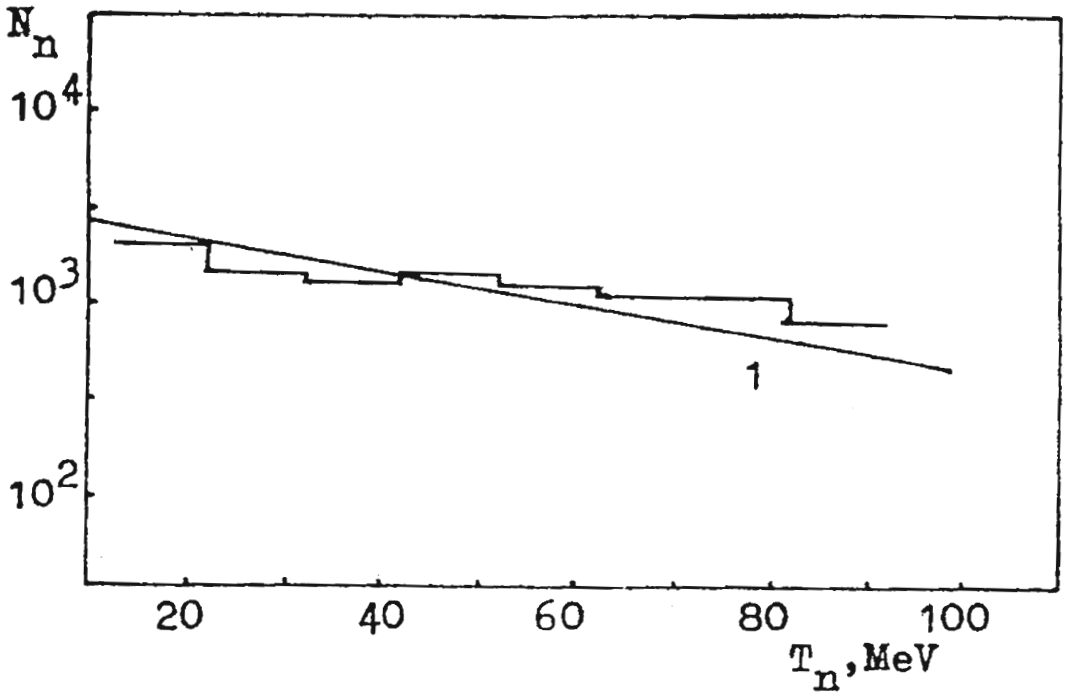

Fig. 1 Energy spectrum of underground neutrons. Histogram - Artemovsk detector data and solid curve correspond to calculated spectrum.

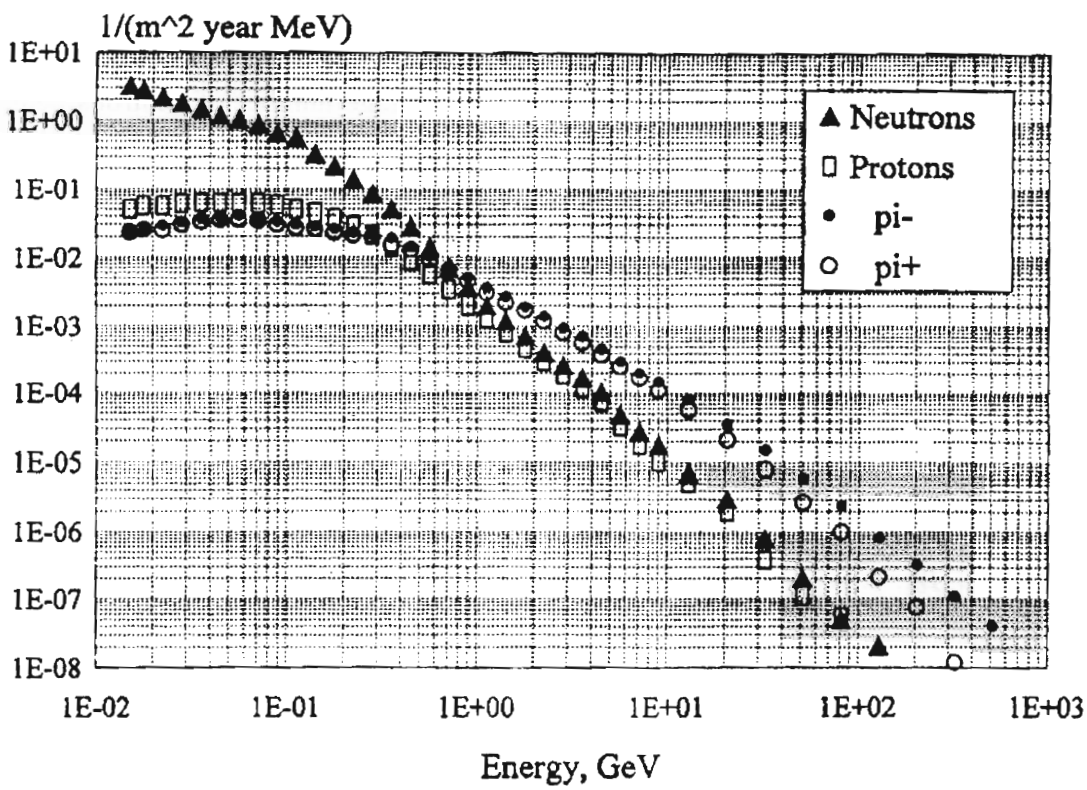

Fig.2. Spectra of particles going into LVD experimental hall from the rock.

3 Results

3.1 Cascade energy determination by ionization signal Potentialities of the INCA in measuring energies of various PCR nuclei of the same energy depends first on dispersion in cascade particle number at a given energy. Figure 1 demonstrates the dependence of the $\sigma(n_{ch})/\langle n_{ch}\rangle$ ratio for the charged particle component integrated over the length of cascades initiated by (a) 10-TeV and (b) 1-PeV primary nuclei on cascade length.

As is seen from Fig. 1, the relative accuracy of energy measurements is low at the initial stage of cascades. However, the standard deviation attains a reasonable value ($\sim$ 30% for protons and less for nuclei), when the device thickness used for energy determination relates to the cascade maximum ($\sim 200 - 250$ g/cm^2 within the energy range under consideration). Simulations show that the use of initial cascade stage decreases the accuracy. Thus, it seems to be reasonable to use for energy determination mainly the close-to-maximum cascade part.

3.2 Cascade energy determination by neutron signal It is very important that the total amplitude of the evaporated-neutron signal can also serve as an additional information on the primary particle energy. As is seen from Fig. 2, the energy dependence of the total cascade evaporated-neutron number $\langle n^{tot}_{neut}\rangle$ integrated over various values of the INCA thickness initiated by protons is linear in the doubly logarithmic scale in a wide energy range. Nuclei demonstrate a similar behavior.

It should be noted that the used energy threshold (10 MeV) is rather high because the cross section of the giant resonance process in lead is significant at $E_\gamma > 6$ MeV. Estimations show that the correct average values of neutron number n^{tot}_{neut} can increase by $\sim$ 15% in proton-initiated cascades and less in nucleus-initiated cascades.

As is seen from Fig. 3, the magnitudes of differential evaporated-neutron yields in proton- and iron-initiated cascades does not exceed the factor of two beginning from $\sim$ 200 g/cm^2. At small depths the signal highly correlates with primary particle type. The multiple-peak behavior is related to INCA's interlayered structure.

To estimate INCA's potentiality in applying the neutron signal for energy determination, Fig. 4 demonstrate the dependence of the $\sigma(n^{tot}_{neut})/\langle n^{tot}_{neut}\rangle$ ratio for the neutron component integrated over the length of cascades initiated by 10- TeV and 1-PeV primary nuclei on cascade length.

As is seen from Fig. 4, the relative accuracy of energy measurements is low at the initial stage of cascades. However, the standard deviation attains a reasonable value ($\sim$ 30% for protons and less for nuclei), when the device thickness used for energy determination relates to the range behind the cascade maximum ($\sim 300 - 350$ g/cm^2 within the energy range under consideration). Simulations show that similarly to the ionization component, the use of initial cascade stage decreases the accuracy. Thus, it seems to be reasonable to not use the initial stage for energy determination.

4 Conclusion

New method based on measuring the neutron yield is proposed to study the energy spectrum of primary cosmic rays in the "knee" region ($10^{15} - 10^{16}$ eV).

References

Dement'ev, A.V. & Sobolevskii, N.M., Proc. Special. Meeting Intermed. Energy Nucl. Data: Models and Codes (Paris 1993) NEA OECD, 237.

Fedorova, G.F. & Mukhamedshin, R.A., Bull.Soc.Sci. Lettr.Lodz, Ser.Rech.Def. 1994, XVI 137.

INCA Collaboration I, Proc. 26th ICRC (Salt Lake City, 1999), OG 1.2.33

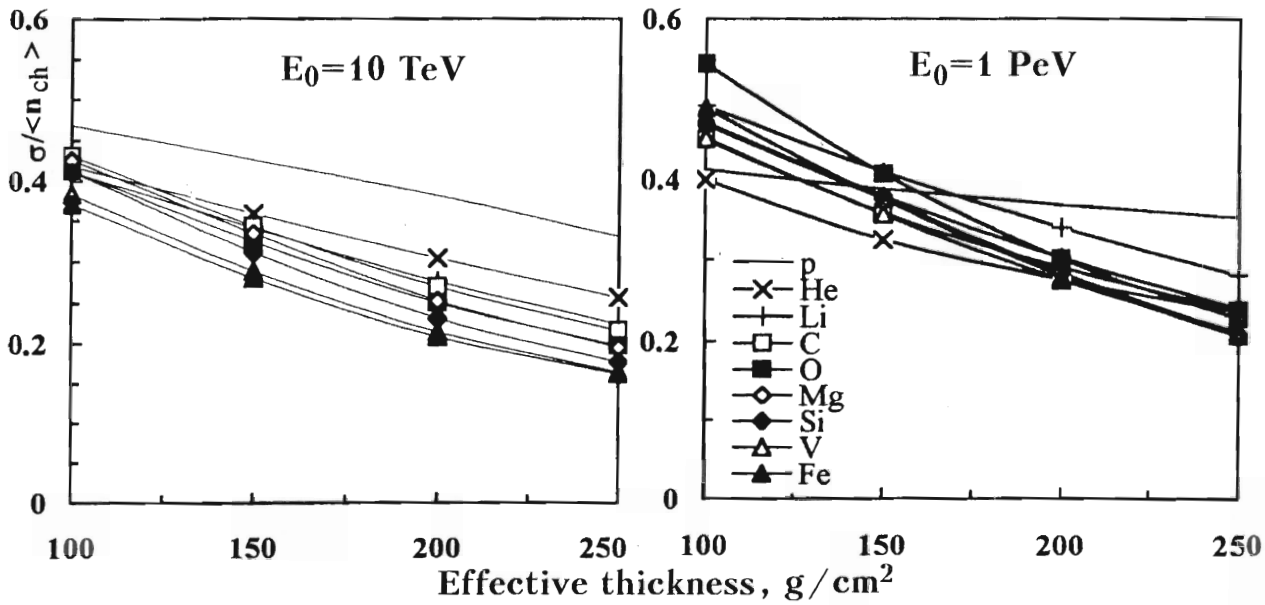

Figure 1: Dependence of the $\sigma(n_{ch})/\langle n_{ch}\rangle$ ratio for the number of charged particles, integrated over the length of cascades initiated by 10-TeV and 1-PeV protons and nuclei, on cascade length.

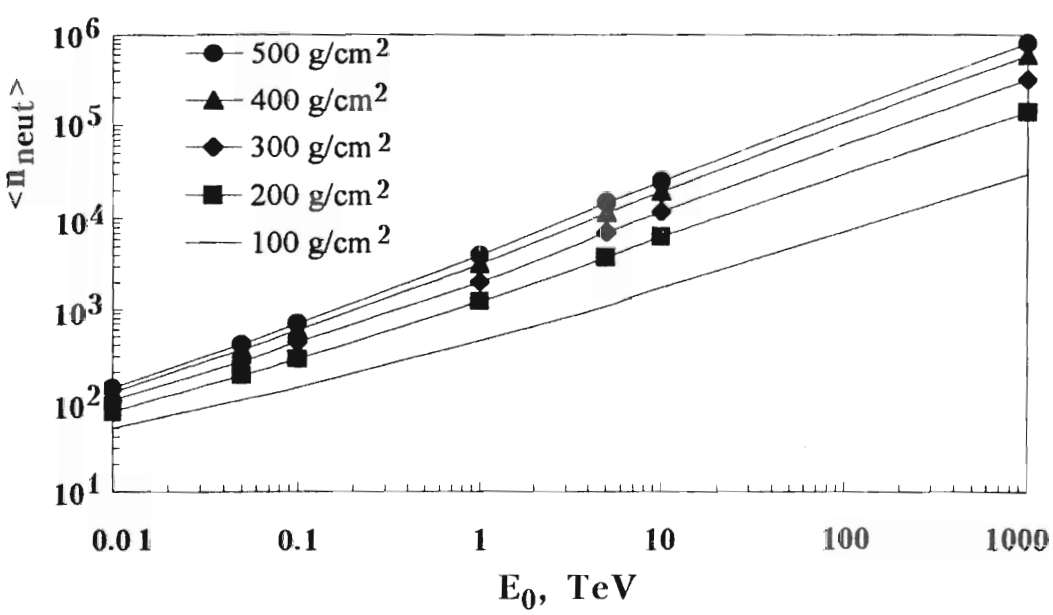

Figure 2: Energy dependence of the total evaporated-neutron number $\langle n^{tot}_{neut}\rangle$ at various INCA's thickness in cascades initiated by protons.

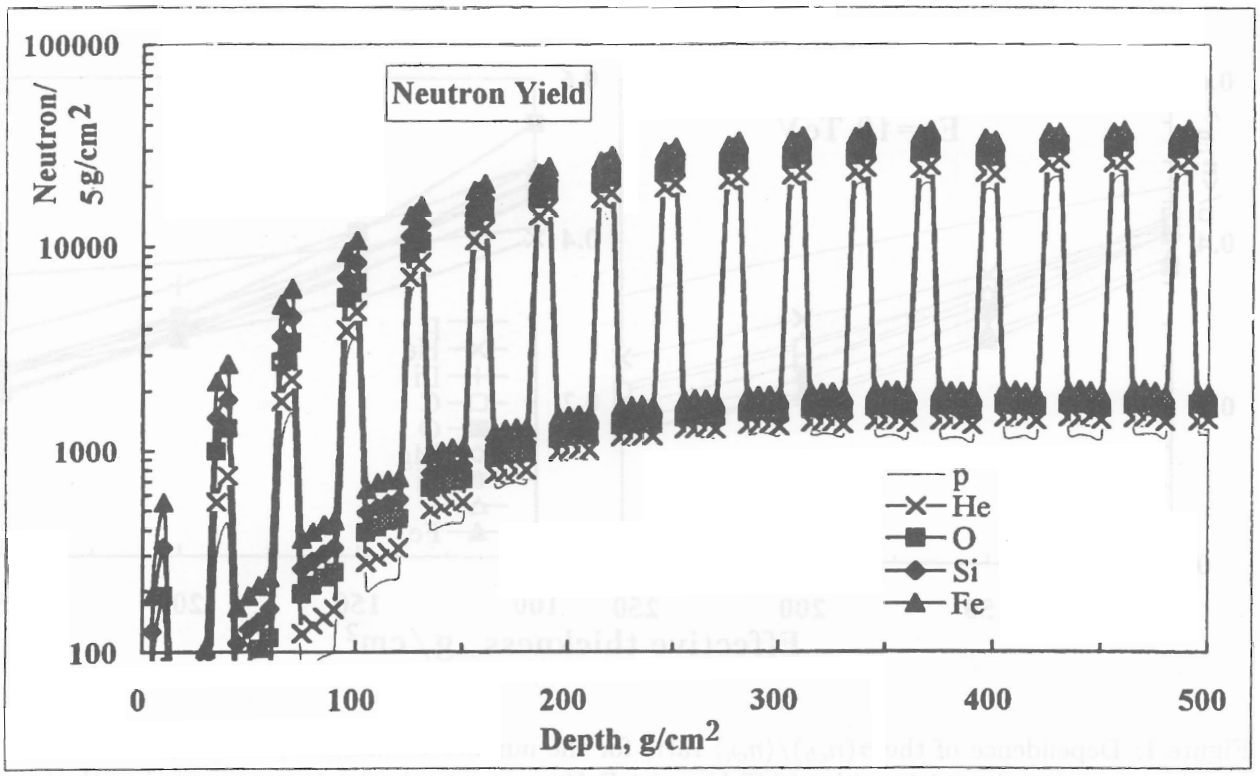

Figure 3: Depth dependence of the neutron yield per 5 g/cm^2 in cascades initiated by 1-PeV protons and nuclei.

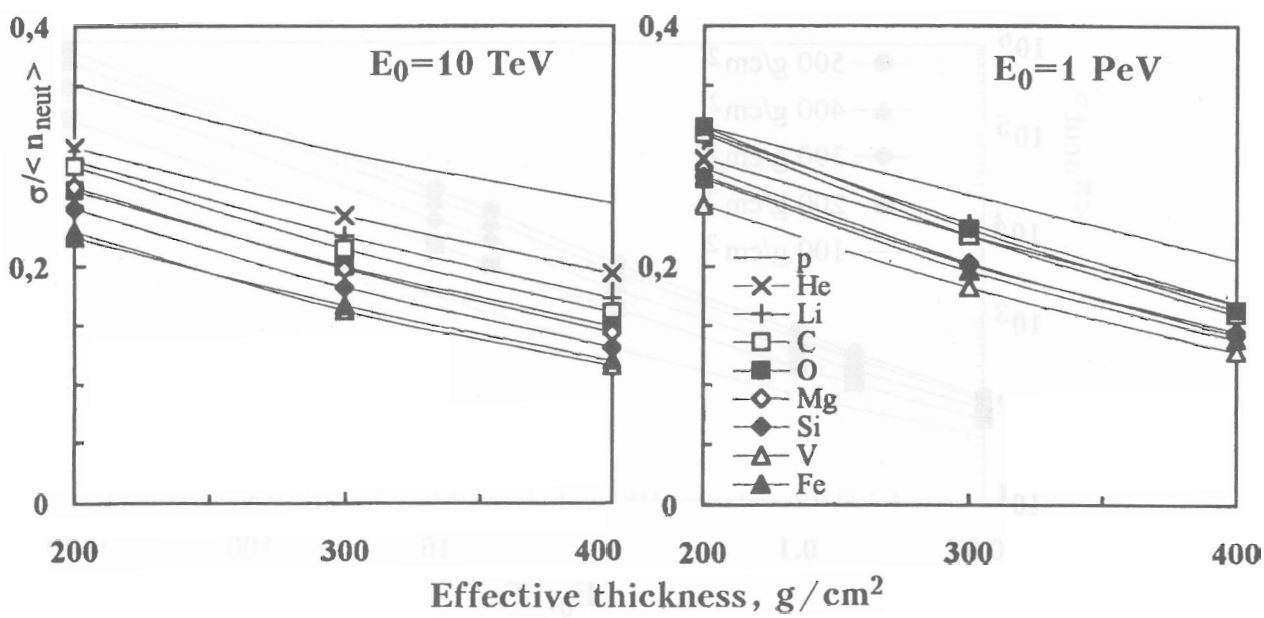

Figure 4: Dependence of the $\sigma(n^{tot}_{neut})/\langle n^{tot}_{neut}\rangle$ ratio for the number of evaporated neutrons, integrated over the length of cascades initiated by (a) 10-TeV and (b) 1-PeV protons and nuclei, on cascade length.

New Method for Separation of Electromagnetic and Hadron Cascades in Detection of Primary Electrons and Gamma-Rays

R.A. Mukhamedshin

Institute for Nuclear Research, Moscow, Russia

Abstract

A new method for separation of primary electrons and protons is proposed on the basis of underground cosmic-ray experimental measurements and Monte Carlo simulation to investigate the primary electron spectrum at energies $E_e \gtrsim 1$ TeV. The method is based on the difference in evaporated-neutron yield in cascades initiated by electrons and protons. It provides a total rejection factor of $\sim 10^{-5} - 10^{-6}$ that is several orders of magnitude better as compared with other methods.

1 Introduction

One of the major goals of the INCA Project is to study the spectrum of primary *cosmic-ray* (PCR) electrons at $E_e \gtrsim 1$ TeV. The available data are rather poor, mainly due to difficulties in separation of cascades initiated by electrons in chambers against the background produced by protons because the proton flux exceeds by a factor of about 1000 the electron flux. Until now, no adequate technique has been used to solve this problem. On the other hand, the further extension of the measurements beyond the few-TeV region could bring rather dramatic new conclusions on acceleration and propagation of primary electrons.

Another astrophysical goal is studying the cosmic γ-radiation in the energy interval $30 - 1000$ GeV, which is covered neither by balloon/satellite nor by EAS-array experiments.

We propose to solve both these problems, i.e., to measure the electron spectrum at $E_e \sim 1 - 10$ TeV and spectra of primary diffusion γ- radiation as well as that from known γ-ray sources.

The INCA's capability of separating electrons/γ-rays from protons in mixed particle beams results from the fact that the evaporated-neutron yield in electromagnetic cascades is only (5-10)% as large as that in hadron- induced cascades (Bezrukov et al. 1973). We consider results of Monte Carlo simulation carried out to estimate a possibility to reject electron-like proton-initiated cascades in the INCA and to separate electron-initiated cascades, which confirm this conclusion.

2 Simulation

We simulate processes in an INCA with a periodic structure, so that each layer contains lead and light substance (polyethylene) with a thickness of 10 and 20 g/cm^2, respectively. The lead provides the neutron generation and the light substance provides the necessary cascade development.

A modified version of the MC0 code by Fedorova and Mukhamedshin (1994) used to simulate nuclear-electromagnetic cascades in the INCA additionally accounts for (a) approximation B for electron-photon cascades; (b) neutron evaporation by nuclei due to inelastic interactions of hadrons and γ-rays, and giant resonance processes. The energy threshold for particle simulation is 10 MeV.

Only the neutron generation was considered but not the posterior neutron thermalization and diffusion, which will be analyzed with using the SHIELD code by Dement'ev and Sobolevskii (1993). We believe that the results given in this paper will not be subjected to a qualitative change.

The energy dependence of multiplicity of evaporated neutrons, $\langle n_{neut} \rangle$, per one simulated inelastic hadron/photon interaction with lead nucleus is very weak at $E \gtrsim 2$ GeV ($\langle n_{neut} \rangle \approx 26$). This permits to use the neutron signal for energy measurements of primary high-energy particles (see corresponding paper of the author). Hadron interactions give the predominant contribution into the neutron yield ($\gtrsim$60%) even at the initial stage ($\lesssim 100$ g/cm^2) of proton-initiated cascades at energies under consideration, and this value arises with energy, while this fraction in electron-initiated cascades is only $\sim$5%.

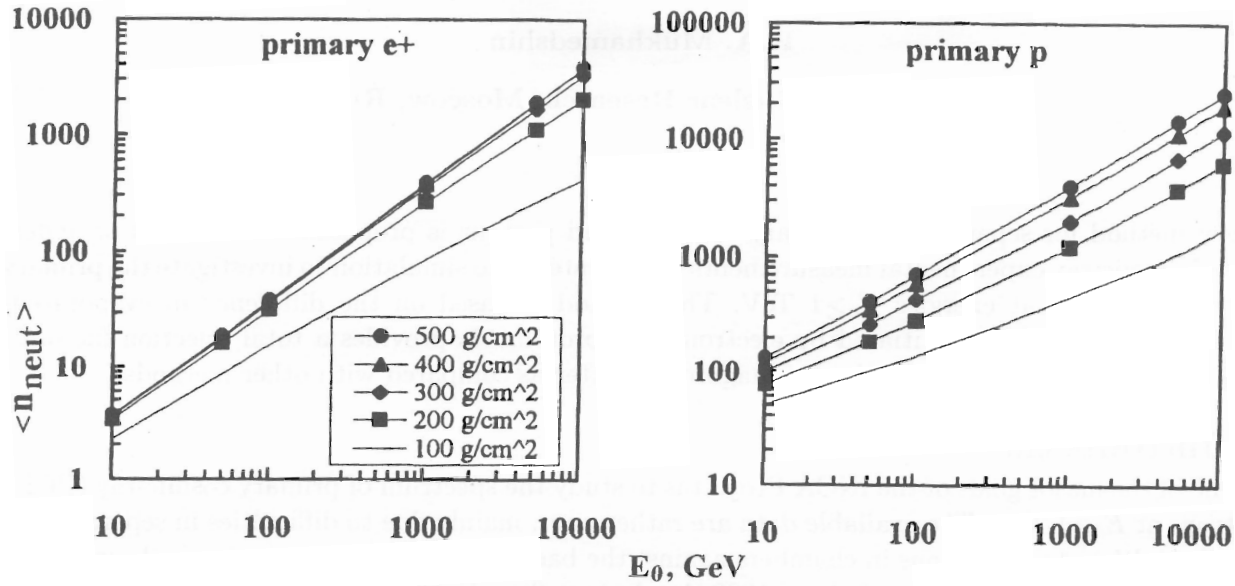

Figure 1: Energy dependence of the total evaporated-neutron number $\langle n_{neut} \rangle$ at various INCA's thickness in cascades initiated by primary electrons and protons.

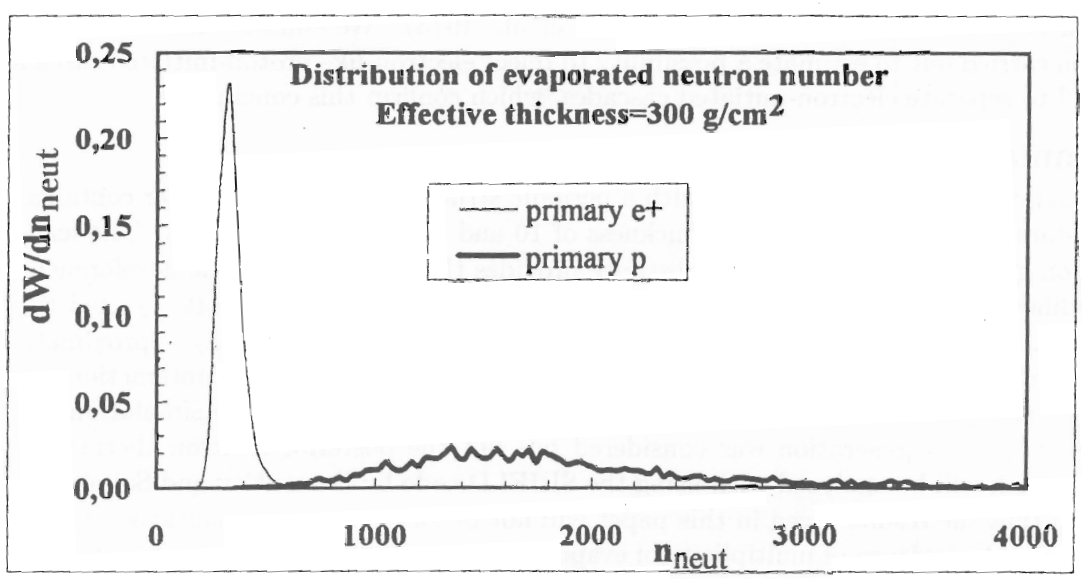

Figure 2: Distribution of the neutron total multiplicity $\langle n_{neut} \rangle$ in cascades generated by 1000-GeV electrons and in the case of 800 – 1200-GeV energy release into the electromagnetic component in cascades initiated by primary cosmic-ray protons in the top 10-g/cm^2 lead layer in an INCA with an effective thickness of 300 g/cm^2.

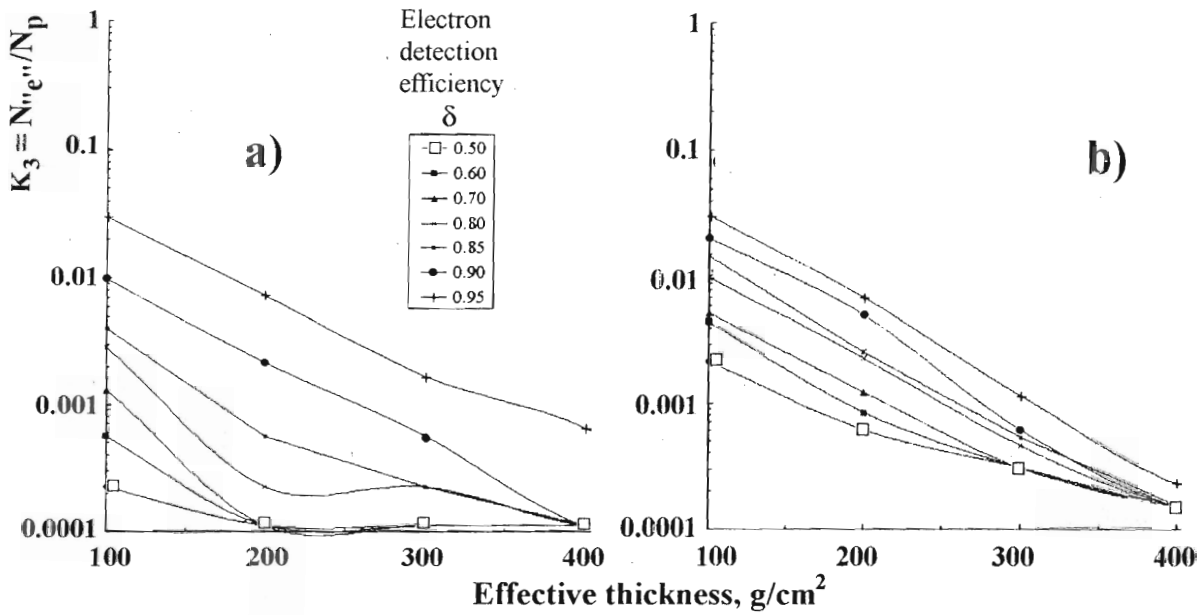

Figure 3: Rejection factor K_3 for electron-like proton-initiated cascades vs. INCA's thickness for various electron detection efficiency δ at (a) $E_e = 100$ and (b) $E_e = 1000$ GeV.

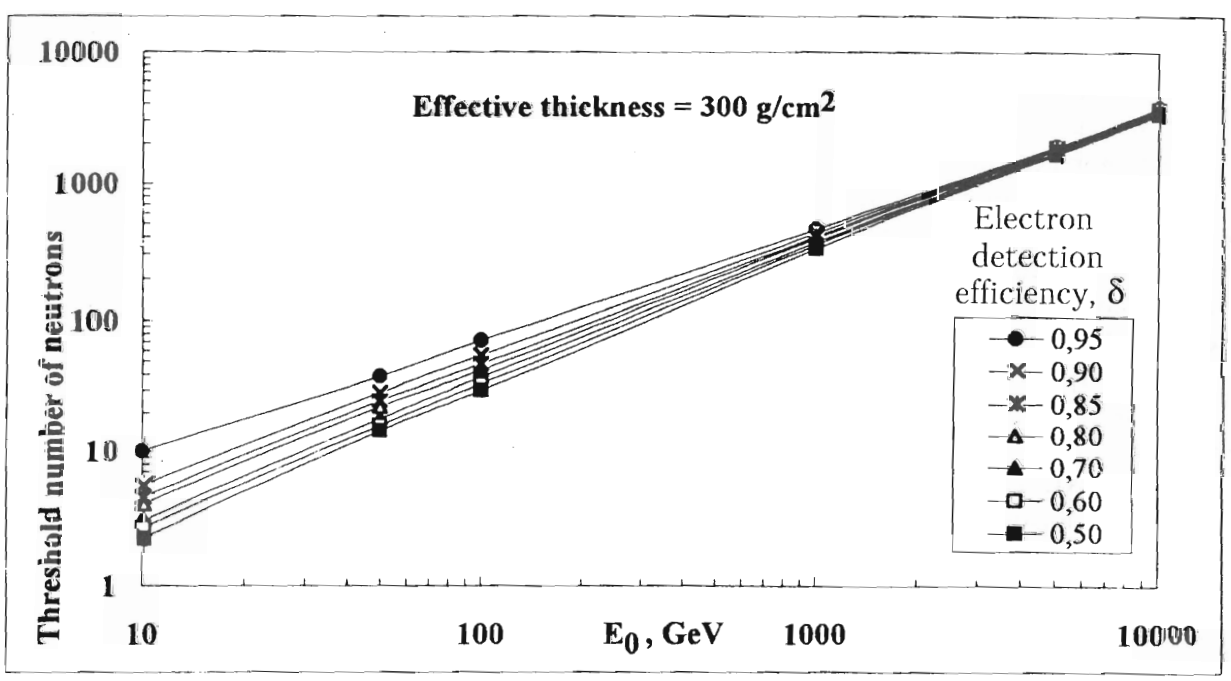

Figure 4: Threshold number of neutrons used to separate electron cascades from proton cascades at various electron detection efficiency δ.

3 Results

Generally, procedures applied to separate electrons against the predominant proton background can be characterized by two rejection factors K_1 and K_2 as follows:

(i) When fixing the cascade starting point within the first lead layer with a thickness of $\Delta x \sim 1$ cm, protons can be discriminated with $K_1 = \Delta x/\lambda_{int}^{p-Pb} \simeq 1/20$.

(ii) If the energy released into the electromagnetic component is E_γ, the average proton energy is $\langle E_p \rangle \approx E_\gamma/K_\gamma \approx 5E_\gamma$. Since the integral proton spectrum decreases as $E_p^{-1.7}$, the effective flux of protons (releasing the same energy E_γ as electrons) must be decreased by $K_2 \simeq 0.2^{1.7} \simeq 1/15$.

The use of these factors permits to consider only proton-initiated cascades which start within the top 10-g/cm^2 lead layer and release the energy $E_\gamma \sim E_e$, namely, $E_\gamma = (0.8 - 1.2)E_e$.

We suggest a new powerful rejection factor associated with the neutron detection.

As is seen from Fig. 1, the energy dependence of the total cascade evaporated-neutron number $\langle n_{neut} \rangle$ integrated over various values of the INCA thickness initiated by electrons and protons is linear in the doubly logarithmic scale. The difference for cascades of different origin is significant. Obviously, the actual separation is possible only in the case of small corresponding dispersions.

Figure 2 demonstrates an example of the distribution of neutron total multiplicity in cascades generated by 1000-GeV electrons and in proton-initiated cascades with $E_\gamma = 800 - 1200$ GeV, i.e., $E_\gamma \sim E_e$) within the top 10-g/cm^2 lead layer in an INCA with an effective thickness of 300 g/cm^2. The narrow distribution for electron-initiated cascades does not actually overlap the broad distribution for proton-initiated cascades. The INCA concept uses this feature of neutron signal to reject electron-like proton-initiated cascades, additionally to the criteria K_1 and K_2. Quantitatively, this idea can be described by the rejection factor K_3 which depends on both absorber thickness and the efficiency δ of primary-electron detection (Fig. 3). Here δ is the fraction of electron-initiated events considered after cutting off their distribution's right wing, which could overlap the distribution of proton-initiated events. Even for a thin (100 g/cm^2) setup, $K_3 \approx 10^{-2}$ at $\delta = 0.8$. For a thickness of 300 g/cm^2, $K_3 \approx 10^{-3} - 10^{-4}$ at $\delta = 0.9$. Calculations show that K_3 weakly depends on E_e up to 10 TeV. Figure 4 illustrates the energy dependence of the threshold neutron signal required to separate electron cascades at varying δ. As is seen, the neutron number corresponding to $E_e = 1$ TeV and $\delta = 0.9$ exceeds 10^2. Thus, we can realize this criterion even in the case of the neutron detection efficiency of about $10 - 20\%$. At the same time, a high level of the neutron threshold signal suppresses the influence of background PCR neutrons.

It should be noted that the used energy threshold (10 MeV) is rather high as the cross section of giant resonance process in lead is significant at $E_\gamma > 6$ MeV. Estimations show that the correct average values of neutron number can increase by $\sim 25\%$ in electron-initiated cascades and $\sim 15\%$ in proton-initiated cascades. On the other hand, in accordance with SHIELD code the average number of neutrons evaporated by lead nuclei at energies in the GeV range must be taken as high as about 30. As a result, the total effect of all the corrections cannot decrease the difference between cascades initiated by electrons and protons obtained in our calculations.

Let us note that corresponding selection criteria, proposed recently by various authors and based on cascade lateral and longitudinal characteristics provide an additional rejection factor only of about 0.1. Moreover, the efficiency of these criteria decreases with increasing energy.

The criterion based on the neutron signal is more efficient by two or three orders of magnitude as compared to other methods. It is simple in realization and keeps its high efficiency at all energies. **The total INCA's e/p rejection factor ($K = K_1 \cdot K_2 \cdot K_3$) can attain $10^{-6} - 10^{-7}$ at the electron detection efficiency $\delta = 0.8 - 0.9$ up to $E_e \gtrsim 10$ TeV.**

References

Bezrukov, L.B. et al., Sov.J. Nucl.Phys. 1973, 17 98.

Dement'ev A.V. & Sobolevskii N.M., Proc. Special. Meeting Intermed. Energy Nucl. Data: Models and Codes (Paris 1993) NEA OECD, 237.

Fedorova G.F. & Mukhamedshin R.A., Bull.Soc.Sci.Lettr. Lodz, Ser.Rech.Def. 1994, XVI 137.

Measurements of the neutron yield from a lead absorber for pion and proton projectiles

V.A. Ryabov

P.N. Lebedev Physical Institute, Russian Academy of Science, Moscow

Abstract

As a part of the program of development of a new instrument called Ionization- Neutron Calorimeter (INCA) aimed at studying primary cosmic radiation, experimental data on average values and fluctuations of the neutron yield from a 60-cm-thick lead target are obtained. The target was exposed to pion and proton accelerator beams with energies of 4 and 70 GeV, respectively, and to an electron beam with an energy of 200 to 550 MeV. The experimental data obtained well agree with the results of a simulation by the SHIELD code used for development of INCA elements. It is shown that the same particle energy, the average neutron yield for electron projectiles is by the factor of approximately 50 lower than for hadrons.

1 Introduction

Characteristics of the ionization signal are well known. In the present study, the following basic properties of the INCA neutron signal are investigated: 1) The mean neutron yield as a function of the energy E0 of a primary hadron; 2) Neutron yield fluctuations for different E0; 3) Thermalization and diffusion times in the INCA layered structure; 4) Neutron signal distribution over the depth of the combined absorber composed of light and heavy substances.

2 Experimental prototype setup

We used an INCA with the absorber containing six lead layers each 10 cm thick and 20 cm × 20 cm in area interlayered by polyethylene plates 6 cm thick (Figure 1). SNM-18 ^{3}He proportional counters 30 cm long and 3 cm in diameter served as neutron detectors. Three counters were placed in holes drilled in polyethylene plate installed beyond every layer of the INCA absorber. The distances between centers of two adjacent counters of the same layer and between rows of counters in two neighboring layers were 6 and 15 cm, respectively. The total number of neutron counters in the INCA was 18.

To increase the detection efficiency for evaporated neutrons generated in the INCA, the lead absorber was completely screened by the polyethylene moderator and reflector 10 cm thick. The calibration measurements with Po−Be radioactive sources having activities of $2.25 \cdot 10^5$ and $2.25 \cdot 10^6$ s^{-1} were carried out to determine the detection efficiency for thermalized evaporated neutrons. The sources were placed in turn at different points of the INCA, and the total neutron counting rate in 18 INCA channels was determined. The average neutron detection

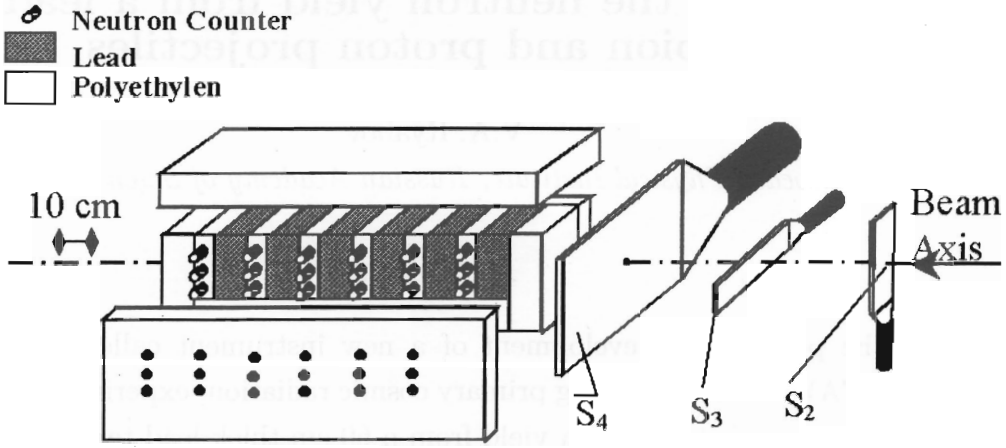

Figure 1: Experimental setup

efficiency obtained for 20 different positions of the sources within the INCA turned out to be $\langle\varepsilon\rangle = 7.4 \pm 0.4\%$.

The measurements of the neutron yield were performed in pion and proton beams with energies E_π= 4 GeV and E_p=70 GeV, respectively, at the IHEP U-70 accelerator (Ammosov V.V. et. al., 1998). The stretched beams were used in which the hadron flux within every burst was uniform during 2 s, and the total number of particles per beam burst did not exceed 10^4. Thus, the average time gap between hadrons incident onto the INCA was $\geq 200\mu$s.

Mean neutron yields $\langle n\rangle$ were also measured for electron energies of 0.2, 0.3, 0.4, 0.5 and 0.6 GeV at the LPI electron accelerator (Chubenko A.P. *et al.* 1998).

The INCA trigger provided (1) recording of the neutron signal induced by a single beam particle passing through the center of the INCA; (2) the absence of overlapping neutron signals induced by two or more primary hadrons; (3) suppression of signals caused by background particles.

Four scintillation counters S_1, S_2, S_3, and S_4 installed along the 20-m base were used to form the trigger. The counter S_1 was disposed immediately downstream of the beam collimator output, while the counter S_3 was installed directly in front of the INCA. The coincidences $S_1S_2S_3$ selected events corresponding to the incidence of beam particles onto the experimental setup. To reject background events and scattered beam particles, we used a large anticoincidence counter S_4 (30×30 cm^2) with a central hole 2 cm in diameter.

After the 10-μs delay, each trigger signal $S_1S_2S_3\bar{S}_4$ opened the time gate with a duration from 30 to 420 μs (depending on the measurement series). This is the time window that was used in the INCA for recording neutron signals.

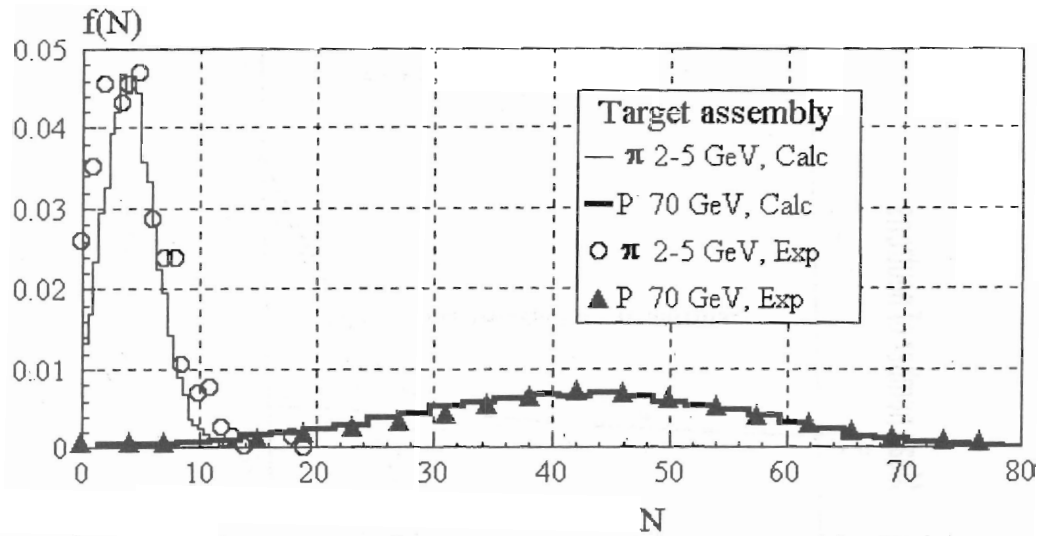

Figure 2: Distribution of the number of evaporation neutrons detected by INCA prototype.

3 Experimental results for hadrons and electrons at accelerator energies

Figure 2 demonstrates distributions $P(m)$ of a number m of neutrons detected by the INCA prototype in cascades that were initiated by protons ($E_p = 70$ GeV) and pions ($E_\pi = 4$ GeV). The distributions measured for protons are well approximated by a Gaussian, whereas those for pions are described by a superposition of two Poisson distributions. This fact is a consequence of the complicated nature of the process of nuclear disintegration in the INCA absorber under the action of beam particles.

The characteristic lifetime of neutrons in the INCA was determined using the dependence of the mean value $\langle m \rangle$ of recorded neutrons on the time-gate duration t. This lifetime turned out to be equal to $130 \pm 10\,\mu s$. All values of $\langle m \rangle$ given below correspond to $t = 330\,\mu s$, when the neutron collection efficiency attained, approximately, 95%.

For comparison, the calculated data for the mean number m of evaporated neutrons initiated by pions and protons with $E_0 = 4$ and 70 GeV, respectively, are also given in Figure 2. These data are obtained on the basis of the program package SHIELD (Dement'ev and Sobolevskii, 1993) based on the cascade-evaporation model of nuclear disintegration. The calculation was performed for real setup geometry with $\epsilon = 8\%$. There is a good agreement between calculation and experimental results.

In our experiment, we also have measured the distribution of a number of observed neutrons for the INCA with a combined absorber composed of light and heavy substances. To do this, in the INCA with the absorber made of complete polyethylene, we have replaced the polyethylene plate in the sixth row by the lead plate 5 cm thick. The measurements were performed in the 70 GeV proton beam.

The experimental results are given in Fig. 3. As is seen, the replacement of polyethylene by lead led to a very sharp increase (by the factor of 20) a number of neutrons recorded in channels of the sixth row as compared to the first four rows. Such a polyethylene-lead transition effect

Then the transport of these neutrons throughout the device is simulated taking into account the interactions mentioned above. The act of detection of a neutron by a counter was simulated in the following way: if the neutron with energy $E_n<1$ eV entries the counter, the neutron is detected with the probability of 80% and the neutron history is finished. With the probability of 20% this neutron cross the counter (as a vacuum) and its history is continued. Neutrons with energy En >1 eV cross counters without detection.

3. Results.

The total of eleven variants of the simulation were performed at different numbers of the counters arranged inside three and five counter planes. Outer planes L and R contain 48 counters for all variants while the number of counters in the planes LM, M, and RM was variable. Variants of the simulation are presented in Table 2.

Table 2. Number of counters in counter planes L, LM, M, RM, R for different variants of simulating.

Variant	Number of counters					
	L	LM	M	RM	R	Total
1	48	-	5	-	48	101
2	48	-	12	-	48	108
3	48	-	24	-	48	120
4	48	-	48	-	48	144
5	48	-	55	-	48	151
6	48	-	70	-	48	166
7	48	-	92	-	48	188
8	48	6	48	6	48	156
9	48	12	48	12	48	168
10	48	24	48	24	48	192
11	48	48	48	48	48	240

The number of simulated neutron histories (i.e. the number of source neutrons) was 100000 for all variants. Numbers of neutrons detected by each counter plane are presented in Table 3.

Table 3. Number of neutrons detected in counter planes L, LM, M, RM, R per 10^5 source neutrons.

Variant	Number of detected neutrons					
	L	LM	M	RM	R	Total
1	4187	-	1264	-	4143	9594
2	4113	-	3054	-	4012	11179
3	3951	-	5467	-	4007	13425
4	3848	-	9076	-	3787	16711
5	3705	-	10509	-	3772	17986
6	3620	-	11700	-	3794	19114
7	3516	-	13474	-	3640	20630
8	3732	1149	8646	1066	3649	18242
9	3706	2120	8143	2102	3634	19705
10	3575	3887	7312	3774	3628	22176
11	3463	6482	6238	6497	3430	26110

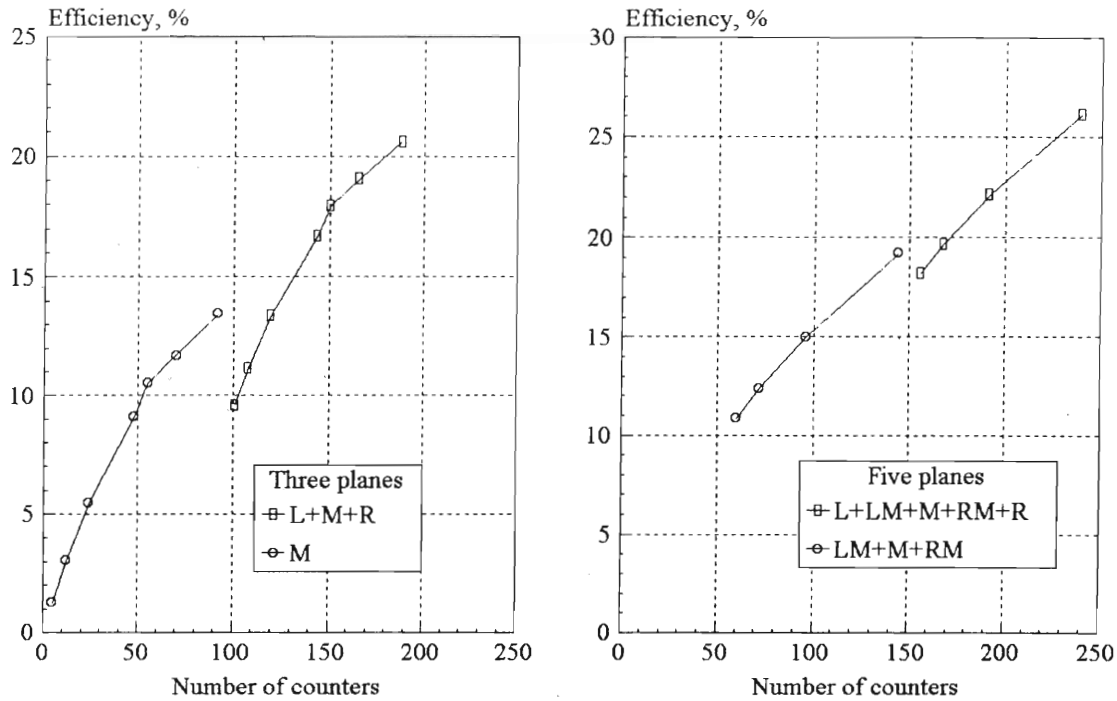

Fig. 2. Efficiency of neutron detection as function of the number of counters for three (a) and five (b) planes of counters. Squares - efficiency for all planes, circles - inner planes only (without planes L and R)."

As one can see from Table 3, the required efficiency of neutron detection, determined as the ratio of total number of detected neutrons to total number of source neutrons, lies in the range 9.6% (Variant 1) to 26.1% (Variant 11). Obviously, the efficiency of neutron detection may be enhanced by means of further increase of the number of counters, but the total number of counters inside the calorimeter cannot exceed some reasonable limit.

Fig. 2 presents the data of Table 3 in the graphic form. Fig. 2(a) concerns the case when the counters are arranged in three planes L, M, and R only, while Fig. 2(b) corresponds to arrangement of the counters in all five planes L, LM, M, RM, and R.

References

1. A.V.Dementyev, N.M.Sobolevsky. SHIELD - Universal Monte Carlo Hadron Transport Code: Scope and Applications. Proc of Third Workshop on Simulating Accelerator Radiation Environments (SARE3), KEK, Tsukuba, Japan, May 7-9, 1997. KEK Proceedings 97-5, Ed. H.Hirayama, p.21; A.V.Dementyev, N.M.Sobolevsky, Yu.Ya.Stavissky. Nucl. Instr. Meth. A374 (1996) 70.

2. L.P.Abaguan, N.O.Bazazyants, M.N.Nikolaev, A.M.Tsibulya. Neutron Group Constants for Reactors and Shielding Calculations. Atomizdat, Moscow, 1981.

INCA DESIGN AND REALIZATION STAGES

Merzon G.I.

P.N.Lebedev Physical Institute, Russian Academy of Sciences, Moscow

1. Requirements to INCA modules

To solve the problems of the spectrum and composition of primary cosmic rays in the "knee" region, i.e., at energies of 1 to 10 PeV, and energy spectrum of primary electrons near 1 TeV, we need an INCA with the following characteristics:

- Geometry close to 4π (i.e., close to spherical or cylindrical);
- High geometry factor (i.e., a detector with the maximum area at a given volume, e.g., ring-shaped);
- Minimum mass (i.e., based preferably on light absorbers);
- Good radiation resistance (i.e., containing radiation-hard detectors and electronics);
- Capability of long-term operating in space (i.e., a high reliability of an experimental device as a whole).

In addition, the detector must satisfy the following requirements:
- High determination accuracy for the particle arrival direction (of a few angular degrees). To realize this requirement, a cellular detector structure is necessary with the cell size of about 1–10 mm;
- Energy measurement accuracy of 20 –30%;
- Mass-number measurement accuracy of about 30%;
- Particle-charge measurement accuracy of about 20%;
- Absence of an effect of the reverse current;
- e/p rejection factor of 10^6
- 10^7 at the measurement efficiency exceeding 90%.

2. General approach to the INCA design

The general approach to the INCA design is based on the concept of an ionization-neutron calorimeter supplied with position-sensitive and particle's charge (scintillation and semiconductor) detectors, acoustical detectors for recording exotic massive particles, etc.

A usual idea of a sandwich-type calorimeter consisting of thin lead plates and thick graphite and/or polyethylene absorbers is exploited. The heavy absorber multiplicates the cascade electromagnetic component. The light absorbers provide the multiplication of the nuclear component and serve as a neutron moderator that makes it possible the thermal-neutron detection by conventional methods of neutron physics.

It is important that the moderation and diffusion lengths for neutrons in polyethylene and graphite are about 2 cm. This implies that evaporation neutrons produced by cascade particles as a result of nuclear disintegrations are concentrated (at short diffusion times) in the vicinity of their parent absorber nuclei. This fact makes it possible, in particular, to measure the partial neutron flux near the cascade generation point, i.e., to determine the mass number A of a projectile nucleus.

3. Stages of the INCA project realization

We propose a gradual approach to construction of several INCA versions differing in their design and capabilities. Thus, we suggest to solve the above problems step by step in three stages.

The first stage includes manufacturing of a balloon-born INCA module (Mini-INCA) aimed at verifying the INCA concept and engineering solutions, Fig.1. In this case, the INCA mass and exposure time are limited by about 1 t and 10-day flight, respectively. At this stage, the engineering aspects of the simplest INCA version exposed to cosmic rays can be tested. Refined data on PCR electrons under conditions of a strongly suppressed predominant proton background (the resulting proton admixture is expected to be lower than 1%). The module could be constructed and tested during 2 or 3 years. The cost of this stage is estimated to be 100 –300 k$.

The second stage is constructing an INCA module (Midi- INCA) with a mass of 2 –3.5 t to be installed at a Space Station or a dedicated satellite (e.g., VOSTOK) Fig. 2. This module must be capable of directly measuring the PCR hadron and electron spectra up to energies of 1000 TeV and 10 TeV, respectively. The Midi-INCA makes also it possible to solve other problems related to physics of diffuse galactic gamma-rays with energies up to 1 Tev, solar neutrons and gamma-rays, search for exotic particles with the anomalously low ratio Z/A, etc. Solving these problems will require 3 to 5 years and 200 –500 k$.

Finally, a full-scale INCA module with a mass of 4 –18 t for installation at a dedicated satellite will be consttructed, Fig. 3. This version is intended for directly studying the composition and spectrum of PCR hadrons at energies up to 10 PeV in the knee region. Solving this problem will require the 3-year exposure in space. A rocket with an enhanced carrier capacity is necessary for launching. The cost of this project is more than 1 M$ and its realization time is 8 to 10 years. The realization of all these projects in parallel is possible.

4. The Mini-INCA design

We consider the INCA structure using the balloon-born version as an example (Fig. 1). This Mini-INCA has the shape of a thin parallelepiped 0.24 m wide and is composed of absorber plates with an area of 1.1 x 1.1 m^2. Such a version contains six 0.5-cm lead plates (i.e., 3 cm), six 2.5-cm graphite plates (15 cm), and six rows of 1-cm plastic scintillators on the basis of polysterene (6 cm). The INCA faces are covered by the 4-cm neutron moderators made of polyethylene. The total Mini-INCA's thickness and mass are 82 g/cm2 and 992 kg, respectively. To provide the optimum energy resolution the thickness of 200 to 300 g/cm2 is necessary. This requirement restricts particle's arrival directions and the fiducial detector area, so that we detect about 0.1 fraction of the isotropic cosmic-ray flux from the upper hemisphere. The effective geometry factor of the Mini-INCA turns out to be about 0.26 m^2 sr. Thus, it is able to detect about 4 x 10^4 primary electrons with energies exceeding 0.1 TeV per one flight day. The Midi-INCA (Fig. 2) with an area of 1 m^2 and thickness of 200 g/cm2 (mass of 2 t) installed aboard of an aligned satellite or space station has the geometry factor of about 0.5 m^2 sr and is more efficient compared to the balloon-born version.

Finally, the geometry factor of a large-scale INCA version (Fig. 3) with a mass of >= 10 t, which uses an advantage of cylindrical design, can attain 10 m^2 sr that allows studying the hadron spectrum in the knee region. Here, the expected numbers of hadrons for 3-year operation are (2–6) x 10^3 and 40–120 events with energies exceeding 1 and 10 PeV, respectively. The expected number of PCR electrons with energies E > 1 TeV is about 10^6.

5. INCA detectors

In all versions of INCA, detectors of various types are used to determine particle's coordinate, energy, charge, and mass number. For example, the Mini-INCA contains:

- About 200 scintillation detectors in the form of bars with a cross section of 1 cm x 2 cm and 1 m long;
- About 100 neutron detectors, i.e. proportional counters 2 cm in diameter and 30 cm in length filled with 3He at a pressure of 7 at and installed in holes drilled in graphite or polyethylene absorbers;
- We intend also to employ silicon detectors for coordinate, ionization, and time-of-flight measurements with the spatial resolution of 0.1 –1 mm and signal-to-noise ratio of about 100/1 for minimum ionizing particles;
- Acoustical detectors for recording very massive exotic particles.

6. Conclusion

We can conclude that the gradually progressing INCA versions are capable of solving by the direct way basic urgent problems of cosmic-ray physics, which were listed above. Further studies involving mathematical simulation and irradiation in accelerator beams are necessary to optimize these versions and determine the yield of detected events.

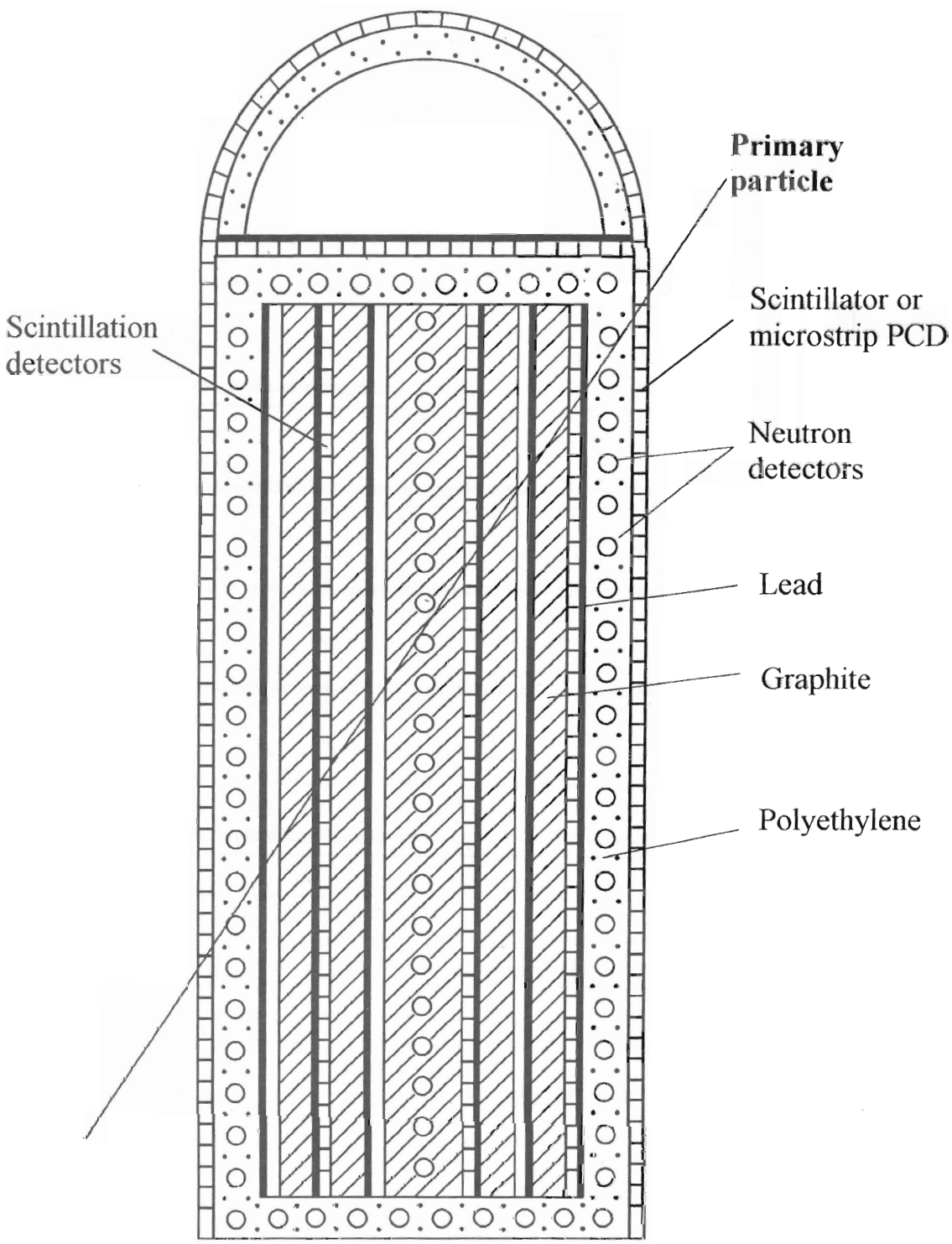

Fig. 1 Mini-INCA version designed for balloon flights

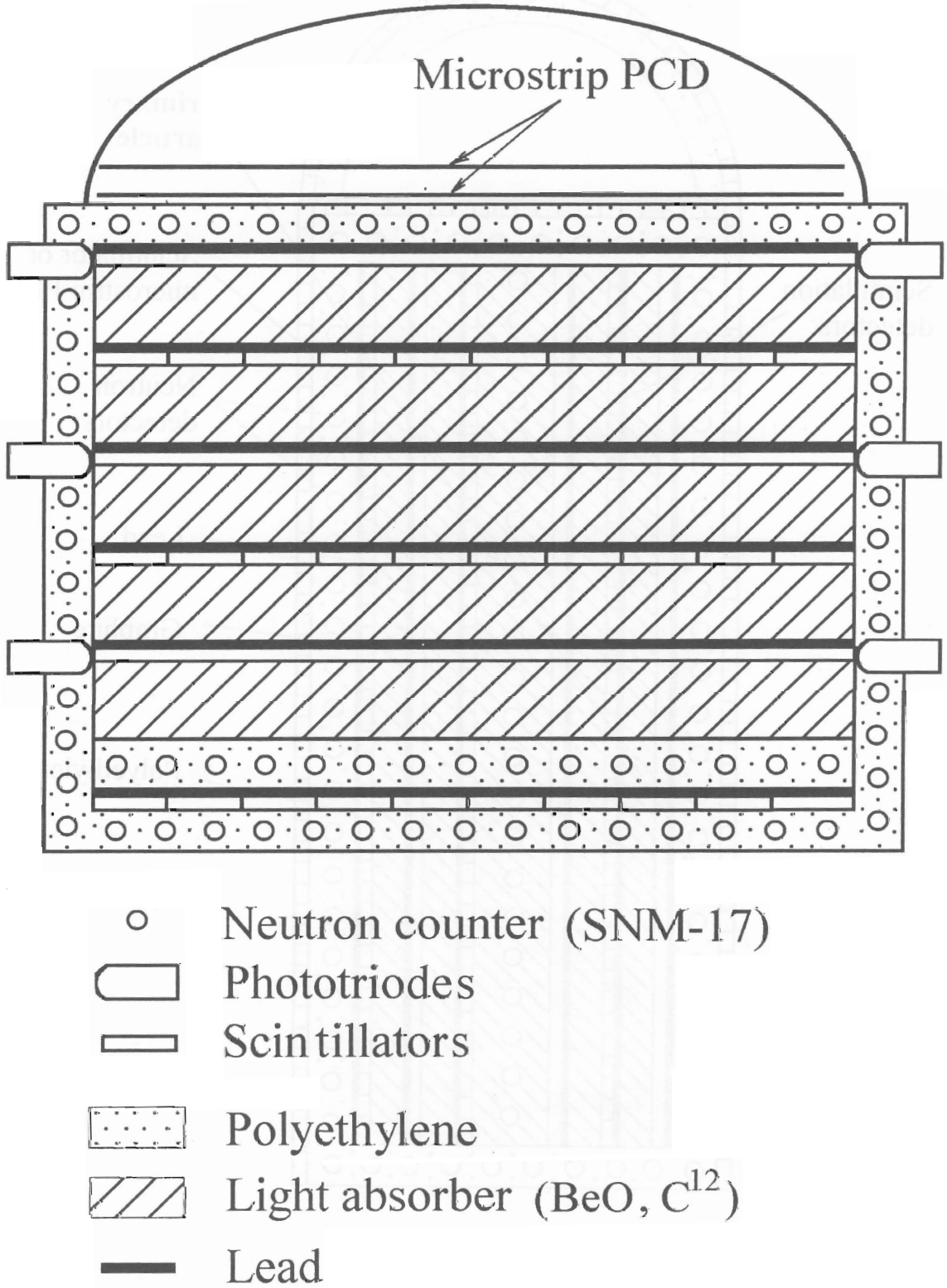

Fig. 2. Mini-INCA version designed for a space mission.

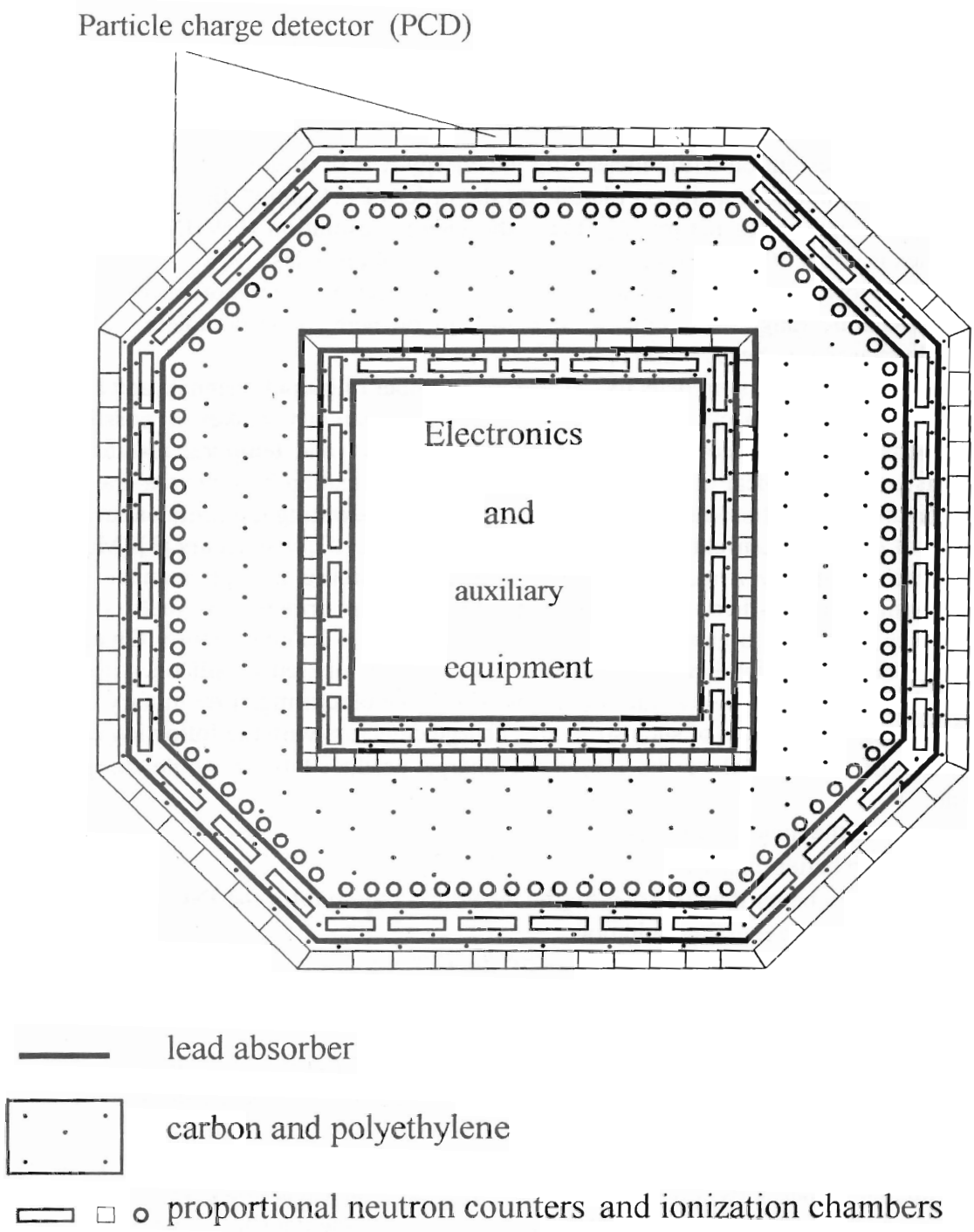

Fig. 3 Cross section of the Ionization-Neutron CAlorimeter (INCA) with the Particle Charge Detector (PCD). Basic parameters are: weight = 4.6 - 9 t; $S\Omega$ =10 - 30 $m^2 \cdot sr$ (up to 20 - 60 $m^2 \cdot$ sr for iron nuclei); height = 1.5 m; diameter = 1.8 - 2 m; absorbers are carbon and polyethylene.

Investigation of signal amplitude dependence upon the high voltage supply.

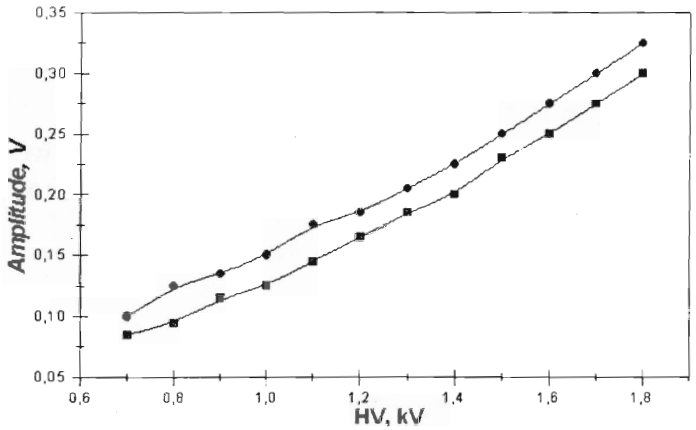

Experimental test of phototriode.

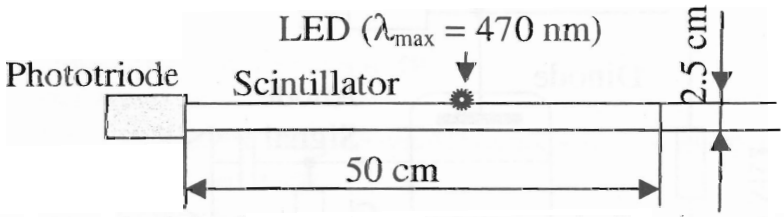

1) We investigated minimal phototriode response to the LED light flashes. The LED was fixed at the middle of scintillator strip.

2) Decreasing the brightness of LED flashes we reached the ratio $U_{signal}/U_{noise} \cong 3\text{-}4$, where U_{signal} – is amplitude of phototriode output signal, U_{noise} is a height of the noise.

3) After that, the brightness of LED flashes was fixed and phtotriode was replaced by PMT. We measured amplitude of PMT output signal (U_{LED}) for the same brightness of LED.

4) We irradiated the scintillator at the muon beam ($I_\mu = 10\ cm^{-2}\ s^{-1}$), and measured amplitude of PMT output signal ($U_{particle}$) corresponding to one relativistic particle, crossing through the middle of scintillator (2.5 cm thickness)

5) We obtained minimal number of particles which is possible to register using scintillator with phototriode as photodetector:

$$N_{min} = U_{LED} / U_{Particle} \cong 20$$

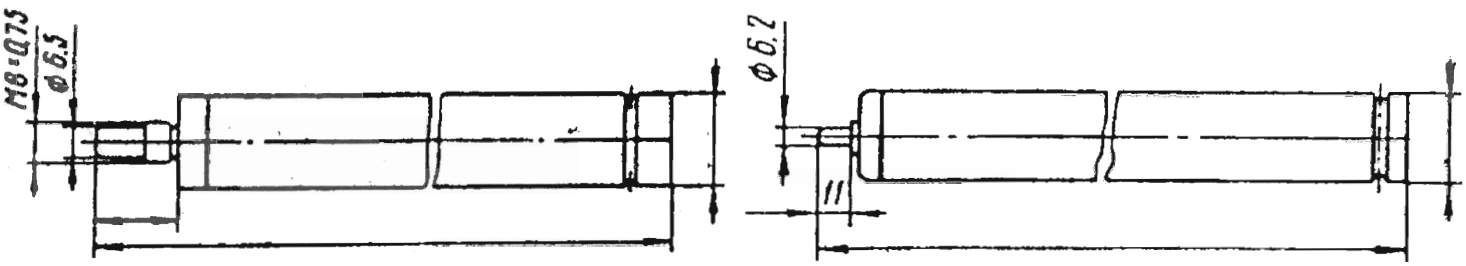

Counter type	SNM 17	SNM 18
Rated thermal-neutron detection efficiency	80%	70 %
Relative counter sensitivity spread	15%	10%
Inherent counter background, pulse/s, max	0.05	0.05
Temperature range, °C	-50...+ 150	-50...+ 150
Pilling gas pressure, Kgf/cm^2	7	4
Mass, g	≤40	≤150
Cost, $	100	100

The main counting gas of the counters is Helium-3.

Neutrons are detected from the reaction:

$$^3He + n \rightarrow p + {}^3T_1 + 770\ KeV.$$

Typical ADC spectrum of ^{3}He Nutron Counters SNM - 17, 18.

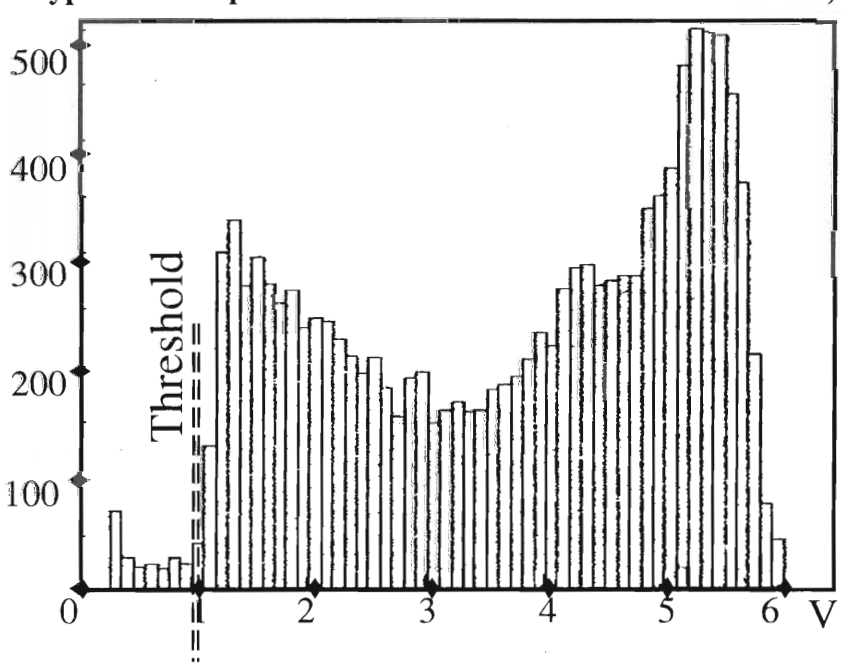

Detectors and Electronics of Balloon borne Strange Quark Matter Telescope

T. Yanagita
square College of Technology
Y. Hatano
Institute for Cosmic Ray Research
University of Tokyo

Anomalous massive nuclei of charge $Z \approx 14$ and mass of about 370 amu was observed for the first time in the galactic cosmic rays by a balloon borne experiment.(Saito et al., 1990). These nuclei are supposed to be SQM (Strange Quark Matter). In order to search for SQM with higher detection sensitivity, a series of international balloon experiments with a new telescope was conducted under the collaboration between Japan and Italy (Saito, 1991).

The SQM hybrid telescope is shown in Fig.1. It consists of two diffusion box type scintillation counters, S1 and S2, used to define the incident charge, 6 direct viewed(light guide type) scintillation counters, S3, S4, S5, S6, S7 and S8 for determining the dE/dX, two diffusion box type Cherenkov counters C1 and C2 for measuring the particle velocity, 4 layers of Multi Tube proportional counter used to define the trajectory and passive particle detector.

The scintillator S1 and S2 are 100x100cm^2 and 1 cm thick. Each of them is housed in a square light diffusion box and is viewed by eight 5" photo multiplier tubes(PMTs, Hamamatsu R877), which are divided into two groups of four PMTs to provide two independent measurements of the scintillation light. C1 and C2 are also 100x100cm^2 and 2cm thick metha-acrylic plate. The Cherenkov light was collected by 16 5" PMTs(R877) divided into two groups of eight PMTs to provide two independent measurements. A plane of Multi Tube Proportional Counter(MTPC) is made of hundred 1cm^2 square, 100cm length tubes filled with Argon He gas. Two planes build up one X-Y layer. The pre-amp and discriminator(made of chip components to minimize the board size) are equipped inside the container of the counters.

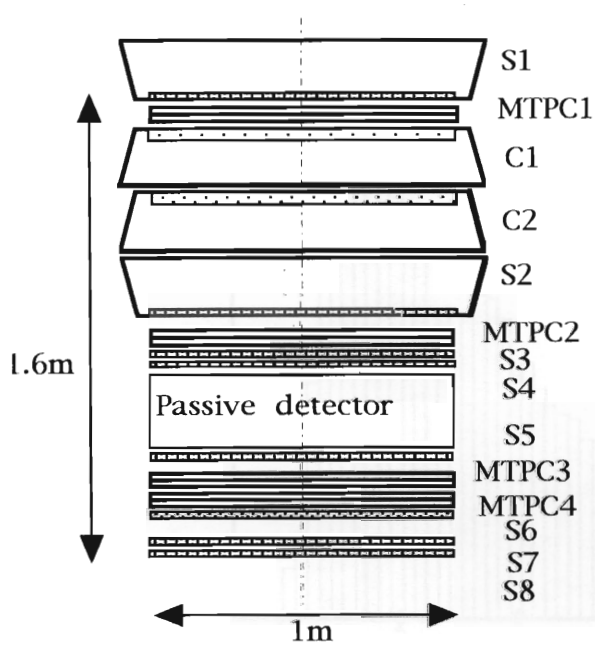

Fig. 1 SQM Counter Telescope

The details of the passive particle detector will be described in elsewhere.

The geometric factor of the instrument defined by S1,S2 and S3 is 8300cm^2 sr.

The whole dimension of payload is 180 cm x 180 cm and 300 cm height, and total weight is 1600 kg. The electric power is about 80W(~1W/Kg) supplied by Li- Battery pack.

Fig. 2 show the Block diagram for the electric system. We will explain the electric system with this schematic diagram. Used electric devices are all C-MOS Logic, and /or low power grade. Especially, we chose the devices carefully which were located at he detector side, because the temperature of circumstance decreases below -40℃.

The signal from the detectors are fed to 2 stage amplifier, pre and main amp. The pre-amp is equipped at the detector side (near the PMT, or sensor), all other of the circuit are mounted on the 24 single width and 5 double width cards inserted inside the EURO-CARD (same size of VME) rack.

Trigger logic is as follows as three fold coincidence.

(S1)*(S2)*(S3+S4)

A burst trigger (>300 minimum ionizing particle)(S5+S6+S7+S8) was also added. The resolving time of this system is about of order of several hundred nanosecond. Actual trigger rate was ~ 30/sec (discrimination level was set above He nuclei)

Each channel starts ADC (successive 10 bits type of 5 μsec conversion time) by self trigger and the data was latched when the trigger condition was satisfied by the three fold master coincidence. The output of MTPC is already digitized at the counter side, thus 800 parallel data were transferred serially to controll system in coincide with triggering.

The house keep data such as the atmospheric pressure and the temperature of outside etc. was manipulated with slow ADC (conversion time, 10msec) and recorded in every trigger.

Data length;

PH	10 bits ADC	x24ch.	=	240
Magnet sens.	10 bits ADC	x2ch.	=	20
MTPC	100ch. x8	(25x4)x8	=	800
HK	Temp. 8bitsx4ch.		=	32
	Press. 10 bits x 1		=	10
others	real time, dead time, trigg. rate			200
Total				~ 1200 bits/event

To decrease the dead time, we compressed the MTPC data as small as possible, so the data length varied by the track pattern. And we also prepared the 3 stages of shift registers in data stream line for the purpose to absorb the fluctuation of the trigger interval. The Z-80 controller was used to construct the serial format for the telemetry transmission and to read out operation from

the MTPC.

Data format is ;

1 word 16 bits
1 frame 16 words
normally 4 frame/events
in case of multiple tracks, frame number increased up to 6.

These data are encoded by PCM and passed to the telemetry system whose transmission speed are 16 to 131kbps through the low pass filter. We used the 64kbps system, so maximum available event rate is around 60 .

Usually , several command channels are prepared for controlling the payload in flight. We used two channels for the High Voltage switching and system reset.

In the latest experiment, the instrument was flown from the Millo base of the ASI in Italy, on July 23th morning, 1997, and recovered in Spain next morning. About 1.4 million events were collected during 20 hours.

Though all of the counter data was transferred by telemetry, we also prepared the on-board data storage system (DAT and Hard disk unit) considering the future program for long duration balloon flight. The DAT and Hard disk can record the data up to 1 Gbytes and 4Gbytes, respectively. (There is one weakness that both requires pressurized container.) We are studying a DVD-RAM which is able to record 4-5Gbytes without air tight container as a next stage storage.

Reference

Saito T. et al. Phys. Rev. Lett. 65, 2094-2097 (1990).
Saito T. Nucl. Phys. 24B, 184-190 (1991).

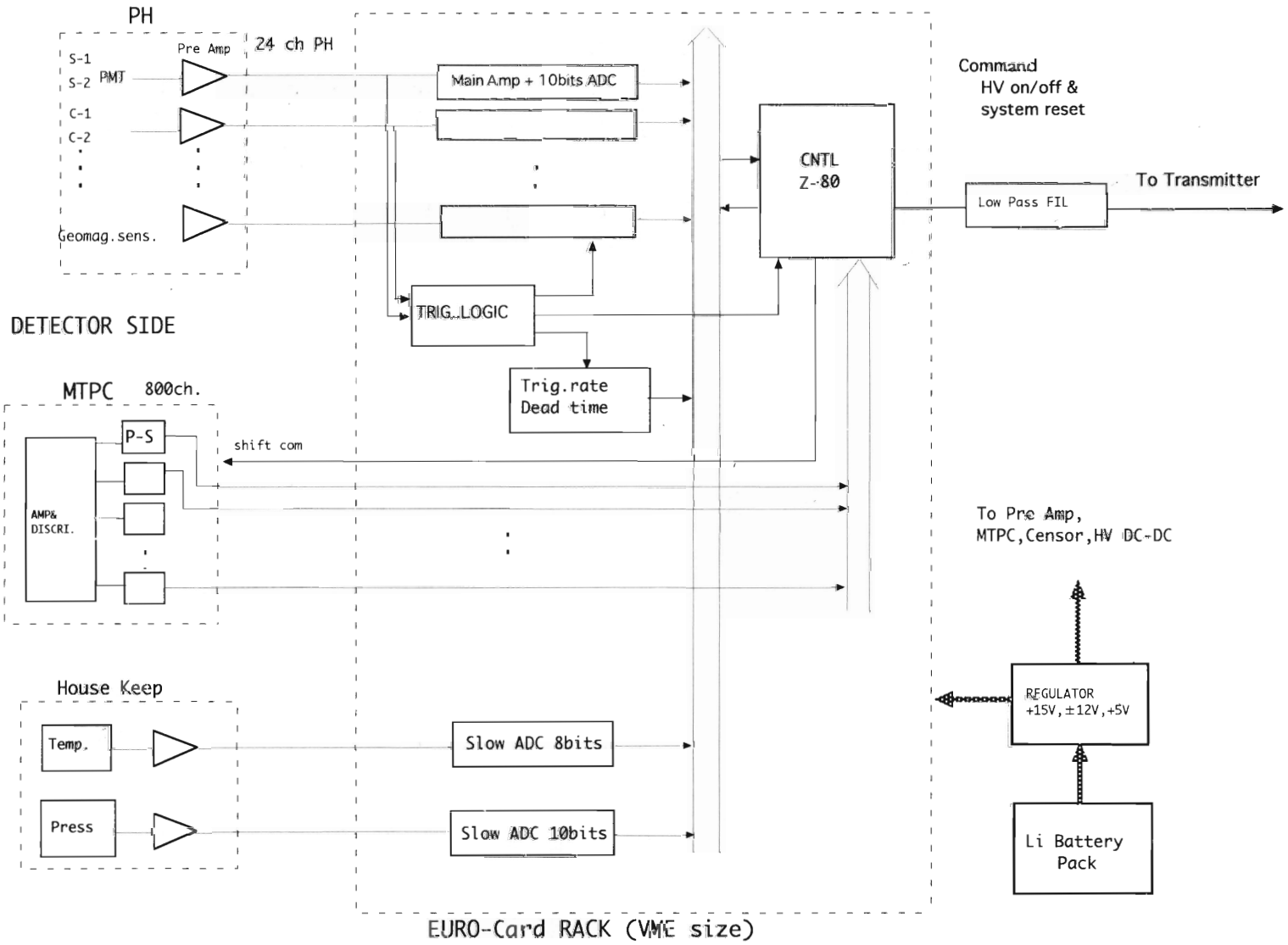

Fig. 2 Schematic Block Diagram for Electronics

Ball antenna and its application

H. Sasaki

Department of Natural Environmental Science, Faculty of Science,

Kochi University, Kochi, 780, Japan

Abstract

The ball antenna system has been developed for the detection of EM waves emitted by nuclearites at deep seabed. The minimum detectable amplitude by the stainless ball antenna is about 3 microvolts per meter. As there is some possibility to utilize the ball antenna for the INCA project, we present its feature and performance of the ball antenna system and some preliminary results of the 3 point's simultaneous measurement of natural ELF/VLF EM waves in the atmosphere and the observation in the sea. Finally the utilization of the ball antenna system for the INCA project will be discussed.

1. Introduction

Research on cosmic ray anomalies, for example long lived massive particles, delayed sub-air shower disks, hadron bundles and Strange-quark matter, became the important subject in cosmic ray physics at the decade of 1980 and many theoretical and experimental proposals were offered. Many scenarios, also, with respect to the candidates of dark matter were offered. S.L.Glashow and A.De Rujula[1] have raised the existence of strange quark matter, named nuclearites, with mass of 10^{-24} to 10^{10} g and have showed the possibility of detecting seismic signals by the nuclearites (whose mass greater than 1 kg) at the passage through the earth.

On the other hand, it has been reported that the anomalous EM (Electromagnetic) waves were observed before the big earthquake (Gokhberg et al., 1979)[2]. Many laboratory experiments to detect the EM wave emission at the rock fracture, also had performed since 1977(Nitsan[3], 1977, Ogawa et al[4], 1985, Cress et al[5], 1987). Ogawa et al.[4] developed the ball antenna system to measure natural ELF/VLF EM (Electromagnetic) signals in the atmosphere relate to the research on the lightning and on the worldwide EM circumstance. Also, there are many scenarios on the emission of EM waves from the fracture of rocks are offered and recently Tsarev and Sasaki had discussed three mechanisms of EM waves emission during development of cracks of the crust.[6], [7]

According to these results and the Glashow's scenario, we had calculated the emission of ELF/VLF (Extremely Low Frequency / Very Low Frequency) EM waves along the path of a nuclearite through the crust of the earth(Sasaki et al.[8], 1990). As the detector of such EM radiation from the rock fracture at deep seabed (where there is no EM noises) we selected the ball antenna developed by Ogawa because of its shape which is convenient to house in a glass sphere and no corrosion problem. Figure 1 shows a schematic view of EM wave observation system for the

study of the global electromagnetic anomalous events in the atmosphere and in the sea. The principle of the ball antenna is the electric potential sensor set in the atmosphere. The electric field near the ground would reasonably be vertical and constant. When a conductor of capacity C_0 is raised in the air to a height of h from the ground surface and connected to the ground through the resistance R and capacitor C, it can receive the electric potential variations at that level. When we measure the electric potential variations near DC region on the ground, however, we must consider the resistivity of air, about 4×10^{13} Ω•m and the input resistance(10 GΩ to 10^4 GΩ) of a voltage follower installed in a stainless sphere.

In the following sections, we will report mainly on the ball antenna system and the multi-point observation of natural ELF/VLF signals in the atmosphere.

2. Ball antenna system

2-1. Block diagram

Figure 2 shows the block diagram of the ball antenna system used at the 3-point simultaneous observation in 1997, autumn. A voltage follower circuit formed by an ultra-high input impedance operational amplifier (IC.AD515, Monolithic precision, low power FET-input electrometer OP amp. Analog Devices) was installed inside the stainless sphere with the battery block for their power supply. The ball antenna circuit is shown in Fig.3. Output signals from a voltage follower are fed into the filter and main amplifier system through a 50m co-axial cable. The first filter is for the ejection of commercial power supply frequency (50/60Hz), the second one is for the elimination of the 22.2kHz (the Maritime Self Defense Force of Japan, for submarine, Miyazaki) and the third is the low pass filter for the ELF output. After 22.2kHz filter the signals are separated to the ELF main amplifier and the VLF main amplifier (IC, AD621, instrumentation amplifier, Analog Devices, gain of 20db). Both outputs are added to the GPS 1pps signal for the accurate arrival time analysis. The GPS 1pps signal have an accuracy of + - 1 microsecond against the UT time. These outputs are recorded on a digital audio tape recorder (DAT, SONY) with sampling frequency of 48 kHz. Therefor the minimum system error of the arrival time is about 20 microsecond. If we take into account of the place of the real arrival time for each rather complex wave form, the expected error of the arrival time is about twice of 20 microsecond which is correspond to + - 12 km error for the position of the source point. Moreover, as the effect of reflection at the ionosphere and the height of source point of EM signals must be taken into account, the accuracy of the source point is about + - 60 km actually.

The frequency response of a filter and amplifier circuit for the VLF region is shown in Fig.4. When we take into account the frequency response of the DAT, response curves for 3 measuring system at Sapporo, Norikura and Kochi change as dot lines in the figure.

On the other hand, in the case of under water experiment we use a two ball antenna system, and the differential amplifier circuit using an instrumentation OP amplifier IC (AD624) with a voltage gain of 60db is used as a main amplifier for the severe attenuation of the sea water. Each ball antenna is

housed in a glass sphere to avoid any contact with seawater for long term observation. Figure 5 shows the system block diagram for the under seawater experiment. The minimum detectable ELF/VLF signal was about several microvolts at the input of the voltage follower (Sasaki et al.[9], 1994).

3. Multi-point simultaneous measurement of Natural ELF/VLF EM waves

The investigation of ordinary atmospherics is important for the development of the under water system and may be useful for the research on the anomalous increase of EM waves before the big earthquake. As the study on the source position of worldwide natural ELF/VLF EM waves from lightning (atmospherics) is interesting for the research on the earth's electrical environment and also on the electromagnetic waves relate to the earthquakes.

The recent estimation of global lighting occurrence using satellites was done by Mackerras et al.[10] Their estimated rate of total flashes into cloud and ground is 65 per second. This rate is low due to inadequate detection of weak cloud flashes. They also reported the ratio of cloud flashes to ground flashes with uncertainty of a factor 2.

Method

Simultaneous measurement of natural ELF/VLF EM waves at 3 sites (Sapporo, Norikura and Kochi) using the ball antenna and the GPS time signal, lead us to decide the source position of each EM wave. Observed EM signals are stored in the DAT with the GPS time signal. By the way, the method of arrival time measurements at different places were used in our previous paper in 1995 by Chechin et al.[11] The aim of this measurement is the detection of the EM waves at explosions of the Shoemaker-Levy-9 (SL-9) comets on the Jupiter. As a results, this measurement did not go well, because of the miss design of devices and the unexpected less mass of SL-9 comets.

To determine the emitting point of each EM wave, the spherical trigonometry will be used in case of the study of atmospheric EM noises. The flatness of the earth is only 0.0034 and the difference between the equatorial and polar radius is about 20 km, there is no necessary to use the spheroidal globe, especially at the case of a position finding in small area, for example around Asia. Then the time difference between two signals, for example Sapporo and Norikura give one curve. Other time difference, Norikura and Kochi, give the other curve and the cross point of these curves is the source location. See Figure 6.

Observation at three points was done 20th and 21st Oct. 1997. Three time intervals are selected as 17:00 to 19:00, 21:00 to 23:00 and 7:00 to 9:00 next morning. These 3 time intervals are nearly coincident with the peak times of the diurnal variation of global thunderstorm activity at Asia and Australia, Africa and Europe, and America.

Results

Figure 7 shows obtained waveform data adjusted their absolute times (or time axis) using 1 pps signals. Data on the DAT tape were fed into a personal computer through the ADC board and were arranged as shown in Fig.7. All most all the wave forms were found on the data tape each other where the pulse height of the wave forms were greater than 1.0mV at the ball antenna except for overlapped data region.

Figure 8 and 9 show the weather chart and the obtained source point distribution when we had two typhoons (southern region) and one low atmospheric pressure region (near Hokkaido). We will find easily their similarity in their locations and also the movement of source locations synchronized well with the movement of the low-pressure region. Obtained distribution of the source point of the global lightning will be legal because of the flight time difference method is a fair means in principle except for the error due to the reflection of the waves from lightning by the layer of ionosphere.

Why 4 points measurement?

Up to now we had tried the 3 point simultaneous observation (Sapporo, Norikura and Kochi) and obtained the fundamental results, as the source point distribution compared with a weather map, classification of observed signals (taxonomy). Due to the small number of observation points (3 points) and near aligned arrangement of the 3 points, the error of the source location is more than 1000km in the case of aligned direction of 3 observation points. If we observe at 4 points (as shown in Fig.6) which makes a rectangular arrangement of observation sites, then more confidential data will be obtained. This is the main reason why we propose the collaboration with the researcher in Vladivostok.

Physics / Geophysics

On the earth we have at least 1000 thunderstorms at any time and the frequency of lightning is about 10 to 100 per one second. Observed waveform data at previous measurement of 3 points showed good coincident in arrival time and similarity in shape, as shown in Fig.7, in case of more than 4 mV/m signal amplitude 99% of the data showed good analogy. If there is another natural EM wave emission whose source points are fixed at one area, then these waves are easily detected and recognized as the emission with one source point. Meteorological condition should be considered, of course. The possibility of such natural EM wave emission, especially related to the earthquake, is discussed. First paper with respect to the abnormal increase of EM wave emission of 81 kHz before the big earthquake of magniude=7.0, are presented by Prof. M.B.Gokhberg.[9] After his report many such results were offered. But due to the statistical problem of such abnormal increase, most of the seismologist has negative images of such increase.

Another study on the relation between lightning and meteorology is expectable, especially between the lightning and the typhoon.

Moreover the EM wave whose source point is out of the atmosphere are also investigated, if we

are lucky. There was an interesting report by Ogawa et al. that one observed EM wave had its source point at outside of the ionosphere.[12)]

4. Application for the INCA project

Astrophysical goals of the INCA project are followings;

(1) Nuclear composition and energy spectrum of the primary cosmic radiation within the energy 1-10PeV,

(2) Spectrum of cosmic ray electrons from nearby sources,

(3) High-energy gamma rays in space,

(4) Neutral radiation from solar flares,

(5) Search for nonrelativistic and high-energy exotic particles.

Among these five aims of the project, the huge cascade produced by 1-10 PeV primaries may be detectable using EM antennas(ball antennas) installed inside the calorimeter under some additional electromagnetic circumstances, for example to feed a electric field which makes a separation of charged particles. Of course scintillation detectors of the INCA device can easily detect the huge cascades and even if we try to use the ball antenna, some theoretical approaches should be requested.

On the point of the astrophysical goals, there will be another interest which relates with the interplanetary radio wave research and with the detection of EM waves from the layer of the ionosphere, for example a detection of small cosmic objects, as shown in Fig.1

Finally, I will recommend the study on the point of CHAOS and Fractal with respect to the high-energy gamma rays and PeV energy cosmic rays with a new parameter of their arrival time duration.

References

1) De Rujula A. and Glashow S.L. , Nuclearites-a novel form of cosmic radiation, Nature 312(1984) 734

2) Gokhberg, M. B., et al., Experimental Measurement of Electromagnetic Emissions Possibly Related to Earthquakes in Japan, J. Geophys. Res. 87(1982) 7824

3) Nitsan, V., Electromagnetic emission accompanying fracture of quartz-bearing rocks, Geophys. Res. Lett. 4 (8)(1977) 336

4) Ogawa, T. et al., Electromagnetic radiations from rocks, J. Geophys. Res. 90 (D4) 6245, 1985.

5) Cress, G. O. et al., Source of electromagnetic radiation from fracture of rock samples in the laboratory, Geophys. Res. Lett. 148, 49(1987) 331

6) Sasaki H. and Tsarev V., Possible mechanisms of electromagnetic emissions associated with earthquake preparation, J. Atoms. Electri., 17, 2 (1997) 77

7) Tsarev V. and Sasaki H., Low frequency seismogenic electromagnetic radiation: How dose it

propagate in the earth's crust and where can it be detected, Atmospheric and Ionospheric Electromagnetic Phenomena Associated with Earthquakes, Ed. M.Hayakawa, Terra Scientific Publishing Company, Tokyo (1999) 383-393

8) Sasaki H. et al., Detectability of super massive nuclearite by ELF EM-waves on the ocean bottom, Proc. Int. Conf. on Cosmic Rays, Adeaid, Vol.10 (1990) 223-226

9) Sasaki H. et al., ELF electromagnetic wave observation system on the seabed.:Electromagnetic Phenomena Related to Earthquake Prediction, Ed. M. Hayakawa and Y. Fujinawa, Tokyo, TERRAPUB, (1994) 193-204

10) Mackerras D. et al., Global lightning: Total, cloud and ground flash estimates, J. Geo. Res. 103, D16 (1998) 19791-19809

11) Chechin V. et al. Global ELF/VLF wave observation at the SL-9 comet crash on Jupiter, Proc. Int. Cosmic Ray Conf. Rome, Vol. 4 (1995) 1168-1171

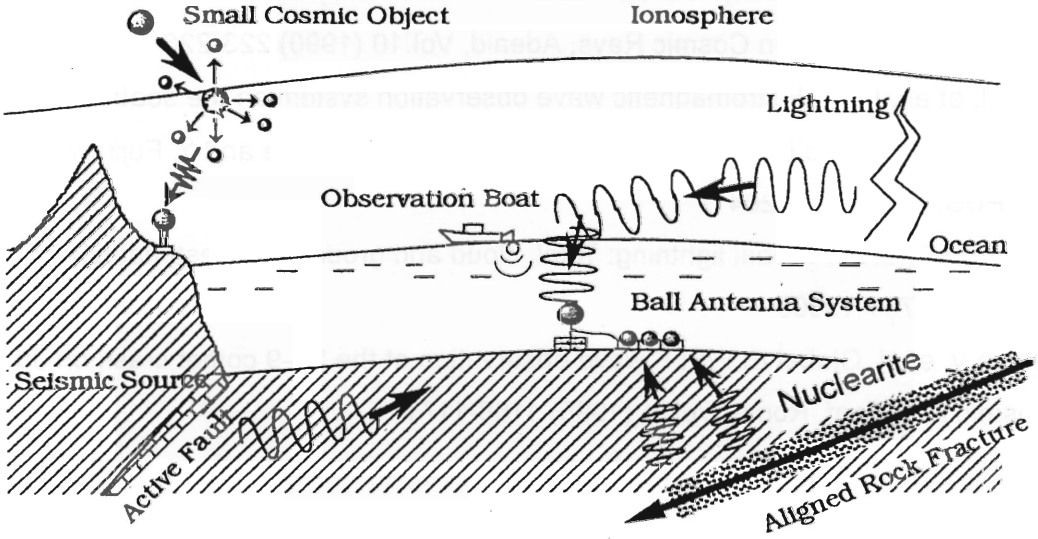

Fig. 1 Shematic view of the ball antenna system in the atmosphere and in the sea.

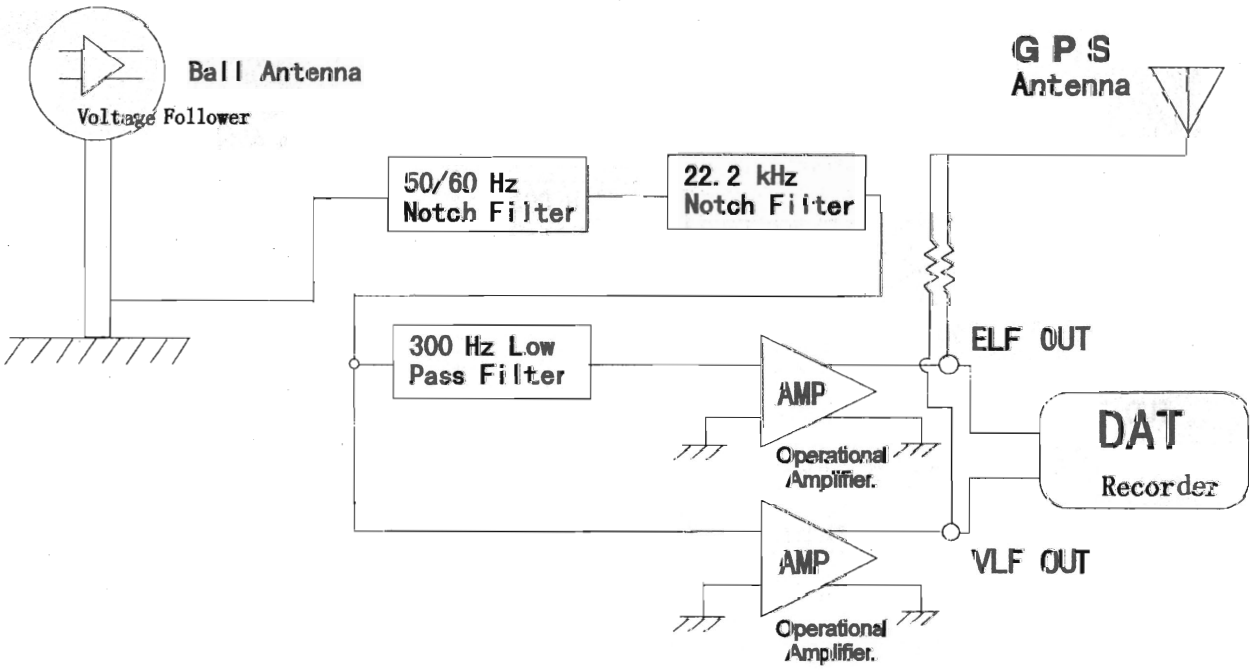

Fig. 2 Block Diagram of the Ball Antenna System.

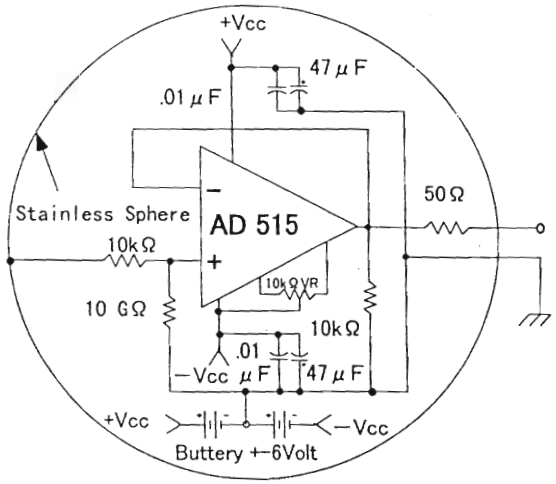

Fig. 3 Circuit diagram of ball antenna.

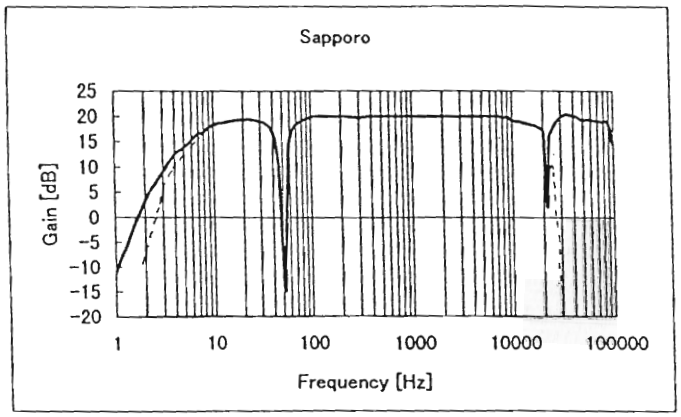

Fig. 4 Frequency response of ball antenna system for VLF output in Fig. 2.

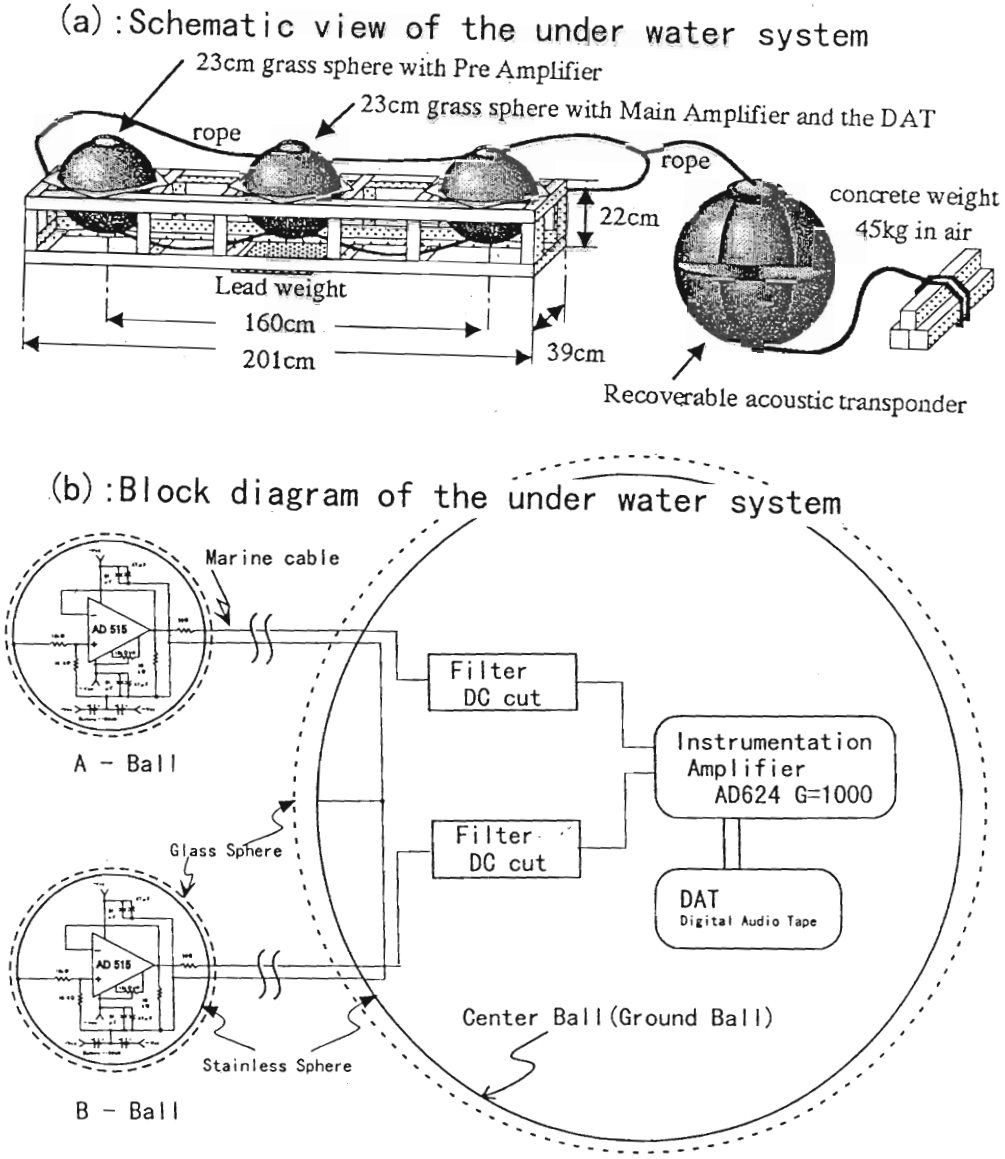

Fig. 5 Two Ball antenna system for the under seawater experiment.

Fig. 6 Network of the ball antenna system around the sea.

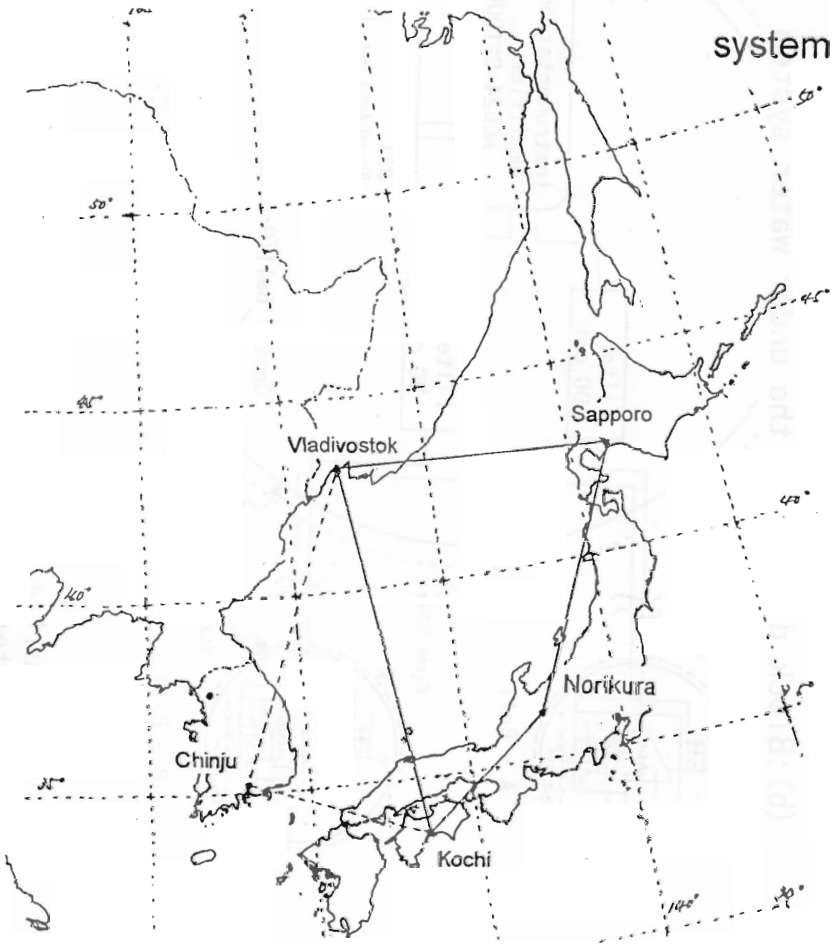

Fig. 7 Example of the obtained wave forms and their source points.
(Abscisas are adjusted at the rise time of a pulse of 1 pps)

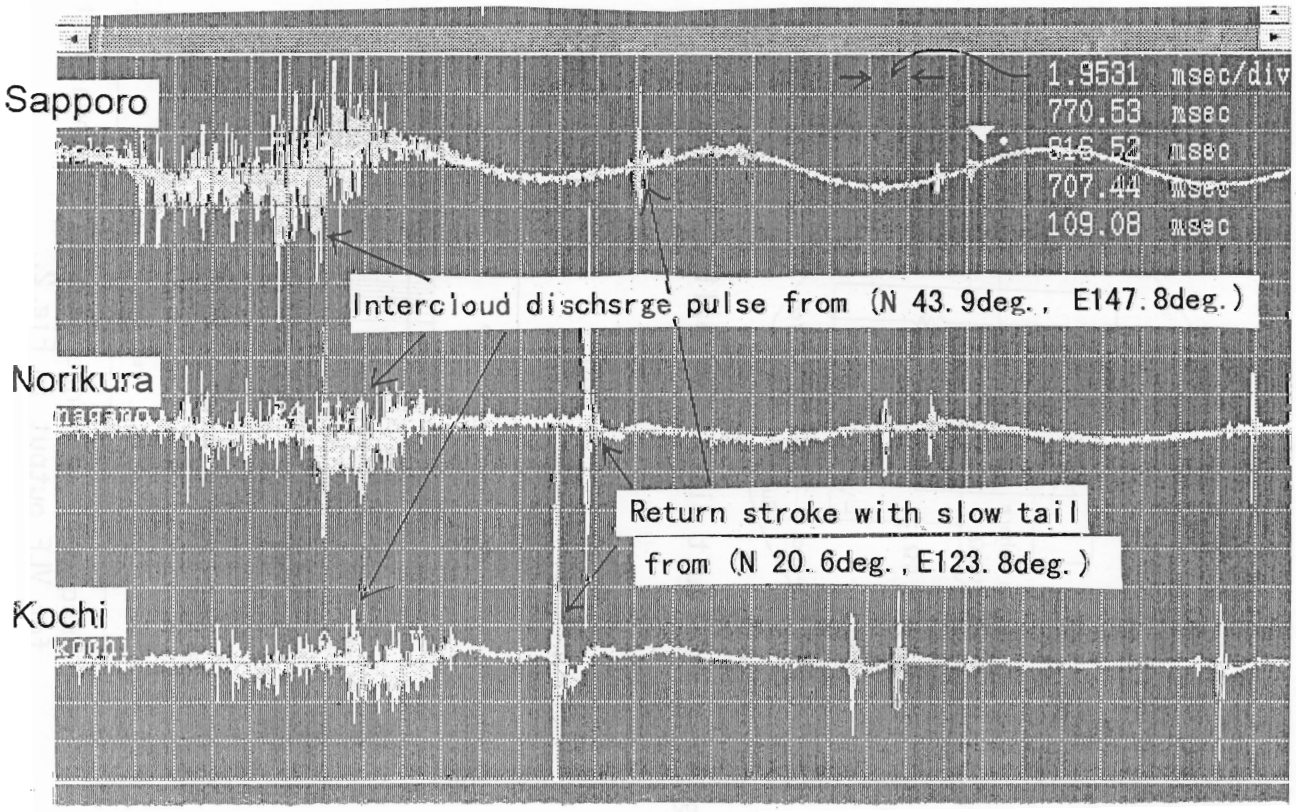

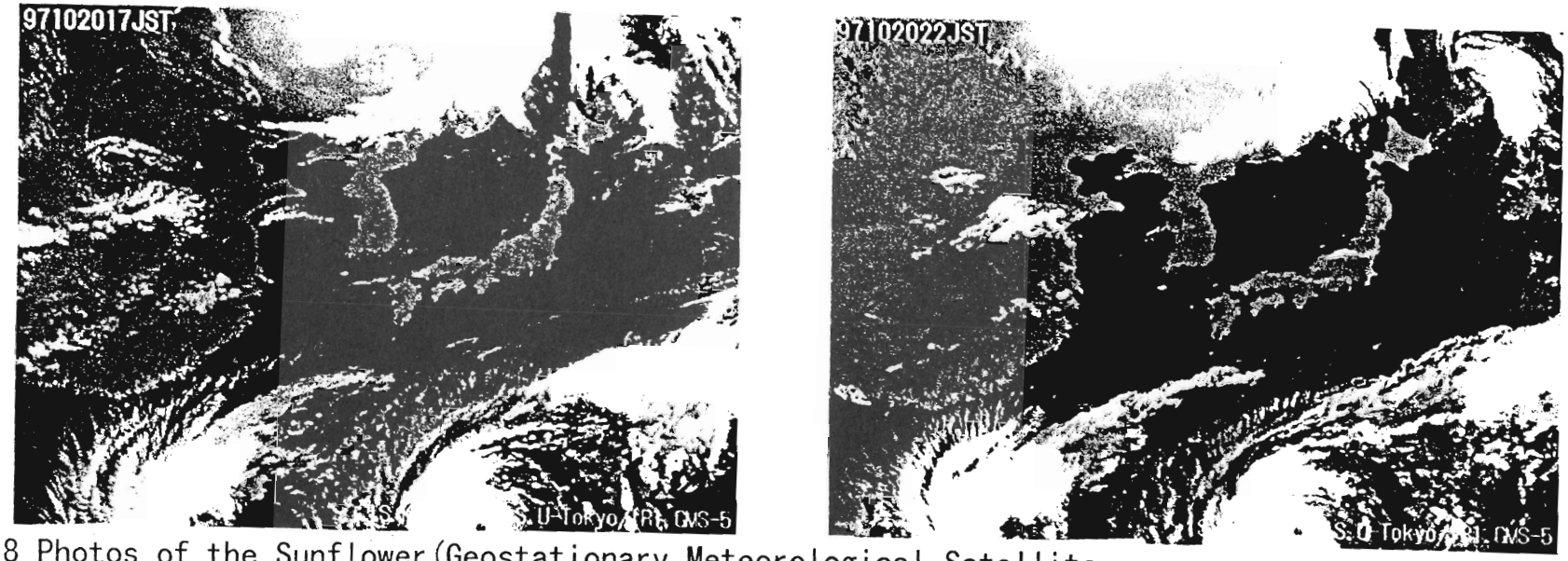

Fig. 8 Photos of the Sunflower (Geostationary Meteorological Satellite : GMS-5) at 17:00 and 22:00 JST on 20th Oct. 1997.

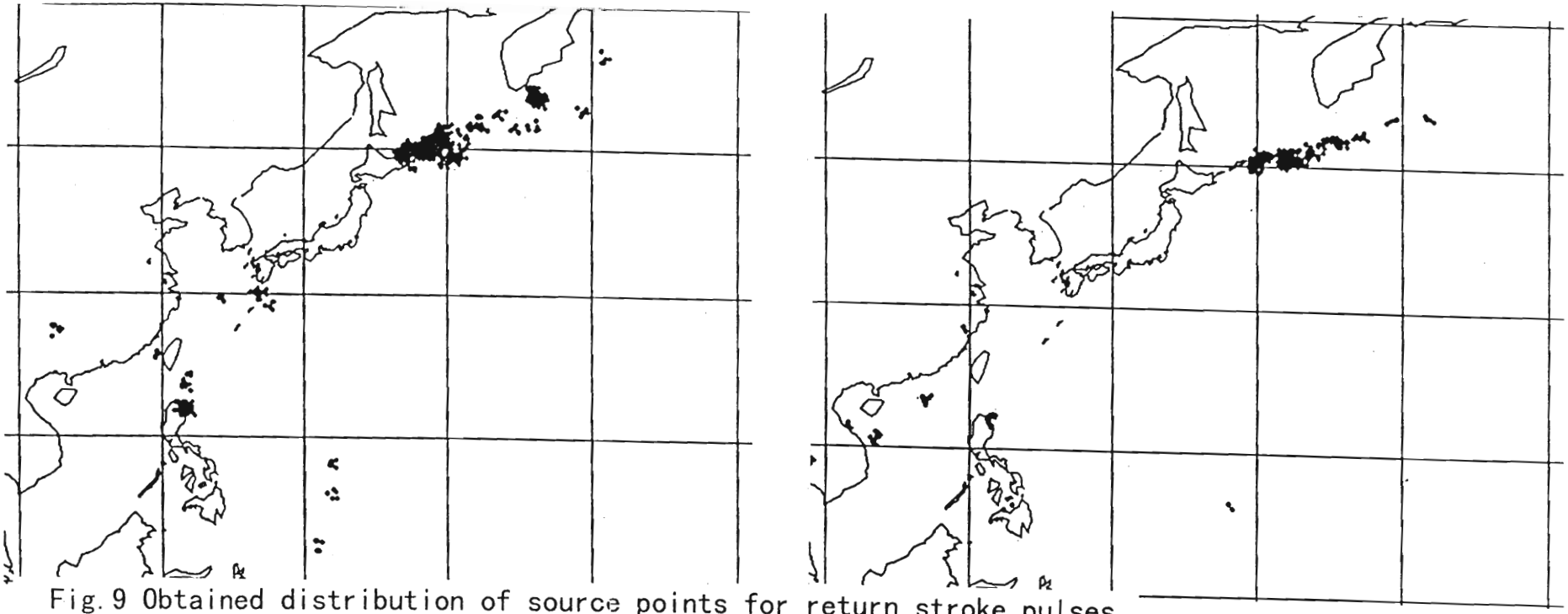

Fig. 9 Obtained distribution of source points for return stroke pulses at 17:00 and 21:30 JST on 20th Oct. 1997. (10min. duration)